Dissertation

Submitted to the

Combined Faculties for the Natural Sciences and for Mathematics

Of the Ruperto-Carola University of Heidelberg, Germany

For the degree of

Doctor of Natural Sciences

Presented by

MSc. Douaa Mugahid (Doaa Megahed)

Born in: Damietta, Egypt

Oral-examination: 24.07.2014

Insights into the regulation of muscle metabolism and growth in mice and hibernating grizzly bears

Referees: Prof. Dr. Ursula Kummer

Prof. Dr. Stephan Frings

Summary

Striated muscle adapts its structure, size, and metabolism to changes in functional demand. This is in part communicated by neural and mechanical input. While the events downstream a neural impulse have been characterised in depth, little is known about the role of mechanotransduction in the regulation of muscle size and metabolism. In mice and humans, muscle disuse induces atrophy, while hibernating mammals largely maintain muscle mass. To understand the intramuscular changes that prevent atrophy during this period, I analysed the changes in muscle of hibernating grizzly bears using high-throughput proteomics and RNA-Seq. The changes in protein expression indicate an effect on muscle metabolism, consistent with increased non-essential amino acid levels and a decrease in ATP production. Supplementing murine myotubes with non-essential amino acids increased cell size, suggesting that increased availability of non-essential amino acids in muscle during hibernation helps prevent atrophy in bears. Comparing gene regulation in hibernation to several atrophy-inducing conditions in mice and humans identified a set of genes that might contribute to the bear's specific ability to prevent the loss of muscle mass. For two of these genes, Pdk4 and Serpinf1, the effect on atrophy signalling was validated in murine myotubes. This supports the utility of the hibernating bear in identifying novel regulators of muscle size.

Towards understanding the role of the sarcomeric mechanotransducer titin in growth signalling and metabolism, I studied transcriptional and proteomic changes in C2C12 myoblasts expressing the titin kinase domain and an animal model deficient in this domain. The kinase domain suppresses Akt activation, possilbly via p62, a protein that interacts with titin's kinase domain and affects signalling upstream of Akt. On the other hand, the titin kinase domain activates NfκB signalling in skeletal muscle by stimulating the processing of p105 to p50, and altering p52-RelB transcription, affecting both the canonical and non-canonical pathways.

Changes in Pdk4, Serpinf1 and insulin signalling in hibernating muscle support the relevance of metabolic regulation and signalling molecules to the bears' ability to preserve muscle mass during periods of prolonged disuse or calorie restriction. While titin kinase-dependent regulation of pathways that are affected in disuse or exercise indicates a role for this mechanically activated domain in regulating muscle adaptation. Thus, both models complement our knowledge of molecular adaptations in muscle with insights into the function of different signalling molecules, which could serve as targets for the improved treatment of muscle disease.

Zusammenfassung

Die quergestreifte Muskulatur kann ihre Masse und Stoffwechsel an den funktionellen Bedarf anpassen – unter anderem über neuronale und mechanische Einflüsse. Während die neuronalen Mechanismen gut verstanden sind, ist nur wenig über den Zusammenhang zwischen der Mechanotransduktion und der Regulation von Muskelmasse und Stoffwechsel bekannt. In Maus und Mensch führt der reduzierte Gebrauch von Muskeln zu Muskelatrophie. Im Gegensatz dazu findet man bei Säugern im Winterschlaf in der Regel keine Reduktion von Muskelmasse. In der vorliegenden Studie habe ich Veränderungen im Muskel von Grizzlybären im Winterschlaf mittels Hochdurchsatz Proteomanalyse und RNA-Sequenzierung untersucht, um Rückschlüsse auf intramuskuläre Veränderung zu ziehen, welche Atrophie verhindern. Die assoziierten metabolischen Veränderungen, beeinflussen die Verfügbarkeit nicht-essentieller Aminosäuren im Muskel. Eine Behandlung von murinen Zellen mit nicht-essentiellen Aminosäuren führte zu einer Zunahme der Muskelgröße und deutet darauf hin, dass im Winterschlaf eine erhöhte Synthese von nicht-essentiellen Aminosäuren im Muskelgewebe die Atrophie reduziert. Die Regulation weiterer Gene im Vergleich zu Atrophie in Maus und Mensch ausschließlich während des Winterschlafes deutet auf ihre spezifische Rolle bei der Konservierung von Muskelmasse im Grizzly-Bären hin. Die Funktion zweier dieser Gene, Pdk4 und Serpinf1, wurde in murinen Myotuben validiert und unterstreicht die Relevanz des Winterschlaf-Tiermodells bei der Identifizierung von Genen, die Muskelgröße regulieren.

Zum besseren Verständnis des Mechanosensors Titin in der Regulation von Wachstumssignalen und Stoffwechsel habe ich Veränderungen im Transkriptom und Proteom von C2C12 Myoblasten, welche die Titin Kinasedomäne überexprimieren, und einem Tiermodel, bei dem diese Domäne fehlt, untersucht. Die Titin Kinasedomäne reduziert Akt Aktivierung – möglicherweise über p62, einem Protein, das mit der Titin Kinasedomäne interagiert und Signaltransduction über Akt beeinflusst. Weiterhin aktiviert die Titin Kinasedomäne den Nfκb Signalweg in dem Skelettmuskel durch die Modulation von p105, p50 und die veränderte p52-RelB Transkription und aktiviert sowohl den kanonischen als auch den nicht-kanonischen Signalweg.

Akt und NfκB Signalwege sind abhängig von Muskelaktivität reguliert, was für eine Rolle der mechanisch aktivierten Titin-Kinasedomäne in der Homöostase des Muskels spricht. Veränderungen in der Signaltransduktion im Muskel über Pdk4, Serpinf1 und Insulin während des Winterschlafs zeigt, wie relevant die Regulation von Stoffwechsel und Muskelwachstum für den Erhalt der Muskelmasse ist. Die identifizierten Wachstumssignale könnten eine ähnliche Rolle in Lebewesen spielen, die keinen Winterschlaf halten – beispielsweise bei reduzierter Kalorie-Zufuhr und Immobilisation.

Acknowledgements

بسم الله الرحمن الرحيم

قال تعالى :(لَئِنْ شَكَرْتُمْ لَأَزِيدَنَّكُمْ)

[سورة إبراهيم الآية:7]

I would like to first start by thanking God Almighty for his bountifulness, it is only because of his never ending generosity that I have achieved in life what for others are far-fetched dreams. Second only to God are my parents. Mum and dad, I cannot thank you enough for everything you taught me in life and the freedom you gave me to pursue my dreams, and all the support you provided to help them come true. Without your support and love I am nothing, and this thesis would never have seen the light. My beautiful sisters, I am sure it is your incessant prayers that helped me through some of the hardest times. Thank you for being such wonderful people, and for helping me stay grounded at times when it was hardest to be just that. You make me laugh when I no longer think I can, and the thought of you makes the impossible -for me- possible!

That said, I am immensely grateful to Prof. Michael Gotthardt for the opportunity to complete my PhD work in his lab, and under his supervision. I have learnt a great deal more than I ever thought I would when this all first started. You taught me so much more about science communication than I have learnt in all my previous work places combined, and I believe this will stay with me everywhere and anywhere I go. Prof. Ursula Kummer, thank you for believing in me all these years, even before we ever met. I am forever grateful to you for allowing me the chance to be in the first class of SysBio students and for making that whole experience one of the pleasantest educational periods in my life. You have taught me how to be a humble and caring scientist, yet critical of my own and others' work. Your support means the world to me, and I am lucky to have you as a mentor. Prof. Stephan Frings, thank you for your very helpful critical input at all my committee meetings; your support on these limited occasions gave me the strength to stay much more grounded and focused, shaping my work into what has finally become this thesis. I can never thank you enough.

My wonderful colleague and friend Meghna Thakkar, I owe you so much more than I can ever repay you for by being there for me throughout this ordeal! You have always been the better party, showing selfless support and a strong belief in my abilities. Your presence has

transformed my PhD from bearable to pleasant! And has taught me so many things about selflessness at work! What would I have done without you? My other colleagues in the Gotthardt lab, thank you all for lending a helping hand, or giving a piece of advice no matter how small. Thank you Titin kinase subgroup members; our discussions were critical for what my understanding of Titin kinase function is today. Martin and Poldi, thank you for helping me orient in the lab when I first started. Franzi, you have always shown a willingness to help. Flo, thank you for being so honest and outspoken; you are one of the few people who I think I got right from day one! Vita, your little conversations have always put a smile on my face, and your willingness to listen has helped a lot at times when I needed to be heard. Micha, you are the backbone of so many projects in this lab, and watching you work has been an inspiration. I hope I can be half as thorough as you are one day; you have always been willing to help and answer questions and have always been so efficient and timely. Uta, sharing the office with you was a pleasure, and seeing you work has taught me a lot about perseverance at the bench-side; I am glad we crossed roads, and hope we do again. A special thanks goes to Carmen and Beate who provided enormous help with the technicalities in the lab! You're support has been instrumental to the completion of this thesis as it stands today. Tutku, I couldn't have asked for a better and more pleasant person to work with so closely. The time we spent working on the grizzly bear project was one of the best throughout this PhD! I am so lucky to have had you as my student! Thank you for being such a great one!

I would also like to deeply thank all the members of AG Poy! You guys have always been willing to help whenever asked and were always generous with your time, information and reagents. Thomas and Sudhir you have made my time on the floor and beyond so much more fun than anyone else, and your willingness to help has always blown my mind. Thank you for being so dependable, pleasant and joyful! I don't think this PhD experience would've been the same without you! As you already know…" You rock!".

All our collaborators especially Dr. Stefan Kempa, Dr. Leif Steil and Arthur; thank you for the timely support generating and analysing the different types of high-throughput data used for all the projects.

A lot of thanks goes to TransCard and its coordinators past and present. You have supported my education since day one and I have benefited tremendously from the infrastructure you have provided. I am grateful for all the effort you have put in to helping me and others during our time as students. The same goes for the Helmholtz graduate school at the MDC for supporting

the first three years of my PhD financially, this PhD would certainly never have happened without that.

To the unsung heroes behind the scenes, my childhood friends Sarah E, Sarah G, Amira and Eeso your support and prayers have kept me going always, and every time we talk or meet I am reassured I can make it through another day! Aya Helal thank you for believing in me all these years, you know me better than almost anyone else and having your faith has kept me strong! I love you my friend! Stephen Kraemer, thank you is not enough for all the time and support you have given me! You have been so selfless in your support of me over the past four years, and I deeply wish I can give back even a small part of it to you one day! Katrina Meyer, our tea and coffee evenings have always helped me unwind! Sometimes all you need is to be heard and you did that so well. Thank you for sharing so much of your very precious time. Zuzu and Amira, seeing you in action has been such an inspiration over the years, everything I do you do better! And in doing so have always shown me how much more can be achieved! You are such wonderful friends and incredible women! Thank you for showing me how possible it is to be a wonderful mother, partner and scientist. Lamiaa Bahnassawy, we have shared so much over the past couple of years, it is insane how intense it has been! You have been more than a sister to me, showing me all the love and support a sister and friend could give. You have inspired me to stay strong, and have taught me how dedication to one's work should be! I am grateful we got to make so much memories, and am sure we will continue to forever! Thank you so much for everything! Ameirah, just the thought of you makes me cry with emotion! You have been the mother and sister I miss from back home. Your support and willingness to so selflessly help on every occasion is super-human! You have made my whole Berlin experience so much more than it ever would've become without you! I thank God every day for bringing you to this city just when I didn't want to be here anymore! I love you dearly and can never thank you enough for everything you've done for me. Last but not at all least, I have to deeply thank *you* Mohamed Sherif for your patience and understanding these past couple of years. I know they have been a difficult lot, but you were always so supportive of me and my career! I pray this continues to be the case, and that I can be to you what you have been to me when the time comes. Thank you for sharing this journey so gracefully! And I am looking forward to a wonderful life-long one ahead!

Table of contents

1 Abstract

Mechanotransduction plays an important role in the regulation of muscle growth and metabolic signalling in striated muscle. Muscle disuse reduces mechanical input to the muscle, which results in a loss of muscle mass. Here I describe how titin's mechanically activated kinase domain affects muscle growth and metabolism via p62 and Akt signalling. I also demonstrate how changes in metabolic and growth signalling in hibernating grizzly bear help maintain muscle mass under conditions that induce muscle loss in humans and mice. I validated some of these changes in murine myotubes demonstrating that increasing non-essential amino acid levels, increasing Pdk4 levels or suppressing Serpinf1 has a positive effect on growth signalling that extends to non-hibernators.

2 Introduction

2.1 Adaptability

The ability of living species to survive under various environmental conditions emerges from the adaptability of biological systems. Adaptability here means the ability of a system to regulate its components in response to changes in the environment with which it interacts. This property is key in keeping organisms functional despite changes in temperature, nutrient availability and predator behaviour for example. The ultimate goal is for the organism to be able to sustain its own existence and procreate despite alterations in external stimuli. In unicellular organisms, the survival of a species in a new environment could simply be brought down to the individual cells' ability to produce enough energy under the current circumstances to sustain the next cell division even if at the expense of the less fit counterparts. At a multicellular level, it is slightly more complicated, especially as each cell type starts to serve a different purpose, all of which contributes to the general fitness of the organism. The challenge then becomes sustaining the whole organism, while preserving each cell type or the organ it comprises without much damage (Gardner, 2009). This has led to the emergence of centralized control in higher animals such as mammals, who exert central regulation largely through the brain. Central regulation helps coordinate the response of the various organs to changes in environmental stimuli, while each organ is hard wired to attempt preserving itself in the process.

2.2 Muscle tissue

In vertebrates myocytes are the cells that build up muscle tissue, and their characteristic property is the ability to contract, changing their shape and area, facilitating organ locomotion. This is possible due to the presence of a network of actin and myosin filaments that utilize ATP to produce force. All muscles are under neural control, which regulates how they respond to changes in the environment ensuring concerted action. Some muscles are under voluntary control such as skeletal muscle, while the heart and smooth muscle which lines, among other organs, the internal viscera are not. Together cardiac (heart) and skeletal muscle is referred to as striated muscle owing to the distinct striated pattern they exhibit under a microscope. This striated pattern comes from the organization of their contractile machinery into distinct units, a property smooth muscles lack.

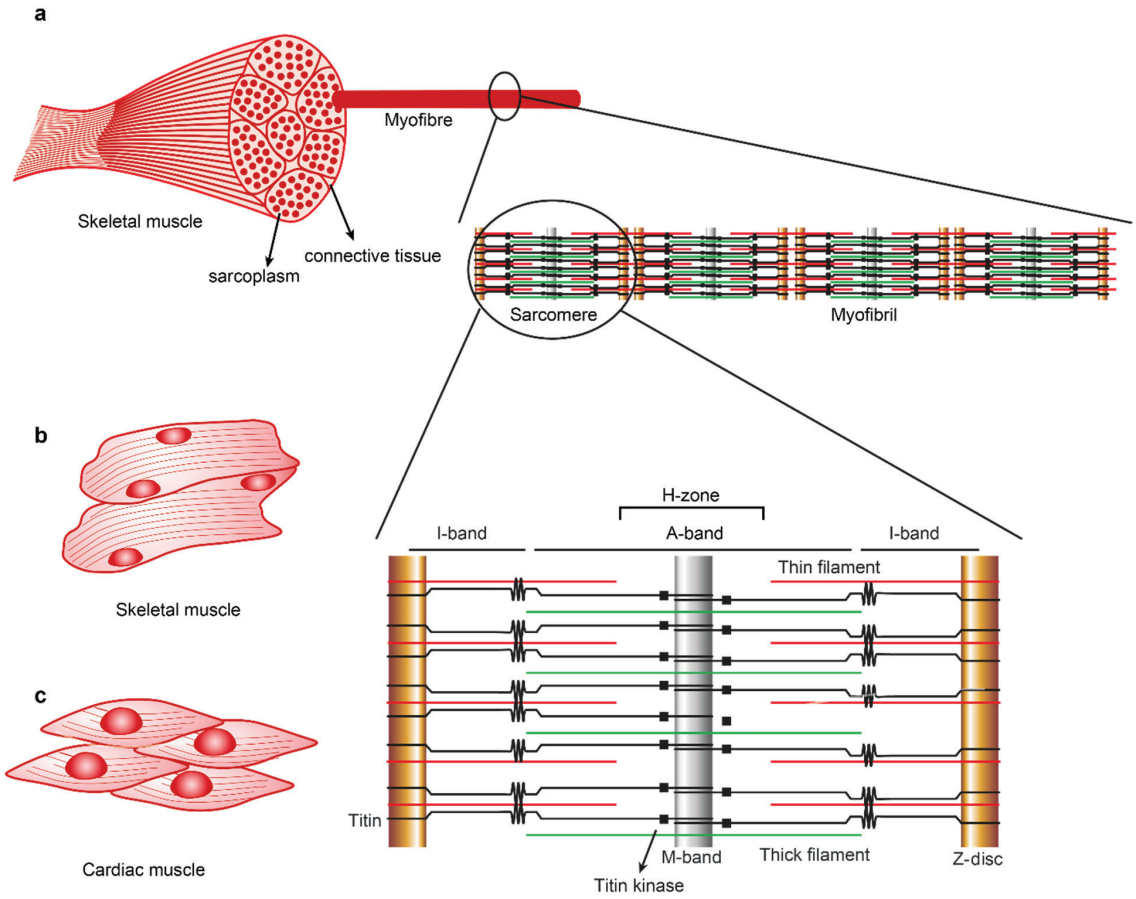

Figure 1 : Structure of striated muscle.
(a) Striated muscle is composed of bundles of myofibres, which are themselves made up of myofibrils. Myofibrils consist of sarcomeres which are constituted of a network of structural proteins intricately arranged to allow muscle contraction. (b) Skeletal muscle cells are formed by the fusion of several individual cells during development, giving rise to elongated, multi-nucleated cells. (c) Cardiac muscle cells are interdigitated mono-nucleated cells, smaller in size than skeletal muscle cells. (Adapted from Junqueira's Basic Histology Text and Atlas)

2.2.1 Striated muscle

Skeletal muscle is made of fibres (cells) arranged in series or parallel to form the whole muscle. The number and arrangement of these fibres determines how fast and strong a muscle contraction is. These fibres are themselves made of smaller contractile units called myofibrils which come together in bundles of 500-10,000 to form one fibre (Figure 1a). The myofibril is an assembly of thousands to millions of smaller contractile units called sarcomeres, which are arranged in series and considered the smallest force-generating units within striated muscle (Figure 1.a). Under the electron microscope a sarcomere can be seen as a structure of alternating light and dark bands, where the light bands are regions of actin-containing thin filaments and the dark bands regions where actin interacts with myosin-containing thick filaments. The light

bands are referred to as I-bands because they are optically isotropic, while the dark bands are anisotropic and therefore called A-bands. However, the sarcomere is not only comprised of thin and thick filaments. Titin molecules span the half sarcomere, with their N-terminus anchored at the Z-disc a structure that separates every two adjacent sarcomeres and also docks the thin filaments. The area in the A-band that is slightly lighter than its surroundings is known as the H-zone and is where the thick filaments extend in the absence of actin. Within the H-zone is the M-line, a thin region where the Titin molecules spanning each half of the sarcomere overlap and where only myosin tails and no heads are present (Clark et al., 2002).

Though both cardiac and skeletal muscle have a similar striated pattern, reflecting the highly organized structure of their contractile machinery, they express different isoforms of contractile proteins and are functionally different. Isoform expression varies depending on the developmental stage, muscle type and muscle load and optimize each type of muscle for its role in the body at that particular time or condition. Faulty isoform expression is the base of various myogenic diseases (Clark et al., 2002).

2.2.1.1 *Skeletal muscle*

During development a skeletal muscle fibre arises from the fusion of several smaller cells, which is why they appear cylindrical and are multinucleated (Figure 1b). Each fibre is separated from the other by connective tissue and is innervated (Figure 1a). Fibres that are innervated by the same nerve contract together and are considered one motor unit. Contraction in a skeletal muscle occurs when the neurotransmitter acetylcholine is released from a nerve's end, changing transmembranal voltage which generates an action potential (AP). This ultimately leads to the release of Ca^{2+} from its intracellular store in the muscle, a specialized compartment known as the sarcoplasmic reticulum (SR). The release of Ca^{2+} synchronizes various intracellular events, including actin-myosin binding which facilitates muscle contraction. Skeletal muscle fibres consist of three main types; I, IIa and IIb. Fibre type composition differs between muscle types and can change in response to changes in muscle use and load (Schiaffino and Reggiani, 2011). Fibres differ largely in their contraction speed and energy source. Type I fibres are rich in mitochondria, but relatively poor in glycogen, making them incapable of rapidly generating large amounts of glycogen-derived ATP, but nevertheless capable of generating higher amounts of ATP overall through fatty acid-driven oxidative phosphorylation. This makes them ideal for the slow and stable muscle contractions required to support muscle function over long periods of time. On the other hand, type IIa fibres have comparatively less mitochondria, but contain more glycogen than type I fibres. This makes them capable of producing sustainable amounts

of ATP via oxidative phosphorylation, but also capable of rapidly producing ATP through glycogen breakdown and anaerobic respiration. These fibres are thus ideal for supporting relatively long periods of intense muscle use, such as required by runners. The third fibre type is type IIb, which constitutes fibres that are poor in mitochondria, but generate ATP rapidly from the breakdown of glycogen-derived glucose; they are highly fatigable and generate a lot of lactic acid. This makes them ideal for fast responses, but not long-lasting ones. The three fibre types also express different isoforms of contractile molecules to match their contractile abilities (Schiaffino and Reggiani, 2011).

2.2.1.2 *Cardiac muscle*

The mechanism of force generation in the heart is similar to skeletal muscle but cardiac structure and cellular composition is somewhat different. Because the heart is constantly beating, cardiac muscle cells (cardiomyocytes) are rich in mitochondria, and ATP production is sustained primarily through fatty acid oxidation. Glycogen is also present, but in low amounts (Stanley, 2005). Unlike skeletal muscle fibres that are long and multinucleated (Figure 1b), cardiomyocytes are smaller and much easier to distinguish as individual cells (Figure 1c). Adjacent cells interdigitate holding the heart together as a well-connected mesh; and the membrane between them is organized into distinct gap-junction-rich regions called intercalated-disks (Clark et al., 2002). These low resistance areas facilitate the rapid transfer of an action potential from one cell to the next, a key property for a well-functioning heart. This ability of cardiac cells to relay an action potential throughout the heart, together with the presence of specialized auto-excitatory cells makes the stimulus for contraction inherently different from skeletal muscle. Unlike skeletal muscles, which need innervation for the generation of an action potential and subsequent contraction, cardiac cells can synchronize their beating in response to locally-generated action potentials, making innervation unnecessary for each and every cell. Only certain parts of a cardiac muscle are extensively innervated to regulate the rate of cardiac contraction in response to external stimuli (Zaglia et al., 2013; Shen and Zipes, 2014).

2.2.2 Striated muscle and the adaptation in size

Striated muscle size changes in response to alterations in their load and frequency of use (Alway et al., 1988). This is evident in the increase in skeletal muscle size in athletes with consistent training. Once an athlete stops training, their muscle size is no longer put to stringent use and their skeletal muscle size decreases to within the average range (Faulkner et al., 2008). Similarly, the hearts of hypertensive patients exhibit left ventricular hypertrophy to compensate

for the increased resistance in the blood vessels through which the heart needs to pump oxygenated blood. Although compensatory at first, this increase in size often becomes pathological and increases mortality among hypertensive patients (Berenji et al., 2005). Such is an example of a situation where controlling adaptational changes in striated muscle is necessary. Similarly, decreased use and/or load is the reason why immobilized patients often suffer from skeletal muscle loss as do astronauts in space (Glass, 2003). Muscle size also declines in aging and malnourished individuals, as well as cachectic and spinal cord injury patients (Thuret et al., 2006). Characterizing the pathways that control muscle growth and adaptation can thus help prevent undesired changes in muscle size, minimizing mortality in some cases and improving the quality of life of patients in others.

2.2.3 Striated muscle and metabolism

Together, the heart and skeletal muscle constitute about 40% of an average individual's body weight. They contribute to 30% of the body's resting energy consumption, and almost 100% of it during exercise (DeFronzo and Tripathy, 2009; Baskin et al., 2015). Skeletal muscle is also the major site of postprandial glucose uptake (80%), and is where most of the body's glycogen is stored under resting conditions. This makes striated muscle important in regulating blood glucose levels and whole-body metabolism, and its failure to do so can be of consequence on the whole body. For example, skeletal muscle, together with adipose tissue, was found to be an important contributor to the development of diabetes in some genetically prone populations (Pratipanawatr et al., 2001). Studies on normal glucose tolerant offspring of type II diabetic parents in these populations have shown that the skeletal muscle of the asymptomatic children was often insulin resistant long before they developed the full blown symptoms and that the children were glucose tolerant mostly because of a compensatory increase in B-cell insulin release. The children who failed to increase B-cell insulin secretion where those that were most likely to develop diabetes later on in life (DeFronzo and Tripathy, 2009). In a reverse type of interaction, some diabetic patients develop diabetic cardiomyopathy, a heart condition that involves left ventricular hypertrophy, systolic and -in 30-60% of cases- diastolic dysfunction (even after correction for age, hypertension, obesity, hypercholestrolemia and coronary heart disease) (Boudina and Abel, 2007). Part of the pathoetiology is attributed to the changes in the heart's metabolic machinery during diabetes, where there is a reduction in the mitochondrial enzymes required for oxidative phosphorylation, decreasing the heart's ability to efficiently produce ATP from FAs, its major energy source (Boudina and Abel, 2007). Thus striated muscle is affect by and is important for maintaining metabolic homeostasis (Baskin et al.,

2015). This has made the study of metabolic control in striated muscle a topic of interest not only to muscle biologists but to many of those interested in metabolic diseases.

2.2.4 Molecular regulation of skeletal muscle size and metabolism

Several pathways have been implicated in the orchestration of both metabolic and trophic changes in response to increased muscle utility, including Ca^{2+}-CaM-CaMK, PI3K-AKT-mTOR and NFKB signalling (Glass, 2003). All these signalling pathways work in part by facilitating changes in the expression of genes that alter metabolism and the rates of protein turnover in response to different stimuli.

2.2.4.1 *Ca^{2+}-CaMK signalling*

Ca^{2+} release is a critical step in the response of striated muscle to an action potential as it binds to TroponinC allowing crossbridge formation, which is necessary for muscle contraction. Ca^{2+} is not only important in muscle, but is a ubiquitous secondary messengers in all cell types and its intracellular concentration is altered in response to various stimuli (Clapham, 2007). The specificity of the calcium response is coded in the amplitude and periodicity of the Ca^{2+} waves propagated through the cytosol, which is generated in a stimulus-specific manner (Berridge et al., 2003). In muscle, an action potential changes membrane potential increasing Ca^{2+} influx into the cell via voltage sensitive channels. These receptors are also coupled to Ryanodine receptors (RyR) along the sarcoplasmic reticulum (SR), the major compartment for Ca^{2+} storage in a muscle cell (Figure 2). This enhances the rise in cytoplasmic Ca^{2+} levels. Also the binding of Acetylcholine (Ach) to the muscarinic Ach receptors or of catecholamines to the α1-adrenergic receptor induces the formation of IP3, which activates IP3R channels another Ca^{2+} channel along the SR membrane (Fill and Copello, 2002). Elevated cytoplasmic Ca^{+2} not only binds to Troponin C but many other proteins as well, which allows it to couple changes across different intracellular processes. One class of Ca^{2+}-binding proteins is Calmodulin (CaM) which acts as a Ca^{2+} receptor that binds many other proteins and regulates their function in a Ca^{2+}-dependent manner. These proteins include kinases, phosphatases and nucleotide phosphodiesterases (Means, 2000). One of the better studied families of CaM-binders are the Ca^{2+}/Calmodulin-dependent kinases (CaMK), a family of 4 kinases that mediate intracellular events in response to changes in intracellular Ca^{2+} concentrations. The kinases of this family are grouped into four classes: the Myosin Light Chain Kinases (MLCK) and the CaMKI, CaMKII and CaMKIV kinases.

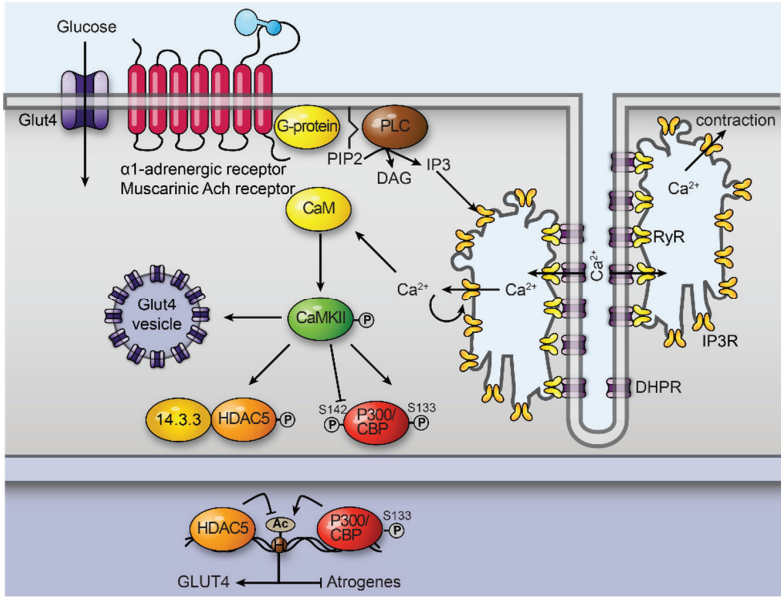

Figure 2 Neurotransmitter-mediated Ca2+-signalling in striated muscle.
Activated muscarinic or α1-adrenergic G-protein coupled receptors activate phospholipase C which cleaves phosphatidylinositol 4,5-bisphosphate (PIP2) into inositol 1,4,5-trisphosphate (IP3) and diacylglycerol (DAG). IP3 binds IP3R on the sarcoplasmic reticulum (SR) enhancing the release of Ca^{2+}. Cytosolic Ca^{2+} mediates muscle contraction, Ca^{2+} release from the ER and activates calmodulin (CaM), which in turn activates CaMKII. Active CaMKII phosphorylates HDAC5, preventing its nuclear localization, while activating histone deacetylases P300/CBP by phosphorylating Serine (S) 133, counteracting the effect of HDAC5 in the nucleus. This enhances the expression of the glucose transporter GLUT4 while suppressing atrogene expression. CaMKII can also inhibit P300/CBP activity by phosphorylating S143.

While MLCK almost exclusively associate with actomyocin to phosphorylate the myosin light chains (MLC), the other three families have various targets ranging from cytosolic to membrane and nuclear proteins (Means, 2000). CaM-binding leads to a conformational change in these kinases, displacing their autoinhibitory domain to expose the catalytic core. This leads to their activation and allows subsequent substrate binding. Unlike the other CaMKs, CaMKII functions as a multimeric complex of 10-12 subunits. These are encoded by 4 different genes in mammals, expressed and spliced in a tissue-specific manner. The binding of CaM to two adjacent subunits not only induces the conformational change necessary for the activation of the other CaMKs but also promotes the phosphorylation of the adjacent subunit, making its subsequent activity Ca^{2+}-independent until dephosphorylated (Means, 2000). In striated muscle CaMKII is the main CaMK family expressed and its phosphorylation increases in skeletal muscle of humans and rats in response to acute training (Rose and Hargreaves, 2003). This observation suggests it plays an important role in regulating muscle adaptation to use. Not much

is known about the consequence of this enhanced activity, but the inhibition of CaMKII in skeletal muscle inhibits contraction-mediated glucose uptake, but not that stimulated by insulin (Witczak et al., 2010). This can be explained by CaMKII's ability to increase GLUT4-vesicle fusion at the membrane, increasing glucose uptake. Exercise-induced CaMKII activation however seems to have no consequence on glycogen breakdown rates, but could affect GLUT4 expression levels (Ojuka et al., 2012). More functions of CaMKII in the muscle adaptive response can be envisioned based on the function of some of its known targets, among which are the Class II histone deacetylases (HDAC) HDAC4 and 5. These HDACs play an important role in muscle growth and metabolic regulation (Moresi et al., 2010; Karpac and Jasper, 2011) and their nuclear localization is phosphorylation-dependent (Karpac and Jasper, 2011). HDAC phosphorylation promotes their nuclear export and cytosolic sequestration by 14-3-3 proteins thereby preventing them from regulating gene expression (Figure 2) (McKinsey et al., 2000). HDAC5 inactivation decreases atrogene expression, preventing muscle wasting and enhancing muscle growth (Moresi et al., 2010). It also increases glucose uptake, glycogen synthesis, mitochondrial respiration and ATP production in skeletal muscle (Raichur, 2012; McGee, 2014). Thus an increase in CaMKII activity upon muscle use could inhibit HDAC-mediated atrogene expression and enhance energy production, thereby helping the muscle adapt to this increase in demand. CAMKII also phosphorylates the histone acetyltransferases (HATs) CBP and P300, which counteract the activity of HDACs; an event that activates them if phosphorylation takes place on ser133, but inhibits them if ser142 is phosphorylated (Means, 2000). Moreover, the over expression of various CaMKII isofroms in the hearts of mice leads to changes in cardiac muscle size and function, demonstrating their importance in maintaining these processes in the heart (Anderson et al., 2011).

2.2.4.2 *PI3K-Akt-mTOR signalling*

The PI3K-AKT-mTOR signalling cascade is the pathway downstream of insulin (INS) and the insulin-like growth factors (IGF) (Figure 3). Upon INS/IGF binding, the receptors dimerize and cross phosphorylate one another, which enhances their kinase activity. This results in a tyrosine phosphorylation of the insulin receptor substrates (IRS1-6), which function as adaptor proteins that relay the signal to downstream effectors. These effectors include the regulatory subunit of PI3K (p85), which leads to the activation of the catalytic subunit and the generation of phosphatidylinositol 3-phosphate (PIP3) which serves as a binding platform for proteins with a pleckstrin homology (PH) domain (Taniguchi et al., 2006). One of the most well studied PH-containing proteins recruited to the membrane and activated downstream of INS/IGF signalling

is Protein kinase B (AKT). This protein is phosphorylatable at two amino acids both of which lead to its activation. Phosphorylation at Thr-308 is catalysed by another PH-containing kinase, PDK1 which is also recruited to the membrane upon INS/IGF binding; and Ser-473 which is catalysed by the RICTOR-mTOR-containing mTORC2 complex (Sarbassov et al., 2005). When activated, AKT regulates many other proteins such as GSK3B which inhibits glycogen synthesis; mTOR, which regulate rates of protein synthesis, AS160 a GTPase-activating protein that mediates GLUT4-vesicle transport to the membrane and FOXO1 which - when unphosphorylated and deacetylated - activates the transcription of gluconeogenic and muscle-specific ubiquitin ligases (Manning and Cantley, 2007) (Figure 3).

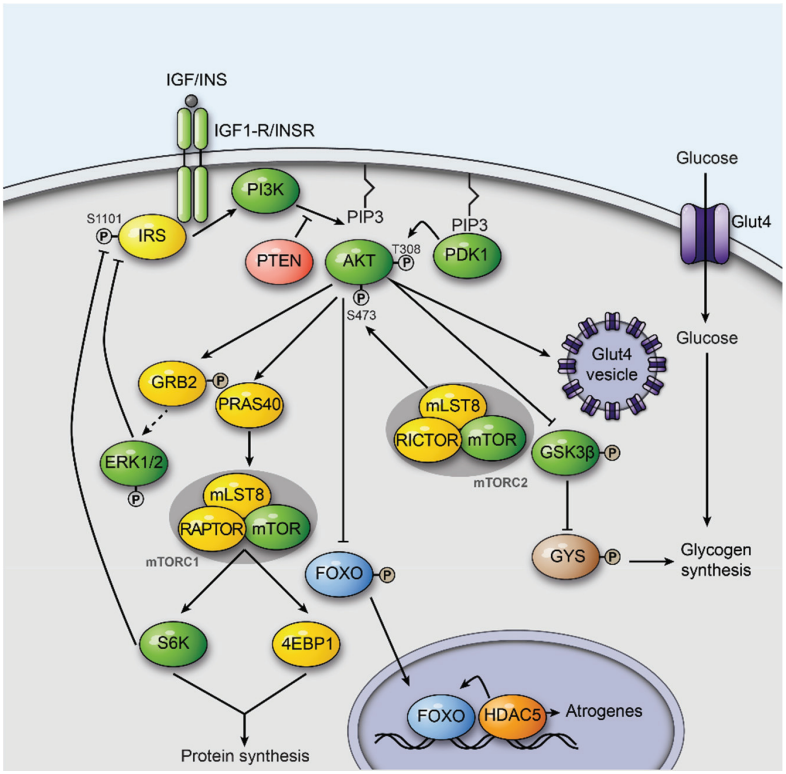

Figure 3: Insulin/Insulin-growth factor signalling in striated muscle.
IGF/INS binding to receptor tyrosine kinases (RTK) induces phosphorylation and activation. This recruits IRS, which in turn activates PI3K, catalysing the generation of phosphatidylinositol (3,4,5)-trisphosphate (PIP3). AKT and PDK1 move to the membrane. PDK1 and mTOR phosphorylate AKT, contributing to its activation. Active AKT activates the TORC1 complex, which is upstream of S6K and 4EBP1, both involved in protein synthesis. AKT also inhibits FOXO transcription factors upon phosphorylation and inhibits their nuclear import, where they are deactylated by HDAC5 to activate atrogene expression. AKT enhances glucose uptake via GLUT4 and inhibits GSK3-beta activity. This enhances glycogen synthesis via glycogen synthase (GYS). AKT activation also helps set in a negative feedback loop by activating GRB2 which mediates ERK1/2 phosphorylation. The ERKs inhibit IRS by its phosphorylating a serine.

While HDAC phosphorylation is CaMK-dependent, FOXO1 deacetylation is HDAC-dependent (Mihaylova et al., 2011) suggesting that FOXO1 might serve as an integration node for signals from different pathways (Karpac and Jasper, 2011). AKT has three isoforms which are very homologous, but expressed at different ratios in different tissues, and have relatively different functions (Taniguchi et al., 2006). In muscle both AKT1 and AKT2 are present, but AKT3 is mostly neuron specific. While AKT1 has been linked to the regulation of cell growth, AKT2 has been shown to affect intracellular metabolism to a greater degree (Taniguchi et al., 2006). Another of the important IRS binding proteins is GRB2, which plays an important role in activating the MAPK pathway leading to changes in cellular growth, division and differentiation (Taniguchi et al., 2006). The MAPK signalling components ERK1/2 can inhibit IRS activity by serine phosphorylation and so play a role in insulin-mediated glucose metabolism (Taniguchi et al., 2006). Indeed studies in muscle show that cardiac and skeletal muscle hypertrophy are associated with an increase in AKT phosphorylation as well as that of its downstream targets, and is prevented by inhibiting mTOR-mediated protein synthesis (Stitt et al., 2004). Others show that insulin resistance in diabetic patients' muscle is associated with a decrease in mitochondrial oxidative phosphorylation, which again links metabolic changes in muscle to changes in insulin signalling (Patti et al., 2003). Exercise can decrease muscle glycogen content independent of insulin activity and in MIRKO mice (a muscle-specific knockdown of the insulin receptor) insulin-mediated glucose uptake and glucose-6-phosphate-dependent glycogen synthase activation in muscle is decreased (Wojtaszewski et al., 1999). However, these mice are more capable of increasing glucose uptake and glycogen synthase activity in response to exercise suggesting the possibility of an exercise-dependent, insulin-independent regulation of glucose uptake and glycogen synthase activity that cross-talks to insulin in some way.

2.2.4.3 *NFKB signalling*

NFKB signalling has long been implicated in inflammation, tumorigenicity and development (Gilmore, 2006). Its components include the NFKB transcription factors (TF), their inhibitors the IKB and the IKB- inhibitors the IKKs. The NFKB transcription factor family consists of several proteins, all of which contain a Rel homology domain that allows DNA binding and protein dimerization (Gilmore, 2006). The differences in the c-termini of these transcription factors splits them into two main subfamilies: the Rel subfamily which comprises RelA (p65), RelB and c-Rel; and the NFKB subfamily which comprises p100 and p105. The Rel subfamily have poorly conserved c-terminal transactivation domains, while the NFKBs are characterized

by their long c-terminal domains that inhibit their TF activity until degraded (Gilmore, 2006). In vivo, all the NFKB TFs can form homo- or heterodimers, except for RelB which only form heterodimers. The NFKB TF dimers bind to 9-10 base-pair long DNA stretches known as kB sites of variable nucleotide composition. Each dimer has its own binding site preferences, making this family capable of regulating a myriad of complex transcription responses (Gilmore, 2006). When bound to the IKB proteins, NFKB transcription factors are inhibited, and are mainly cytosolic (Figure 4).

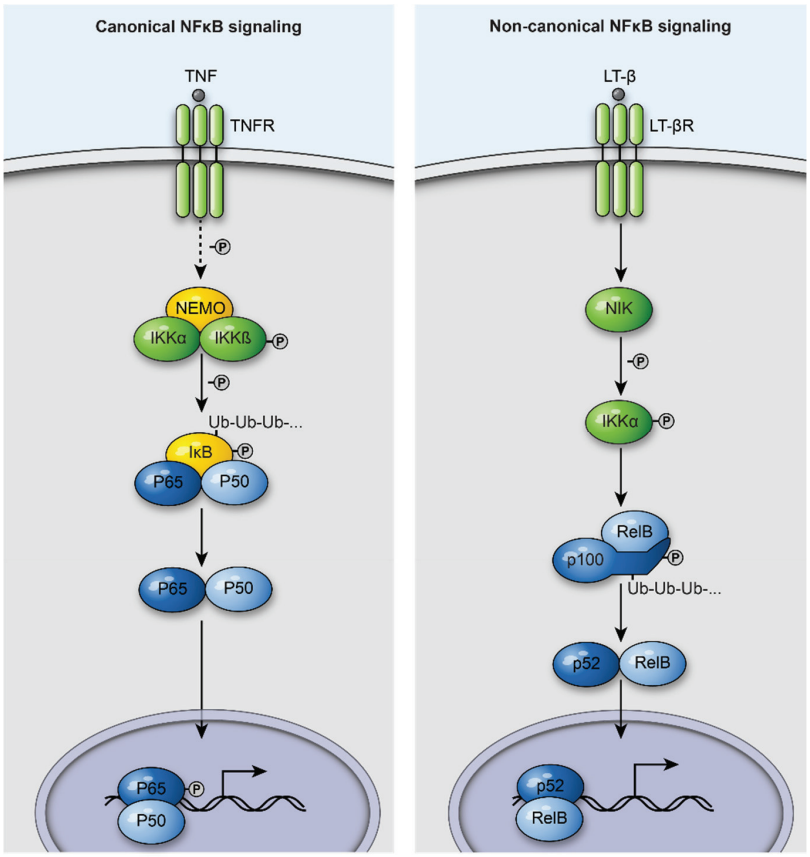

Figure 4: Canonical and non-canonical NFKB signalling.
(a) Extracellular stimuli that activate the canonical NFKB pathway induce the phosphorylation of IKKs, leading to the phosphorylation, ubiquitination and degradation of IKB. This allows p65-p50 heterodimers to move to the nucleus where they are transcriptionally active. (b) Other stimuli lead to the activation of NIK, which phosphorylates IKK-alpha, which in turn phosphorylates the c-terminus of the IKB p100. This leads to the ubiquitination and degradation of the c-terminus of p100, releasing the transcriptionally active p52-RelB heterodimer, which then translocates to the nucleus and initiates transcriptional changes. LT-Beta, lymphotoxin-Beta. Adopted from (Oeckinghaus et al., 2011).

However, in response to stimuli the IKB kinases (IKK) are activated, phosphorylating the IKB proteins which increases their ubiquitination and targets them for degradation (Oeckinghaus et al., 2011). P100 and p105 are also considered to be IKB proteins, the inhibitory domain of which is processed in response to stimuli to release the functional p52 and p50 TFs. The efficiency of p100 processing to p52 is dependent on p105 and p105 proteolysis is in part also dependent on p100 (Yılmaz et al., 2014). NFKB signalling is involved in disuse skeletal muscle atrophy independent of a local inflammatory stimulus or obvious cytokine activity (Hunter et al., 2002). Nuclear p50 as well as Bcl3 are both elevated in the muscle of unloaded limbs in mice, which results in a 10 fold increase in NfkB reporter activity (Hunter et al., 2002). This is independent of RelA and p52 which are both unchanged in the unloaded hindlimbs or RelB which decreases in unloaded muscle. P105 and Bcl3 knockout mice are both resistant to disuse-induced atrophy (Hunter and Kandarian, 2004). On the other hand, Ikka and RelB regulate of skeletal muscle metabolism, as knockouts of either gene have lower mitochondrial content and are less capable of oxidative respiration, increasing the glycolytic type IIb fibres (Bakkar et al., 2012). These changes are mediated via a RelB-dependent decrease in Pgc1-β levels, which in turn lead to a decrease in mitochondrial gene transcription and abnormal mitochondrial biogenesis.

2.2.4.4 *Mechanical input*

In the previous sections I mentioned examples of how muscle use affects glucose uptake and glycogen synthesis in an insulin-independent manner and how disuse has been reported to enhance Nfκb signalling without obvious involvement of inflammatory players. Such findings and others pose a question as to how a muscle communicates information about its use or disuse to the intracellular signalling pathways controlling glucose uptake, glycogen synthesis and Nfκb signalling. One possibility is the activity-dependent release of Ca^{2+}. With both denervation and disuse, neural input to the muscle is absent/reduced, thus the AP-dependent increase in cytosolic Ca^{2+} is suppressed, and so are all the subsequent Ca^{2+}-dependent signalling events. Although evidence for declined neuromuscular activation in space also exist, the application of more load (force) on the feet of astronauts has improved muscle wasting compared to unloaded astronauts (Layne et al., 1998). This indicates the importance of not only neural input in regulating intramuscular changes, but also mechanical input such as force. Another observation is that treadmill training of patients with spinal cord injury seems to enhance these patients' lower limb abilities despite the absence of supraspinal communication (Dietz et al., 1994), also arguing for a role of mechanical input in regulating neuromuscular

function. Such findings support the presence of intramuscular sensors of mechanical input. These are likely molecules that are responsive to force, undergoing some sort of conformational change that is of consequence on the muscle's signalling pathways (Hoshijima, 2006). One such candidate is the sarcomeric protein Titin, which contains many spring-like immnoglobulin (IgG) and fibronectin type III (FN3) domains important for regulating sarcomere stiffness (Linke and Hamdani, 2014) and serve as binding sites for proteins important in muscle growth (Linke, 2008). Towards titin's c-terminus is an autoinhibited serine/threonine kinase domain (frequently referred to as titin kinase) that is believed to be inhibited in resting muscle, but was shown to unfold its regulatory domain to expose the catalytic domain under physiological force ranges (Puchner et al., 2008). This makes it an ideal mechanosensor in muscle because it is inhibited during rest and activated in the presence of force. Despite its structural similarity to CaMKs, recent reports have indicated that this kinase is a pseudokinase more likely to serve as a binding hub for other proteins in response to stretch (Bogomolovas et al., 2014). One such protein is the muscle specific E3-ligase Murf1, which is known to bind M-band titin but not titin kinase itself (Centner et al., 2001). Murf1 binds titin at a site slightly more N-terminal than the titin kinase domain and was shown to bind significantly better in its presence (Bogomolovas et al., 2014). This links Titin kinase to protein turnover pathways, and suggests the possibility of other similar Titin kinase-dependent binding events at the M-band. Another Titin kinase-dependent interaction partner is Nbr1, which localizes at the M-band in a mechanically-inducible manner, recruiting the protein P62, which then binds another muscle-specific E3-ligase, Murf2. This event sequesters Murf2 from translocating to the nucleus and degrading its target serum response factor (SRF) a transcription factor that is then rendered inactive when the muscle is in use (Lange et al., 2005). A similar effect could be envisioned for Murf1, where mechanical contraction allows its binding to TK and prevents it from substrate ubiquitination. Indeed, Murf1's substrates include structural proteins such as Telethonin (Tcap), Nebulin, Troponin and Myosin light chain 2 as well as metabolic enzymes such as muscle creatine kinase, NADH dehydrogenase, pryuvate kinase, pyruvate dehydrogenase-β (PDHB) and the mitochondrial ATP synthase beta subunit (Centner et al., 2001). The consequence of such an interaction would thus be the preservation of these proteins from degradation to help maintain muscle structure and metabolic function. Nevertheless, these are only single examples that link titin kinase to intracellular effectors, but the functional effects of titin kinase on muscle have yet to be studied.

2.3 Hibernation and atrophy resistance

Despite the detrimental effect of caloric restriction, muscle disuse and denervation on muscle size in humans and mice, nature has presented us with models that are largely resistant to this phenomenon under similar conditions. Such exceptions are mammals that hibernate for prolonged periods every year, a period of caloric restriction and muscle disuse that is not accompanied by significant muscle loss. While smaller hibernators such as squirrels seem to go through extreme measures to reduce demand on skeletal muscle protein such as reducing core temperature to ~0 degrees for stretches at a time to suppress enzymatic function and metabolism, bigger hibernators such as the black and brown bears are capable of the same despite a mild decrease in body temperature (~ 6 degrees) (Carey et al., 2003). This makes them very interesting models for scientists and clinicians interested in understanding how to prevent atrophy in human patients (Bodine, 2013). For one thing, hibernating bears reduce whole body metabolism to decrease metabolic demand during this time. This is independent from the decrease in core body temperature reported during hibernation (Tøien et al., 2011). Also, bears compensate for the lack of ingested nutrients by accumulating large amounts of adipose tissue before hibernating. During hibernation their adipose tissue becomes insulin resistant alleviating insulin's inhibitory effect on lipolysis (Nelson et al., 2014). The result is an increase in circulating triglycerides and glycerol which serve as energy alternatives, reducing the demand on protein catabolism. They also efficiently reabsorb amino acids in their kidneys allowing their recycling into protein (Stenvinkel et al., 2013b). Part of these animals' ability to preserve muscle mass despite disuse was also attributed to regular neural stimulation of the muscle, which serves as a signal of muscle use. However, even denervated bear muscle is resistant to wasting during hibernation (Lin et al., 2012) suggesting that other intramuscular changes must be contributing to muscle preservation during this time, not just neural stimulation. Little is known about the intramuscular changes in hibernating bears besides findings that suggest that transcriptional changes that suppress metabolism, oxidative damage and enhance protein synthesis seem to be prevalent at this time (Fedorov et al., 2014).

2.4 Aim of the study

In this thesis I study how mechanical input affects muscle size and function, and how -despite its absence- hibernating grizzly bears are resistant to changes in muscle size. This thesis is thus split into two parts: the first is concerned with identifying intracellular mechanisms that protect grizzly bear (*Urus arctos*) skeletal muscle from atrophy during hibernation. With this project we hoped to identify novel mechanisms nature has adapted to fight muscle loss, and determine if they could be beneficial in reducing muscle loss in non-hibernating species. In the second part of this thesis I focus on understanding how Titin kinase affects intracellular signalling *in vivo*, shedding light on its previously unknown contributions to intracellular signalling on a cellular and organ level. With such knowledge we hope to better understand how exercise, and more generally muscle use, communicates to the muscle's intracellular machinery even in the absence of neural input. Such knowledge could help improve the treatment and quality of life of patients with debilitating neural injury such as paraplegics as well as of patients suffering from metabolic disorders such as diabetes mellitus, both of which have been shown to be responsive to increased skeletal muscle stimulation.

3 Material and methods

3.1 Material

3.1.1 Chemicals and kits

Chemicals were purchased from GE Healthcare, Invitrogen, Roth, or Sigma-Aldrich if not stated otherwise.

Table 1. Kits.

Kit	Manufacturer
Supersignal West Femto / Pico Chemiluminescent Substrate	Pierce Chemical Co.
Pierce BCA protein assay kit	Thermo
Bradford protein assay kit	Bio-Rad
PureLink™ Quick Plasmid Miniprep Kit	Invitrogen
PureLink™ HiPure Plasmid Filter Maxiprep Kit	Invitrogen
RNeasy Mini Kit	QIAGEN
QIAquick Gel Extraction Kit	QIAGEN
QIAquick PCR Purification Kit	QIAGEN
RiboMinus™ Transcriptome Isolation Kit (Human/Mouse)	Invitrogen
Illumina® Total™ Prep-96 mRNA amplification kit	Ambion
Quant-iT™ dsDNA HS Assay Kit	Invitrogen
Illumina® Genomic DNA single end sample prep kit	Illumina
Illumina® Genomic DNA paired end sample prep kit	Illumina
GS FLX Titanium General Library Preparation Kit	454 Life Sciences
XF Glycolysis Stress Test Kit	SeaHorse

3.1.2 Enzymes

Table 2. Enzymes.

Enzyme	Manufacturer
DNase I	QIAGEN
Nucleic acid Restriction enzymes	NEB
Taq DNA polymerase	Invitrogen
Trypsin, cell culture grade	Invitrogen
Immobilized Trypsin	Applied Biosystems
LysC	Wako
DNA restriction enzymes	NEB
T4-ligase	NEB

3.1.3 Oligonucleotides

Table 3. Primers for cloning.

Primer	Sequence (5'-3')
T7TKCD_Fwd	TTTTTGATATCACCAGGATGGCATCGATGACAGG
T7TKCD_Rev	AATCAAGGGTCCCCAAACTC

Fwd: Forward; Rev: Reverse

Table 4. Primers for genotyping.

Primer	Sequence (5'-3')
Neo_Fwd	AGAGGCTATTCGGCTATGACTG
Neo_Rev	AGCCATGATGGATACTTTCTCG
Puro_Fwd	CAAAGCATGCATCTCAATTAGTCAGCATGACCGAGTACAAGCCCA
Puro_Rev	CAGATTGTACTGAGAGTGCACCATACCAGGCACCGGGCTTGCGG

Fwd: Forward; Rev: Reverse

Table 5. Primers and probes for quantitative real-time PCR (qRT-PCR).

Gene	Sequence/Assay	Dye/Quencher	Company
Pdk4	Mm01166879_m1	FAM/MGB	LifeTechnologies
Serpinf1	Mm00441270_m1	FAM/MGB	LifeTechnologies
Actb	4352341E	VIC/MGB	LifeTechnologies
18S rRNA	4310893E	VIC/TAMRA	LifeTechnologies
IGF-1	Fwd: TGTCGTCTTCACACCTCTTCTACCT Rev: CCACACACGAACTGAAGAGCAT Probe: TCACCAGCTCCACCACAGCTGGAC	FAM/TAMRA	MWG

Fwd: Forward; Rev: Reverse

Table 6. Oligonucleotides for shRNAs.

Oligo	Sequence (phospho-5'-3')
shPDK4-693F	GATCAGACGCTATCATCTACTTAATCGAGTTTAAGTAGATGATAGCGTCTACTTTTTG
shPDK4-693R	TCGACAAAAAAGACGCTATCATCTACTTAAACTCGAGTTTAAGTAGATGATAGCGTCT
shSERPINF1-900F	GATCTCACCTTCCCGCTAGACTATCCTCGAGGATAGTCTAGCGGGAAGGTGATTTTTG
shSERPINF1-900R	TCGACAAAAATCACCTTCCCGCTAGACTATCCTCGAGGATAGTCTAGCGGGAAGGTGA

F: forward, R: reverse

Table 7 Plasmids.

Backbone	Company
pTET-OFF	CloneTech
pTRE2	CloneTech

3.1.4 Antibodies

Table 8. Primary antibodies used for Western blotting (WB).

Antibody	Species	Dilution	Manufacturer
Akt	Rabbit	1:1000	CST
pAkt (ser473)	Rabbit	1:1000	CST
Fhl2	Rabbit	1:200	Bethyl
Gsk3β	Rabbit	1:1000	Millipore
pGsk3β (ser9)	Rabbit	1:1000	Millipore
Hdac4	Rabbit	1:1000	CST
Hdac5	Rabbit	1:1000	Abcam
NfκB1	Rabbit	1:1000	Sigma
NfκB2	Rabbit	1:1000	CST
Pdk4	Rabbit	1:1000	Abcam
Pten	Rabbit	1:1000	CST
P62	Mouse	1:200	Abcam
Serpinf1	Rabbit	1:2000	Abcam
γ-Tubulin	Mouse	1:1000	Sigma
T7	Mouse	1:10,000	Novagene

Table 9. Secondary antibodies and fluorescent-labelled reagents used for Western blotting (WB).

Antibody	Species	Dilution WB	Manufacturer
Anti-rabbit IgG HRP-conjugated	Goat	1:1000	Sigma-Aldrich
Anti-mouse IgG HRP-conjugated	Goat	1:1000	CalBiochem

3.2 Methods

3.2.1 Cloning

3.2.1.1 *PCR amplification*

All PCR amplifications were done using a high fidelity Taq (Invitrogen), on a PeQstar 2x thermocycler (PeQlab) unless otherwise specified.

3.2.1.2 *Nucleic acid digestion*

All nucleic acids were digested with the specified restriction enzymes as follows unless otherwise specified:

Table 10. Test digestion mix.

Reagent	Amount
Restriction enzyme	0.5 µl
BSA	0.5 µl
DNA	Equivalent of <= 1 µg
NEB buffer (10x)	5 µl
ddH20	To 50 µl

Incubate at 37 °C for 1 h

3.2.1.3 *DNA ligation*

All ligation reactions were done as follows:

Table 11. DNA ligation mix.

Reagent	Amount
T4-Ligase	1 µl
Ligase buffer (10x)	2 µl
Vector	100 ng
Insert	5 x Vector (M)
ddH2O	To 20 µl

Incubate O.N. at 37 °C

3.2.1.4 *Bacterial transformation and plasmid amplification*

Chemically competent DH5alpha *E. coli* bacteria were used for the transformation of all the plasmids generated. 5 µl of the ligation was added to the DH5alpha competent cells and then incubated for 30 min on ice. The bacteria were then heat-shocked at 42 °C for 45 seconds and immediately transferred to ice for 2 minutes. 500 µl of super optimal broth with catabolite repression (SOC) medium was then added to the mixture and incubated at 37 °C for 1 hour

while shacking at 600 rpm. The mixture was then transferred to Luria Broth (LB) -agar plates containing either Ampicillin (Sigma; 100 µg/ml) or Kanamycin (Sigma; 50 µg/ml), and left to dry before incubation at 37 °C overnight. The next day clones were picked and incubated in 5 ml of liquid-LB medium with the corresponding antibiotic. Plasmid DNA was then isolated using a DNA miniprep kit (Qiagen) for subsequent use. For greater amounts of DNA, bacteria were they were cultured in 200 ml of liquid-LB and DNA isolation was done using Qiagen's Maxiprep kit as per the manufacturer's instructions.

SOC medium

2% tryptone (Roth), 0.5% yeast extract (BD Biosciences), 10 mM NaCl (Roth), 2.5 mM KCl (Roth), 10 mM MgCl2 (Roth), 10 mM MgSO4 (Roth), and 20 mM glucose (Roth).

LB-Agar

171. µM NaCl (Roth), 1% tryptone (BD Biosciences), 0.5% yeast extract (BD Biosciences), 1.5% agar (BD Biosciences).

Liquid LB

171.1 µM NaCl (Roth), 1% tryptone, 0.5% yeast extract (BD Biosciences).

3.2.1.5 *DNA plasmid quality control*

All plasmids generated were test digested to ensure the success of the ligation and subsequently sent for sequencing. Validated plasmids were then amplified and isolated using a maxi-prep kit (Invitrogen) as per the provider's instructions. DNA concentration was determined using a Nanodrop ND-1000.

3.2.1.6 *DNA agarose gel electrophoresis*

Unless specified otherwise, DNA molecules were resolved on a 0.8% UltraPure ™ agarose (Invitrogen) gel in 0.5x Tris-acetate-EDTA (TAE) buffer in the presence of Ethidium bromide to allow visualization upon ultra violet (UV) exposure. Gels were poured into a casting tray and left polymerize. Gels were then transferred to an electrophoresis chamber (Cosmo Bio Co) containing TAE, after which DNA samples were mixed with loading buffer at a ratio of 1:5 and loaded. Fragments were separated at 100 V for 20 minutes before visualization on a Gel Doc 2000 UV transilluminator (BioRad).

0.5 x TAE buffer

20 mM Tris-base, 0.05% acetic acid, 0.5 mM EDTA pH 8.0

Loading buffer

0.5% orange G, 50% glycerol, 25 mM EDTA pH 8.0

3.2.1.7 *pTetOff-TKCD plasmid:*

T7-tagged TKCD was PCR amplified from a pre-existing plasmid (pCGT7-TKCD) using T7TKCD_Fwd and T7TKCD_Rev primers. The following program was used for amplification on a PTC-225 thermal cycler (MJ research):

Table 12. PCR program for amplification of TKCD.

Temperature °C	Time (s)
95	5
Start loop	
95	20
50	30
72	90
End loop	
Repeat loop 30 x	
72	600
8	Hold

The amplification products were resolved on a 0.8% Agarose gel, after which they were extracted and kit purified from the agarose gel (Qiagen). They were then digested together with 1 µg of the pTRE2-puro plasmid (Clontech) with *EcoRV* and *BamHI* in NEB buffer 3.

The digest PCR product was then ligated into the digested pTRE2-puro plasmid at a molar ratio of 5:1.

3.2.1.8 *shRNA expression plasmids:*

The sequence of the shRNAs used were determined based on entries in the RNAi consortium database (https://www.broadinstitute.org/rnai/public). Constructs with the highest efficiency and least off-target effects were chosen and synthesized with a 5'-phosphate group and *BglII*/ *XhoI* restriction overhang on each of the forward and reverse oligos respectively.

Oligos were mixed as in table 13 after which they were incubated first at 95 °C for 1 minute then in a beaker of boiling water and left to cool in it overnight. This allows for their annealing to form the final double-stranded (ds) shRNA construct.

Table 13. ds-shRNA construct annealing mix.

Reagent	Volume
Fwd_shRNA oligo	Equivalent of 20 uM
Rev_shRNA oligo	Equivalent of 20 uM
NEB buffer 2 (10 x)	5 ul
ddH2O	To 50 ul

The ds-shRNA constructs were then ligated into pSUPER-Retro-puro (Oligoengine) that was digested with *XhoI* and *BglII* in NEB buffer 3.1. Minipreped plasmid DNA was then test digested with *XhoI* and *SacII* in NEB CutSmart buffer.

3.2.1.8.1 Genotyping C2C12-TetOFF/pTRE2-T7-TKCD stable cell lines

Cells were lysed in RIPA buffer after which 10 µl was used for genotyping. Cells were genotyped for the incorporation of the pTetOFF plasmid using primers for the Neomycin resistance gene (NeoR; Neo_Fwd/Rev primers) and for the pTRE2-T7-TKCD plasmid using primers for the Puromycin resistance gene (PuroR; Puro_Fwd/Rev primers) according to the following PCR program:

Table 14. PCR program for NeoR/PuroR amplification.

Temperature (°C)	Time (s)
95	5
Start loop	
95	20
50	30
72	90
End loop	
Repeat loop 34 x	
72	600
8	Hold

3.2.2 Cell culture

Cells were maintained and passaged in Dolbecco's Modified Eagle's Medium (DMEM; Gibco) supplemented with 10% fetal bovine serum (FBS; Invitrogen) and 5% of 1x penicillin and streptomycin (P/S) solution (Invitrogen). The aforementioned medium is referred to as growth medium throughout the following sections. For passaging, cells were washed in 1 x phosphate buffered saline (PBS; diluted from 10x PBS; Lonza) before they were trypsinized in 0.2% Trypsin solution (Invitrogen) for 5 minutes. Trypsinization was stopped by adding growth medium, after which the appropriate number of cells were seeded for passaging.

3.2.2.1 *DNA transfection*

DNA was transfected into cells using PEI40 (40 kD poly-(ethylene imine); Polysciences Europe GmbH) complexed with DNA at a ratio of 6 mg PEI40: 1 mg DNA. The total volume of DNA was always 10 µg and when two plasmid was transfected at a time, 5 µg of each was used.

3.2.2.2 *Generating Tet-OFF Titin kinase-expressing C2C12 cells*

C2C12 cells were grown to 80% confluence on a 10 cm dish before they were transfected with the pTet-OFF vector (CloneTech). 48 h post-transfection, medium was changed to G418-sulphate selection medium (600 µg/ml of growth medium) and maintained under selection until single clones remained (~10 days). Individual clones were picked and expanded independently. A single clone of those genotyped to be positive for the Neo-marker was selected and transfected with the pTRE2-T7-TKCD plasmid described above. Selection was done in Puromycin-dihydrochloride (50 µg/ml growth medium, Calbiochem). Dox induction was done using 5 µg/ml of Dox dissolved in DMSO (Sigma). Controls were treated with DMSO only.

3.2.2.3 *Generating shRNA-expressing C2C12 cells*

ShRNA constructs were transferred to C2C12 cells via viral infection to enhance the efficiency of DNA delivery, as C2C12 cells are relatively difficult to transfect at a high efficiency with PEI40. In this case, Phoenix cells were grown to ~ 80–90% confluency and 10 ml fresh growth was added before transfection. 30 µg plasmid DNA was mixed with 62.5 µl 2 M sterile CaCl2 (Roth) and the volume brought up to 500 µl with ddH2O. Using a pipette, air was bubbled continuously through 500 µl of 2X HEPES buffered saline to which the DNA-$CaCl_2$ mixture was added dropwise. The mixture was incubated for 5 min at room temperature and added dropwise to a 10 cm plate of Phoenix cells. To increase the transfection efficiency, 11 µl of 25 mM chloroquine (Sigma-Aldrich) was also added to the cells. 24 h after transfection, the

medium was changed to 6 ml fresh growth medium and 48 h post transfection 6 ml of virus-containing supernatant was collected and filtered through a 0.45 µm syringe filter before transferring onto a 50% confluent 10 cm dish of C2C12 cells. 16 µl of polybrene (Sigma-Aldrich; 4 mg/ml) was added to increase the infection efficiency. After removal of the viral supernatant, Phoenix cells were washed with 1X PBS before addition of 4 ml fresh growth medium. C2C12 cells were infected a second time 6 h later by transferring 4 ml of fresh viral solution to the previous round's. 24 h after the first infection, the viral solution was removed from C2C12 cells and two more infection steps were performed. C2C12 cells were thus infected a total number of four times to obtain a higher infection efficiency. The infected cells were subsequently selected with puromycin-dihydrochloride (50 µg/ml, Calbiochem) for one week before use and were subsequently kept under selection at all times.

3.2.2.4 *C2C12 cell differentiation*

C2C12 cells were grown to ~90% confluence in growth medium before switching to differentiation medium. Differentiation medium was similar to the normal growth medium except that the 10% FBS was replaced with 2% horse serum (HS; Sigma). Cells were kept in differentiation medium for at least 8 days, and the medium changed every 2 days in between.

3.2.2.5 *Insulin induction of C2C12 cells*

Cells were kept for 8-12 h in serum-free medium containing 0.2% sterile-filtered BSA. Induction was then done using 6 µg/ml of human Insulin (PAN biotech). Cells were then incubated for a minimum of 5 minutes and maximum of 30 minutes, after which cells were washed in PBS and immediately lysed in RIPA buffer on ice.

3.2.2.6 *Dexamethasone treatment of C2C12 cells*

Differentiated C2C12 cells were treated with 10 µM dexamethasone-acetate (Sigma) in DMSO (Sigma) in 2% HS medium for 2 days. Controls were treated with DMSO only.

3.2.2.7 *Non-essential amino acid supplementation of C2C12 cells*

Differentiated C2C12 cells were treated with 10 x non-essential amino acid (NE-AA) solution (Gibco) in 2% HS medium for 2 days and compared to non-treated cells.

3.2.2.8 *Secreted protein preparation and Igf-1 quantification*

C2C12 cells were seeded on 15 cm dishes in 25 ml of growth medium until they reached 80% confluence. Medium was then changed to 0.2% BSA-containing DMEM and cells were incubated in it for 8-12 hours before 10 ml of the medium was transferred to 15 ml Falcon

tubes. The supernatant was spun down once at 200 rpm to pellet debris, then the debris-free supernatant was transferred to a fresh Falcon and snap frozen in liquid nitrogen. The supernatant was later concentrated on a 3 kD, 15 ml Amicon centrifugatl filter for protein concentration as per the manufacturer's instructions. The concentrated protein was then used to measure the amount of secreted Igf-1 using an ELISA kit (Peprotech) as per the manufacturer's instructions.

3.2.2.9 *Metabolic function measurement in C2C12 cells*

C2C12 cells were seeded at a density of 70,000 cells/well on a 24-well XF^{e}24 cell culture micro plate (SeaHorse) one day before they were analysed on a XF^{e}24 analyzer (SeaHorse). The following day the cells were processed as per the manufacturer's instructions for the measurement of metabolic function using the XF Glycolysis stress Test Kit (SeaHorse). Data was analysed using the provider's software and Excel (Microsoft).

3.2.2.10 *Cell size quantification*

Myotube quantification was adapted from a method described previously (Sandri et al., 2004). In short, at least 20 random bright field images were taken at 20 x magnification and subsequently imported into and analyzed in ImageJ by measuring the thickness of the widest area across myotubes of similar morphology. In each group 20±5 cells were used for quantification.

3.2.3 Animal procedures

3.2.3.1 *Grizzly bear samples*

(Conducted by Dr. L. Olson, Washington State University, USA)

Four grizzly bears were used for this study: an adult, a subadult and 2 cubs. All animals were housed at the Washington State University Bear Research, Education and Conservation Center. The animals were maintained according to the Bear Care and Colony Health Standard Operating Procedures approved by the Washington State Institutional Animal Care and Use Committee (IACUC) based on the US National Institutes of Health guidelines. Hibernation began the first week of November when feeding ceased, and ended the second week of March when feeding resumed. Water was available ad libitum, and straw was provided for bedding during hibernation. Bears hibernated in pairs in unheated pens (3 x 3 x 2.5 m^3) with continuous access through a small door to an outdoor area (3 x 5 x 5 m^3). Because the dens were open to the outside, the bears experienced daily light and temperature fluctuations. The dens and runs

were monitored with surveillance cameras (Silent Witness) which confirmed that bears were recumbent for 98% of the hibernation period. The bears were anesthetized with tiletamine HCl and zolazepam HCl (5 mg/kg during the active phase and 2 mg/kg during hibernation) administered intramuscularly by air dart. Isoflurane in 100% oxygen was administered via endotracheal tube to maintain a constant plane of anaesthesia for muscle biopsies. The bears were judged to be in an adequate plane of anaesthesia based on lack of response to the mild stimulus caused by instrumentation, lack of jaw tone and lack of a palpebral reflex. The lateral surface of the leg over the gastrocnemius muscle was shaved, prepped and a sterile field was maintained. An incision (~4 cm in length) was made over the gastrocnemius muscle to excise small biopsies (approximately 1 x 1 x 2 cm^3). The biopsies were immediately frozen in liquid nitrogen and subsequently stored at –80 °C until analysed.

3.2.3.2 *Mouse samples*

(Conducted by Dr. M. Radke, Max Delbrück Centre, Berlin, Germany)

3.2.3.2.1 Sciatic nerve lesion

Denervation was performed as described in (Moresi et al., 2010). In brief, adult mice were anesthetized with isoflurane. The sciatic nerve of the left leg was exposed and a 2 mm piece was removed. The right leg remained innervated and was used as a control. Mice were sacrificed and the gastrocnemius muscle dissected and quickly frozen in liquid nitrogen 2 and 14 days after denervation.

3.2.3.2.2 Endurance running test

Adult male mice were trained on a custom-built running belt for 30 days, 5 days a week at a speed of 23 cm/s. In the 1st week animals were trained for 20 min, in the 2nd week the training time was increased by 5 min per day up to 45 min. Animal tissues were harvested one day after the last exercise.

3.2.4 mRNA expression

3.2.4.1 *RNA extraction and cDNA synthesis for qRT-PCR:*

C2C12 cells were washed twice in PBS after which 300 µl of RTL buffer (Qiagen) was added, followed by subsequent extraction using an RNeasy mini kit (Qiagen). RNA was subsequently quantified on a NanoDrop ND-1000 (Thermo-Scientific). 0.7-1 µg of RNA was equally used for all the samples in one run and reverse transcribed into cDNA using a high capacity RNA-to-cDNA kit (Applied Biosystems) as follows:

Table 15. RNA to cDNA reverse transcription mixture.

Reagent	Volume (µl)
RNA	Equivalent of 1 µg
RT buffer	10
RT enzyme	1
RNAse-free water	To 20

The above mixture was then incubated on a PeQSTAR 2x thermocycler (PeQlab) with the following program:

Table 16 Thermocycler program for RNA reverse transcription.

Temperature (°C)	Time (min)
37	60
95	5
8	Hold

3.2.4.2 *qRT-PCR*

All qRT-PCR assays were run using the TaqMan technology from Applied Biosciences on an ABI-7900 HT. Each biological replicate was pipetted in triplicates and assays were performed using the TaqMan® gene expression master mix (Applied Biosystems) as follows unless stated otherwise:

Table 17. TaqMan gene expression master mix for qRT-PCR.

Reagent	Volume (µl)
cDNA (7-10 ng)	1
TaqMan gene expression master mix	5
Endogenous control	0.5
Gene expression assay (Primer/probe pairs)	0.5
Nuclease-free water (Ambion)	3

3.2.4.3 *C2C12 expression profiling using microarrays*

RNA was extracted from C2C12 cells as mentioned above and three biological triplicates for each condition were pooled. The RNA quality was evaluated on a 2100 Bioanalyzer (Agilent). To reduce ribosomal RNA (rRNA) we used the RiboMinus Kit (Invitrogen). Biotinylated

cRNA was prepared using the Illumina® TotalPrep™-96 RNA Amplification Kit (Ambion) according to the manufacturer's directions starting with ~100 ng total RNA. Expression profiling was performed using Illumina's MouseRef-8 v2.0 Expression Bead chip.

3.2.4.4 *Grizzly bear expression profiling using RNAseq*

(AG Chen, Max Delbrück Centre, Berlin, Germany)

3.2.4.4.1 Full-length enriched cDNA library construction and normalization

The construction of normalized full-length-enriched cDNA libraries for 454 sequencing requires three steps: (1) the synthesis of double stranded cDNA using a modified RACE technique, (2) the subsequent removal of poly(A):T tails using the methylation sensitive type II restriction enzyme *GsuI*, followed by the ligation of a new DNA adaptor, and (3) the normalization of the resulting cDNA library using duplex-specific nuclease (DSN) (Shagin et al., 2002; Zhulidov et al., 2004).

3.2.4.4.2 454 FLX titanium sequencing

The normalized cDNA library was quantified using the Quant-iT dsDNA HS Assay Kit (Invitrogen). A total of 5 mg was used to prepare the sequencing library with the 454 GS FLX Titanium General Library Preparation Kit according to the manufacturer's manual. The 454 library was then sequenced 200 cycles on a 454 GS FLX sequencer according to the manufacturer's manuals.

3.2.4.4.3 Single-end cDNA sequencing using Illumina GAIIX

5 µg of full-length cDNA was used to construct a single-end sequencing library using the Illumina Genomic DNA Single End Sample Prep kit according the manufacturer's manuals. The DNA concentration was measured with a Nanodrop 7500 spectrophotometer, and a 1-mL aliquot was diluted to 10 nM. Adaptor-ligated DNA was hybridized to the surface of flow cells, and DNA clusters were generated using the Illumina cluster station, followed by 50 cycles of sequencing on the GAIIX, in accordance with the manufacturer's protocols.

3.2.4.4.4 Paired-end RNA-Seq using Illumina GAIIX

A total of 300 ng of poly(A) RNA was fragmented at 94 °C for 3.5 min using 5 x fragmentation buffer (200 mM Tris-Acetate at pH 8.1, 500 mM KOAc, 150 mM MgOA) in a total volume of 20 ml. The fragmented RNA was precipitated and converted to first-strand cDNA using Supescript II (Invitrogen), followed by second-strand cDNA synthesis with *E.coli* DNA pol I (Invitrogen) and RNase H (Invitrogen). Then the paired-end sequencing library was prepared

using the Illumina Genomic DNA Paired End Sample Prep kit according the manufacturer's manuals. The DNA concentration was measured with a Nanodrop 7500 spectrophotometer, and a 1-mL aliquot was diluted to 10 nM. Adaptor-ligated DNA was hybridized to the surface of flow cells, and DNA clusters were generated using the Illumina/ Illumina cluster station, followed by 2 x 76 cycles of sequencing on the GAIIX, in accordance with the manufacturer's protocols.

5 x fragmentation buffer

200 mM Tris-Acetate at pH 8.1, 500 mM KOAc, 150 mM MgOA.

3.2.4.4.5 De novo transcriptome assembly

The 454 reads were assembled using Newbler 2.3 (Roche) with default parameters. The Illumina assembly comprised of Illumina paired-end reads was obtained by using the SOAPdenovo software (Li et al., 2010) (http://soap.genomics.org.cn) with default parameters. Contigs longer than 100 bp in the Illumina assembly were combined together with 454 reads for the final assembly using Newbler with default parameters.

3.2.4.4.6 Transcriptome annotation

Out of 43599 transcripts, 22641 were aligned to the human protein database (Ensembl version 66) using BLAST with e-value ≤ 1E-10, corresponding to 9768 human proteins.

3.2.4.4.7 Differential transcript expression

Single-end Illumina reads were aligned to transcripts using SOAP2 allowing at most 2 mismatches to estimate the expression of each transcript. Transcripts corresponding to a total of 4783 genes were aligned. NOISeq (Tarazona et al., 2011) was then used to estimate the likelihood of differential expression (probability > 0.8 considered differential).

3.2.4.5 *Mouse RNA preparation for microarray-based expression profiling*

(Dr. M. Radke and AG Huebner, Max Delbrück Centre, Berlin, Germany)

Skeletal muscle and cardiac left ventricular tissue was homogenized with a homogenizer in the presence of TRIzol (Invitrogen), extracted with chloroform, precipitated in ethanol, and dissolved in nuclease-free water. After quality control (2100 Bioanalyzer, Agilent) and DNAse digestion, RNA was purified using Rneasy columns (Qiagen) and stored at –80°C. To reduce ribosomal RNA (rRNA) we used the RiboMinus Kit from Invitrogen. Biotinylated skeletal

muscle cRNA was prepared using the Illumina® TotalPrep™-96 RNA Amplification Kit (Ambion) according to the manufacturer's directions starting with ~100 ng total RNA. Expression profiling was performed using Illumina's MouseRef-8 v2.0 Expression Bead chip. Cardiac biotinylated cRNA was prepared from 10 µg total RNA using the SuperScript Choice System from Invitrogen and the Affymetrix T7-(dT)24 primer, which contains a T7 RNA polymerase promoter attached to a poly-dT sequence. Following a phenol/chloroform extraction and ethanol precipitation, the cDNA was transcribed into biotin-labelled cRNA using the Retic Lysate IVT™ kit (Ambion). cRNA products were then purified using an RNeasy kit (Qiagen) and fragmented to an average size of 30-50 bases according to Affymetrix recommendations. 15 µg of the fragmented cRNA was used to hybridize the Mouse Genome 430 2.0 Array for 16 h at 45°C.

3.2.4.6 *Analysis of gene expression profiling data*

Illumina chips were quantile normalized without background subtraction in Genome Studio's Gene Expression module version 1.9.0. Genes with an expression p-value of less than 0.05 in all samples were retained for subsequent analysis, while all others were discarded. Affymetrix chips were analyzed using AltAnalyze v.2.0.6 (Emig et al., 2010) with default parameters making further processing unnecessary.

3.2.4.6.1 Denervation data

8 samples were used for comparison in the analysis: GA muscle after 2 and 14 days and the contralateral innervated leg for each animal. Samples were available for three WTs and KOs in each group. For each gene the average value in the control leg was calculated, and used to normalize the value of the gene in the corresponding denervated leg. This reduces the complexity of the data from 8 to 4 triplicates. The effect of denervation and genotype were then determined based on a Two-way Analysis of Variance analysis (TWA).

3.2.4.6.2 Trained animal data

The expression values of each gene in the three trained WT and KO samples were normalized to the average value in the three untrained animals of the same genotype. A t-test was done to compare genes that were regulated between the trained KOs and WTs.

3.2.4.6.3 C2C12 data

Since the returned values per gene in this experiment was already an average of three pooled biological replicates of TK-expressing and TK-null cells, a t-test was not appropriate. Instead, the fold change in gene expression values for each gene was calculated and found to follow

normal distribution. With the assumption that in the presence of TK only a small subset of genes will be regulated on the transcriptional level, we considered the majority of genes unchanged, and only those with a fold change that falls beyond 2 standard deviations from the mean of all genes were considered to be differentially regulated between the two samples.

3.2.4.6.4 Pre-existing transcriptomic datasets

For comparison to our own data more models of muscle atrophy were allocated on the GEO database. Five GEO datasets were selected for this purpose: GSE674 -Aging, HS (Welle et al., 2003), GSE8872 -Ankle fracture, HS (Chen et al., 2000), GSE21496 - Unloading, HS (Reich et al., 2010), GSE25908 - Casting, MM (Bialek et al., 2011) and GSE24504 - Fasting, MM (Hakvoort et al., 2011). Since dataset GSE24504 lacked the associated CEL files, for consistency, all datasets were analysed using GEO2R for differential gene expression. GSE674 gene expression levels from young women aged between 20-29 years (n = 7) were compared to those aged 65-71 years (n = 8). Genes were considered differentially expressed at p-value < 0.01. As for GSE8872, the immobilized (casted) legs from ankle fracture patients were compared to the contralateral leg as controls (n = 4). Significance was considered at p-value < 0.01. In case of GSE21496 the 48 h unloading samples were normalized to the 0 h unloading samples as controls (n = 7). Significance was considered at p-value < 0.01. For GSE25908, the 14-day casted legs (right) were compared to the left control legs from the same mouse (n = 9). Genes were considered significantly regulated if the Benjamini-Hochberg-corrected p-value (p. adj) was < 0.05. Finally, for GSE24504, muscle samples after 72 h of fasting were compared to the controls at 0 h (n = 5). Significance was considered at p. adj < 0.05.

3.2.5 Meta-analysis of global gene expression during atrophy

To help identify genes that play a role in muscle atrophy across the different species under different atrophy-inducing conditions, a meta-analysis with a total of seven datasets was conducted. All data sets were compared using their Official Gene Symbols. Since the data come from different platforms (RNA-seq, Illumina and Affymetrix), comparing the FCs across the datasets could be misleading and contributes little information to our purpose. Thus directionality of regulation was only considered and FCs were discretized as follows:

$$\text{if} \begin{cases} FC < 1,\ FCd = -1 \\ FC > 1,\ FCd = 1 \\ not\ significantly\ regulated,\ FCd = 0 \end{cases}$$

where FC is the ratio of mRNA in the treated group normalized to the control and FCd is the discretized FC. Only genes that were identified in RNA-seq and spotted on the chips were included in the analysis. Genes were then grouped as follows: Regulated in hibernation only if the gene is regulated only during hibernation and none of the other datasets; regulated during hibernation and other conditions if the gene is regulated during hibernation and at least half of the other datasets; not regulated in hibernation but in other atrophy-conditions if the gene is not changed during hibernation but regulated in at least half of the other datasets.

3.2.6 Guilt-by-association functional inference

Co-expressed genes were determined using the software GeneFriends (van Dam et al., 2015), which queries a vast set of RNAseq datasets for genes that are often coexpressed (either increased or decreased) with the input gene list. Genes increased or decreased during hibernation only were used as input gene lists for the algorithm. The resulting list of co-expressed genes were filtered for a p-value ≤ 0.01, then only the genes that were associated with ≥ 5 genes in the input lists were considered and utilized for functional annotation using a KEGG pathway enrichment analysis.

3.2.7 KEGG pathway enrichment analysis

All analyses were done using the CLUEGO plugin in Cytoscape (Bindea et al., 2009; Shannon et al., 2003). Kappa-score threshold was always set to 0.3, min. % genes to 0 and min. number of genes to 2. P-values were Benjamini-Hochberg corrected for multiple testing and denoted (p-adj.).

3.2.8 Transcription factor binding site (TFBS) enrichment analysis

This analysis was done to determine the TFBSs that are enriched in the promoter region of the genes regulated two and 14 days post-denervation. Based on the results of the TWA described above, genes regulated based on genotype were further filtered for those regulated at each of 2 and 14 days post-denervation between WT and KO samples. The regulated genes ($p<0.05$) were then used as an input set for the web-based application DAVID (Huang et al., 2008). As background we used the whole array of genes spotted on the chip. Functional annotation using only protein_interactions > UCSC_TFBS as a term was performed to return information about the TFBSs enriched and the genes downstream of them. TFBSs were considered enriched if assigned a Benjamini-Hochberg-adjusted p-value of <0.05.

3.2.9 Protein expression

3.2.9.1 *C2C12 protein lysate preparation for western blotting*

C2C12 cells were lysed in RIPA buffer containing PhosStop phosphatase inhibitor (Roche) and Complete EDTA-free protease inhibitor (Roche), then treated with Benzonase (Sigma) to digest DNA and facilitate pipetting. Samples were then incubated on an elliptical rotor at 4 °C for 1 h before subsequent use. Protein lysate was subsequently quantified using a BCA assay kit (Thermo). In preparation for immunoblotting, samples were mixed in 4 x Laemmli buffer and boiled for 5 minutes before use.

RIPA buffer

150 mM NaCl, 1 % NP-40, 0.5% sodium deoxycholate, 0.1% SDS, 50 mM Tris (pH 8.0)

4x Laemmli buffer

277.8 mM Tris-HCl, pH 6.8, 4.4% LDS, 44.4% (w/v) glycerol, 0.02% bromophenol blue; 355 mM β-mercaptoethanol.

3.2.9.2 *Polyacrylamide-gel electrophoresis*

Stacking gel was always poured at a 5% polyacrylamide percentage while the resolving polyacrylamide gels of between 15-10% were used, depending on the size of protein of interest. Gels were assembled and run in a Quatro mini-protean electrophoresis cell (BioRad) with 1x running buffer. Equal amounts of 50-100 µg of protein were loaded per sample together with 7 µl of PageRuler™ Prestained Protein Ladder (Fermentas). After proteins were appropriately resolved, the were transferred to a nitrocellulose membrane (Amersham) in a mini-trans blot cell (BioRad) at 200 V for 2 h. Successful protein transfer was determined by staining the membrane in Panceau S after which membranes were subsequently destained in TBS-T. Blocking was done in 5% BSA (in PBS) and membranes were incubated with the respective 1ry antibody (Ab) overnight at 4 °C. Membranes were washed in TBS-T before incubation with the Horse radish peroxidase (HRP)-conjugated 2ry Ab for 2 hours at RT. Membranes were then washed in TBS-T and developed using supersensitive HRP substrate solution (Pierce) and signal was detected and documented using the FUSION-FX7 chemiluminescence detection system (PeQlab).

TBS

50 mM Tris-HCl, 150 mM NaCl, pH 7.4

TBS-T

TBS, 0.1% Tween 20, pH 7.4

3.2.9.3 *Densitometry for relative protein quantification*

Band intensity on the images of the exposed membranes was quantified in ImageJ. The intensity of the protein of interest was always compared to that of γ-tubulin as a loading control across samples.

3.2.9.4 *Total murine protein sample analysis by mass spectrometry*

(Dr. M. Radke and AG Kempa, Max Delbrück Centre, Berlin, Germany)

3.2.9.4.1 Sample preparation for LC-MS/MS

An *in vivo* SILAC-approach was used for protein quantification by mass spectrometry. Muscle samples dissected from age-matched WT and KO mice were immediately frozen in liquid nitrogen then ground using a cooled mortar and pestle. As reference, the muscle of a 129-female mouse fed with heavy ^{13}C6-Lysine was used. Labelling efficiency in this mouse was above 96% as previously determined by LC-MS/MS. 5 mg of sample was re-suspended in urea buffer and sonicated for 30 seconds with 2 pulses at 60% power (Sonoplus HD2070). After centrifugation to remove debris, protein concentration was measured by a Bradford colorimetric assay and 50 µg of protein was mixed with an equal amount of reference heavy sample. The disulfide bridges of proteins were then reduced in 2 mM DTT for 30 minutes at 25 °C and successively free cysteines alkylated in 11 mM iodoacetamide for 20 minutes at room temperature in the dark. LysC digestion was then performed by adding 2 µg of LysC (Wako) to the sample and incubating it for 18 hours under gentle shaking at 30 °C. The samples were then diluted three times with 50 mM ammonium bicarbonate solution, 7 µl of immobilized trypsin (Applied Biosystems) were added and samples were incubated 4 hours under rotation at 30 °C. 18 µg of the resulting peptide mixtures were desalted on STAGE Tips (Rappsilber et al., 2003) and the eluates dried and reconstituted to 20 µl of 0.5 % acetic acid in water.

Urea buffer

8 M Urea, 100 mM TrisHCl, pH 8.25

3.2.9.4.2 LC-MS/MS analysis

5 µl were injected in duplicate on a UPLC system (Eksigent), using a 240 minutes gradient ranging from 5% to 45% of solvent B (80% acetonitrile, 0.1 % formic acid; solvent A= 5%

acetonitrile, 0.1% formic acid). For the chromatographic separation a 30 cm long capillary (75 µm inner diameter) was packed with 1.8 µm C18 beads (Reprosil-AQ, Dr. Maisch). On one end of the capillary, nanospray tip was generated using a laser puller allowing fretless packing. The nanospray source was operated with a spray voltage of 2.0 kV and an ion transfer tube temperature of 260 °C. Data were acquired in data-dependent mode, with one survey MS scan in the Orbitrap mass analyzer (60000 resolution at 400 m\z) followed by up to 20 MS\MS scans in the ion trap on the most intense ions. Once selected for fragmentation, ions were excluded from further selection for 45 seconds, in order to increase new sequencing events.

Solvent B

80% acetonitrile, 0.1 % formic acid

Solvent A

5% acetonitrile, 0.1% formic acid

3.2.9.4.3 Data analysis

(Supported by AG Kempa)

Raw data were analysed using the MaxQuant proteomics pipeline v1.2.2.5 and the built-in Andromeda search engine (Cox and Mann, 2008; Cox et al., 2011) with the International Protein Index Human (version 3.71) database. Carbamidomethylation of cysteines was chosen as fixed modification, oxidation of methionine and acetylation of N-terminus were chosen as variable modifications. 2 missed cleavage site were allowed and peptide tolerance was set to 7 ppm. The search engine peptide assignments were filtered at 1% FDR at both the peptide and protein level. The ‘match between runs’ feature was enabled, ‘second peptide’ feature was enabled, while other parameters were left as default.

The analysis was followed up by normalizing H/L ratio to the sum of the areas under all peaks per animal after correction for errors in sample mixing with the light and heavy label. Proteins with peptides counted less than three times in any of the animals were then emitted. A two-sided Grubbs test was performed for each identified protein within a group to eliminate outliers ($p<0.05$) This was followed by a two-tailed, unpaired t-test to determine significant differences in protein levels between the wild type and titin kinase-deficient muscle.

3.2.9.5 *Phospho-murine protein sample analysis by mass spectrometry*

(Dr. K. Raddatz, University of Greifswald, Greifswald, Germany)

3.2.9.5.1 Preparation of samples for proteome and phosphoproteome profiling

Hearts from titin kinase KO and control mice were dissected washed in ice cold isotonic NaCl solution and snap frozen in liquid nitrogen. Heart tissue was then grinded with liquid nitrogen and suspended in lysis buffer (8 M urea, 10 mM sodium fluoride, 2.5 mM sodium pyrophosphate, 1 mM β-glycerol phosphate, 1 mM sodium orthovanadate, 1 mM tris (2-carboxyethyl) phosphine (TCEP), 1 mM EDTA, and 20 mM HEPES, pH 8.0). The tissue suspension was sonicated and free protein thiols were alkylated by addition of iodoacetamide to a final concentration of 5 mM followed by incubation for 20 min at room temperature. Lysates were clarified by centrifugation (8,700 x g, 15 min) and protein content was quantified using a Bradford assay (Bio-Rad). Peptides were obtained by in-gel digestion using trypsin (Promega). For enrichment of phosphopeptides, 5 mg of protein mixtures were diluted eightfold with 20 mM HEPES, pH 8.0 and digested with trypsin using a protein-enzyme ratio of 20:1. Obtained peptides were purified using C18 Sep-Pak cartridges (Waters) and freeze-dried. Peptides destined for TiO_2-based enrichment were dissolved in buffer A (5 mM KH_2PO_4, 30% (v/v) acetonitrile, pH 2.7) and separated in 15 fractions by strong ion exchange chromatography (SCX) with a Resource S SCX column (1 ml column volume, GE) connected to an Äkta Avant chromatography system (GE) using a binary linear gradient with buffer B (5 mM KH_2PO_4, 350 mM KCl, 30% (v/v) acetonitrile, pH 2.7) at a flow rate of 1 ml/min. Fractions were lyophilized, dissolved in 14 ml TiO_2-binding buffer (73% (v/v) acetonitrile, 10% (v/v) lactic acid, 2% (v/v) TFA) and 100 µl from a TiO_2-stock solution (30 mg / ml Titansphere TiO_2 bulk material (GL sciences) in 100% acetonitrile) was added, followed by incubation for 20 min at room temperature. Samples were centrifuged, beads were washed four times with 80% (v/v) acetonitrile, 2% (v/v) TFA and phosphopeptides were sequentially eluted with 5% (v/v) NH4OH and 30% (v/v) acetonitrile. For LC-MS/MS phosphopeptides were vacuum-dried and resuspended in 1% formic acid, 0.1% HFBA and 7.5% acetonitrile.

Lysis buffer

8 M urea, 10 mM sodium fluoride, 2.5 mM sodium pyrophosphate, 1 mM β-glycerol phosphate, 1 mM sodium orthovanadate, 1 mM tris (2-carboxyethyl) phosphine (TCEP), 1 mM EDTA, and 20 mM HEPES, pH 8.0

Buffer A

5 mM KH_2PO_4, 30% (v/v) acetonitrile, pH 2.7

Buffer B

5 mM KH2PO4, 350 mM KCl, 30% (v/v) acetonitrile, pH 2.7

TiO2-binding buffer

73% (v/v) acetonitrile, 10% (v/v) lactic acid, 2% (v/v) TFA

TiO2-stock solution

30 mg / ml Titansphere TiO_2 bulk material (GL sciences) in 100% acetonitrile

3.2.9.5.2 Mass spectrometry and spectra analysis

LC-MS/MS analyses were performed using an EASY-nLCII nanoflow HPLC system coupled directly to an LTQ Orbitrap Velos hybrid mass spectrometer (Thermo Fisher Scientific). Peptide samples were dissolved in 20 µl 5% (v/v) acetonitrile, 0.1% (v/v) acetic acid and loaded onto a 20 cm-long self-packed C18 (Aeris Peptide 3.6 µm, pore size 100 Å; Phenomenex) analytical column. Gradual elution of peptides was achieved by running a binary linear gradient from 1% (v/v) acetonitrile/0.1% (v/v) acetic acid to 75% (v/v) acetonitrile / 0.1% (v/v) acetic acid over a period of 46 minutes with a flow rate of 300 nl/min. The MS was operated in data-dependent mode, automatically switching between full survey scan (m/z 300–1700) with a resolution of 30,000 followed by fragmentation analyses of the top). 20 precursors with a charge state greater than one. Fragmentation by CID was performed in the linear ion trap with an AGC target value of 5×10^4 ions and normalized collision energy of 35%. Precursors were dynamically excluded for repeated fragmentation for 30 s for the CID method.

The raw data files were processed using MaxQuant (version 1.2.2.5) with the integrated Andromeda search engine against the reviewed mouse proteome deposited in UniProtKB (Swiss-Prot database, 2011-08-15; 16,384 sequences). Trypsin was specified as enzyme and a total number of 2 missed cleavages were allowed. Carbamidomethylation of cysteine residues was set as fixed modification. Oxidation of methionine, amino-terminal acetylation and phosphorylation of serine, threonine and tyrosine were selected as variable modifications. The ‘requantify’ and ‘match between runs’ options were enabled. For peptide, protein or site-specific identifications a FDR cut-off of 0.01 was applied.

3.2.9.6 *Grizzly bear protein quantification by mass spectrometry*

(AG Völker, University of Greifswald, Greifswald, Germany)

3.2.9.6.1 Protein sample preparation of LC-MS

Tissue samples were frozen in liquid nitrogen and disrupted using a bead mill as described earlier (Hammer et al., 2011) with slight modifications. The powder resulting from the bead mill treatment was dissolved in an appropriate volume of sample buffer (8 M urea; 2 M thiourea) and sonicated three times for three seconds on ice (Sonoplus HD 2200). After removal of insoluble cell debris by centrifugation (15,300 rpm; 1 h; 4 °C) the supernatant, containing the soluble cytosolic proteins, was transferred and used for further analysis. Protein concentrations were determined by Bradford assay (BioRad).

Sample buffer

8 M urea; 2 M thiourea

3.2.9.6.2 Peptide Sample Preparation

Two times 4 µg of each protein sample were prepared for tryptic digestion as technical duplicates. Thus duplicates were diluted with 20 mM ammonium bicarbonate (ABC) to obtain a final concentration of less than 1 M urea, after which they were reduced using 2.5 mM DTT (1 h; 60 °C) and alkylated by 10 mM iodoacetamide (30 min; 37 °C). Tryptic digestion (1:50) was performed overnight at 37 °C. The digestion was stopped in 1% acetic acid. The peptide mixtures were desalted using C-18 reverse phase material (ZipTip µ-C18 Millipore Corporation).

3.2.9.6.3 Mass spectrometry FTICR Analysis

The resulting peptide mixtures were separated using nanoAcquity UPLC reverse phase column (BEH130, C18, 100 µm - 100 mm) on a nanoAcquity UPLC system (both Waters, Waters Corporation) as previously described in (Hammer et al., 2011). MS data were generated using a LTQ-FT mass spectrometer (Thermo Electron). For each sample two technical replicates were measured.

3.2.9.6.4 Quantitative Analysis and Protein identification

(With assistance from AG Völker)

The raw data from the LC-ESI-MS/MS measurement were imported into the Rosetta Elucidator software version 3.3 (Ceiba Solutions) and processed as described in (Thiele et al., 2012) with

slight modifications. The following workflow was used: (i) feature detection; (ii) feature alignment across all 16 MS runs; (iii) feature identification via SEQUEST database search (via Sorcerer build 4.04, Sage-N Research Inc.) against a forward reverse database containing human entries obtained from Uniprot; (iv) feature annotation based on protein teller score (> 0.95), (v) median normalization using the annotated features, (vi) Filtering for unique peptides. The obtained feature intensities were averaged for each sample, summed up to peptide and protein intensities. These steps were carried in a visual script within the software Elucidator. The obtained protein intensities were exported to Excel for further analysis.

3.2.9.6.5 Differential protein expression

Differential protein expression was determined based on results of a two-way ANOVA taking age and activity state as factors. Proteins significantly regulated based on activity were used for all further analyses (p-value < 0.05).

3.2.9.6.6 Non-essential amino acid (NEAA) distribution in regulated proteins

Since the majority of the identified peptides in *U. arctos* were based on their homology to peptides in the *H. sapiens* database the amino acid composition for each protein regulated during hibernation was determined based on the corresponding reference human protein sequence (UniProt). The percentage of all NEAA and only those regulated were determined as a percentage of the total number of AAs per protein.

3.2.10 Metabolic modelling

Condition specific models were constructed from Recon2 as a reference model since not much is known about grizzly bear metabolism and how it deviates from metabolism in other mammals, while Recon2 is the most exhaustive reconstruction of a mammalian system to date (Thiele et al., 2013). Also most proteins were identified based on their homology to human counterparts impeding the identification of any bear-specific metabolic enzymes, even if they existed. The GIMME algorithm (Becker and Palsson, 2008) within the *createTissueSpecificModel* function in the COBRA toolbox (Schellenberger et al., 2011) was used with the biomass reaction as the objective function. Expression data was provided as 0/1 based on relative changes in expression levels between the 2 conditions compared. If a protein/mRNA species was increased in one condition compared to the other it was assigned a value of 1 for that condition and 0 for the other, while a value of 1 was assigned for all species expressed but unchanged between the conditions.

When creating the hibernation and activity-dependent models for *U. arctos* the expression data was provided based on changes in protein levels, while in case of the aging models of *H. sapiens* muscle mRNA levels were used.

All computations were done locally on a 64-bit machine and optimization was done using a CPLEX solver (version 7, Tomlab) in MATLAB.

3.2.11 Metabolomics

3.2.11.1 *GC-MS analysis and sample preparation*

(Dr. M. Radke and AG Kempa, Max Delbrück Centre, Berlin, Germany)

Frozen muscle tissue was homogenized and 50 mg powder were extracted with 1 ml methanol-chloroform-water (MCW) (5:2:1/v:v:v) (Methanol LC-MS-grade, Chloroform Reagent Plus ® 99.8% Sigma-Aldrich) with cinnamic acid as internal standard (Sigma Aldrich). After the addition of 500 µl of distilled water, the supernatant was collected and transferred to safelock 1.5 ml Eppendorf tubes. MilliQ water was added in an amount corresponding to 0.5 of the MCW-volume to each muscle sample, then samples were shaken at 750rpm at 4°C for 60 minutes on a Thermomixer comfort 1.5ml (Eppendorf). This was followed by centrifugation for 10 min to separate the polar (top), lipid (bottom) and interface (tissue debris) layers. Polar and lipid phase were then dried under vacuum (SpeedVac RVC 2-33 CD plus, Martin CHRIST) over night. Dried samples were chemically modified by derivatization as described in (Kempa et al., 2007).

Metabolite analyses were performed with a Pegasus III mass-spectrometer (LECO) equipped with an Agilent 6890N gas chromatograph and a VF-5ms column with 30m length and 250 µm inner diameter (Agilent). 1 µl of sample was injected into a baffled liner (Gerstel) with a 1:5 split-ratio under a helium-flow of 1.2 ml/min using a gradient ranging from 70°C to 350°C with 5 °C/min to 120 °C and 7 °C/min to 350 °C followed by a 2 minute hold time. Scan rates of 20 Hz and mass ranges of 70-600 Da were used. The GC-MS chromatograms were processed with the ChromaTOF software (LECO) as described in (Kempa et al. 2007) and the data matrices for relative quantification were generated using the MetMax software (Kempa et al., 2009).

3.2.11.2 *Metabolomic data analysis*

For each sample, the area under the peak corresponding to a metabolite was normalized to the area under the peak of the added control. A two-sided Grubbs test was performed within each group to eliminate outlier values with a p-value <0.05. This was followed by a two-tailed,

unpaired t-test to determine significant differences in protein levels between the wild type and titin kinase-deficient muscles at levels of basal muscle activity.

3.2.12 Statistical analysis

Statistical analysis and data visualization was mostly done in R. While graph generation was done using Excel (Microsoft) or GraphPad Prism 5.

4 Results

This study aimed to understand how striated muscle adapts its size and metabolism during times of altered demand. Specifically, we studied:

(1) How hibernating grizzly bears maintain their muscle mass despite a decrease in activity and reduced food intake during this period.

(2) The role of titin kinase as a mechanosensor in mediating muscle mass and metabolic signalling.

The first question was addressed by analysing global changes in mRNA and protein expression in the skeletal muscle of four Grizzly bears before and during hibernation. Findings were validated in a murine muscle-like cell line (C2C12) to confirm the relevance and adaptability of such findings to non-hibernating species. The second question was addressed by generating and analysing C2C12 cells that stably expressed the catalytic domain of Titin kinase in a doxycycline-dependent manner. Cell culture data was combined and compared to a study done on murine striated muscle lacking the catalytic domain of titin's kinase. The latter included the analysis and integration of transcriptomic, proteomic and metabolomic changes in the muscle of these animals. This data collectively helped build a more detailed picture about how titin kinase affects growth and metabolic signalling in both skeletal muscle and the heart.

4.1 Changes on the proteomic and transcriptomic level reflect alterations in metabolic and signalling pathways during hibernation.

To identify the proteomic changes occurring in the skeletal muscle of hibernating grizzly bears, we extracted proteins from gastrocnemius (GA) muscle biopsies of two cubs, an adult and a sub-adult grizzly bear before and during hibernation (October and February respectively; Figure 5). Proteins were subsequently identified and quantified using mass spectrometry. Since a published grizzly bear genome was not available at the time of the analysis, proteins were identified based on their homology to human homologues. Intensities across samples were compared by a two-way ANOVA to determine the changes contributed by the activity state (active versus hibernating) and/or age (cubs versus adult and sub-adult). The majority of proteins identified enriched to terms related to metabolic processes. A significant number of the components of the electron transport chain (oxidative phosphorylation) and the TCA cycle were regulated based on the activity state of the bears (p-value < 0.05; Figure 6).

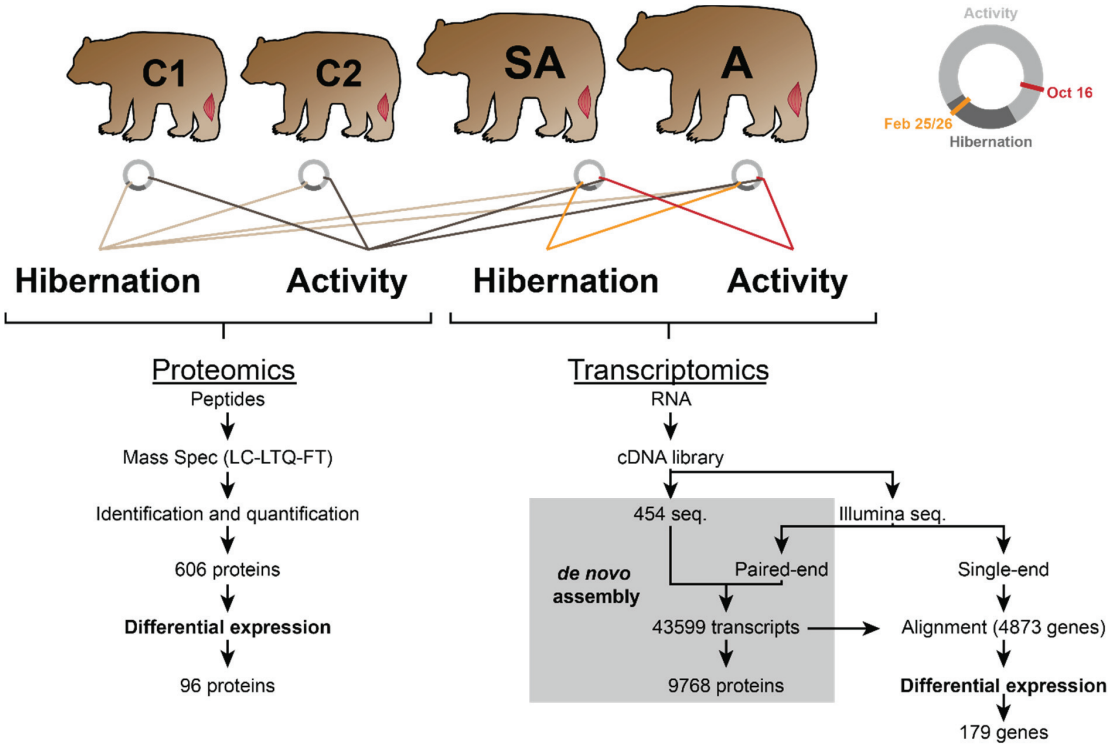

Figure 5: Experimental layout for the identification and quantification of grizzly bear proteome and transcriptome.
C: cub, SA: subadult, A: adult.

Since proteins of non-metabolic processes were not prominent in the protein analysis, we complemented it with a transcriptomic analysis. RNA from the adult and sub-adult biopsies used for the proteomic analysis were used for deep sequencing. Again, transcripts were annotated based on their homology to human transcripts and those differentially regulated between hibernating and active samples were determined using NOIseq (cut-off >= 0.8) (Tarazona et al., 2011). A KEGG-pathway enrichment analysis indicated that genes associated with a wide variety of intracellular processes were identified on the transcriptional level, extending on the proteomic changes (Figure 6c). The mRNAs regulated during hibernation included those associated with the insulin signalling pathway, which affects cells size and metabolism in other organisms (Manning and Cantley, 2007). Components of the Hif1α pathway, which has also been implicated in the regulation of muscle growth and metabolism (Ren et al., 2010), were also regulated in hibernation, as were structural proteins that have been previously associated with hypertrophic cardiomyopathy (Figure 6c). Only seven genes were regulated on both the protein and mRNA level in these datasets (Figure 6a).

4.1.1 Transcriptional changes of insulin signalling components could improve insulin-sensitivity during hibernation.

As changes in insulin signalling affect organ size (Stitt et al., 2004), I mapped the changes in the significantly regulated mRNAs of this pathway to the corresponding human KEGG pathway to visualize its overall regulation during hibernation (Figure 7). There was an increased production of the more insulin-sensitive insulin Receptor Substrate (Rondinone et al., 1997), Irs-1, and a decrease in the less sensitive counterpart, Irs-2. The Irs-1 inhibitor Socs2 was decreased, while the Irs-1 effectors Grb2 and Pi3k were increased. Further downstream, deptor (the mTor inhibitor) was supressed together with a component of Akt's target phosphorylase kinase complex (Phkg1), while Ppp1r3c was increased. Together, these transcriptional changes could improve insulin-sensitivity in muscle if maintained on the post-transcriptional level.

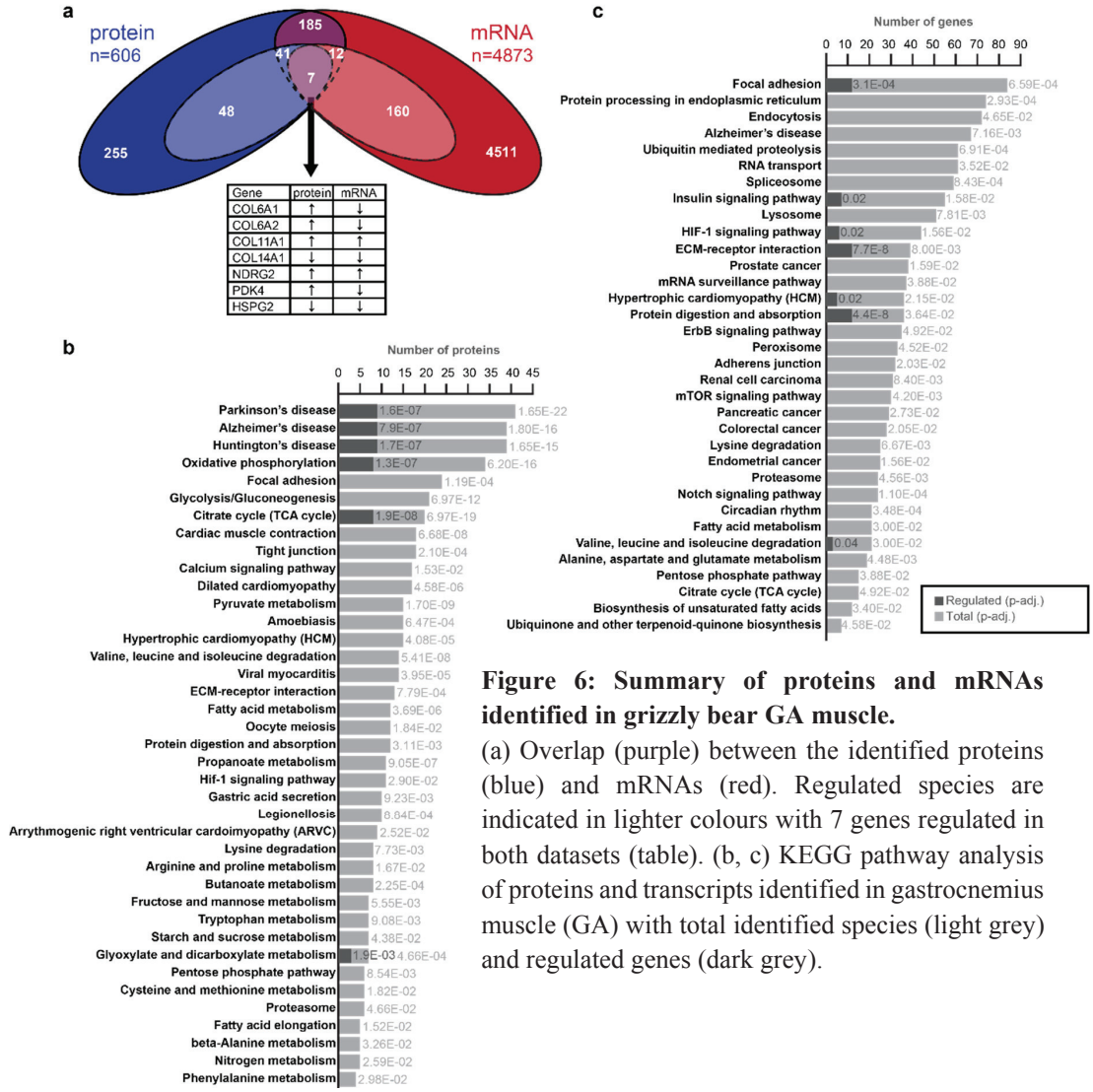

Figure 6: Summary of proteins and mRNAs identified in grizzly bear GA muscle.
(a) Overlap (purple) between the identified proteins (blue) and mRNAs (red). Regulated species are indicated in lighter colours with 7 genes regulated in both datasets (table). (b, c) KEGG pathway analysis of proteins and transcripts identified in gastrocnemius muscle (GA) with total identified species (light grey) and regulated genes (dark grey).

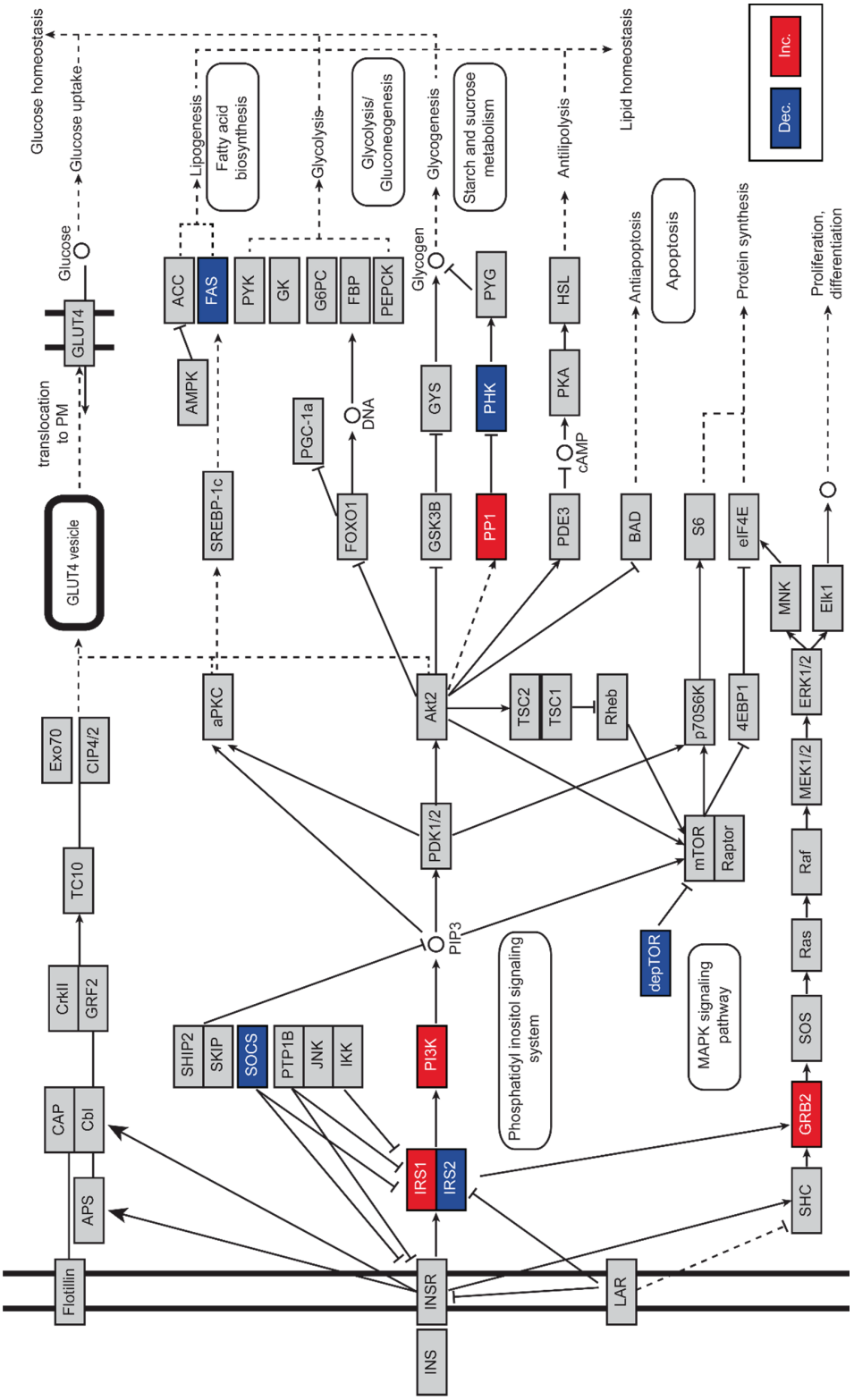

Figure 7: Mapping changes in mRNA levels of the insulin signalling components of GA muscle during hibernation (adapted from KEGG). Positive regulators of insulin signalling are mostly increased (Inc.) on the mRNA levels, while the negative regulators are decreased (Dec.).

4.1.2 Metabolic changes in hibernation suggest a change in central glucose metabolism.

Since components of the TCA cycle and oxidative phosphorylation were significantly enriched among proteins regulated during hibernation, we summarized the changes connected to central glucose metabolism (Figure 8a). The relative changes in the expression of the glycolytic/gluconeogenic enzymes and TCA cycle components were incorporated into a pathway diagram (Figure 8b). An increase in a single glycolytic/gluconeogenic enzyme, Gpi, was observed, accompanied by a decrease in all the regulated enzymes of the TCA cycle, except Ogdh, which was increased. Pdhb and Pdha1 - both components of the pyruvate dehydrogenase complex that shuttles pyruvate into the TCA cycle as acetyl-coA - were decreased, while the inhibitor of the Pdh complex - Pdk4 - was increased. Taken together, the data suggest that components of the aerobic respiratory pathway are decreased on the protein level, supporting reports previous reports of decreased of metabolic rates during hibernation in bears (Tøien et al., 2011). These were accompanied by changes in the muscle's capacity to buffer ROS as evident by changes in some of the ROS neutralizing genes (Figure 8a).

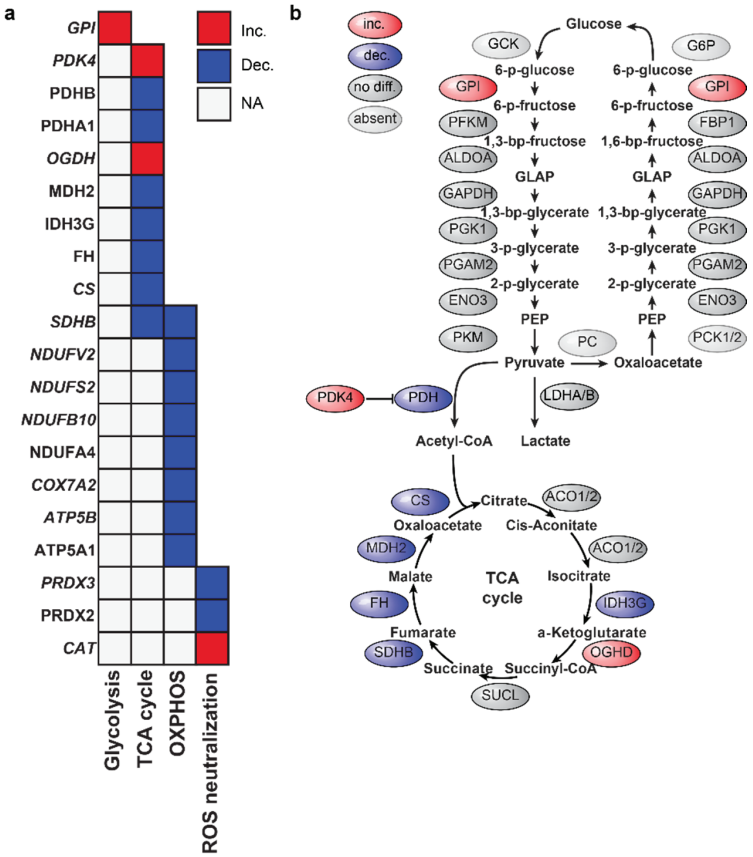

Figure 8: Enzymes related to glucose metabolism are regulated at the protein level in skeletal muscle during hibernation.
(a) Summary of changes in enzymes related to central glucose metabolism in hibernation (versus activity) that occur irrespective of age (p-value < 0.05, two-way ANOVA). (b) Pathway of central glucose metabolism overlaid with hibernation associated changes in proteins depicted in (a). Proteins in red are increased (inc.) during hibernation, proteins in blue are decreased (dec.). No diff.: No difference; NA: not applicable.

4.1.3 Metabolic changes occur in aging human muscle

To determine whether the metabolic changes observed in the hibernating grizzly bear muscle were specific to this type of muscle disuse, or an adaptation to other environmental conditions that affect muscle function and size, we compared hibernation associated changes to a publicly available dataset of aging muscle (GSE674). This dataset compares genome-wide changes in mRNA levels in skeletal muscle biopsies from 15 women; seven aged between 20 and 29 years (younger) and eight between 65 to 71 years (Welle et al., 2003). mRNAs with significantly different expression levels between the two age groups associated with several metabolic processes (Figure 9a).

Enzymes involved in central glucose metabolism were decreased on the transcriptional level (Figure 9b), and are predominantly involved in the TCA cycle and oxidative phosphorylation (Figure 9c). Enzymes important for ROS neutralization were also mostly decreased. Together these changes suggest that a decreased metabolic capacity in aging, is accompanied by a difference in ROS levels which mediate intracellular damage (Finkel and Holbrook, 2000).

4.1.4 Metabolic modelling suggests that non-essential amino acids increase in the muscle in hibernation and decrease in aging.

The inconsistent increase in Gpi and Ogdh enzyme levels compared to the other enzymes of glucose metabolism during hibernation raised the question whether pathways not primarily related to energy production were affected. Both the glycolytic pathway and TCA cycle are known to provide precursors for non-essential amino acid (NEAA) synthesis which is needed to drive protein synthesis. In hibernation, changes that enhance NEAA synthesis together with metabolic suppression could help maintain muscle mass. In the absence of metabolomic data on hibernating bear muscle we used a modelling approach to assess if these metabolic changes could, in principle, affect NEAA levels during hibernation. Thus, relative changes in protein levels between hibernating and active muscle were used to build metabolic models that capture the effect of enzymatic changes on metabolite levels. The changes were contextualized with respect to the most-comprehensive mammalian metabolic model at the time, Recon2, which was constructed based on human-derived data. As we identified only proteins that have human homologues, the approximation was considered reasonable. After creating the models of active and hibernating skeletal muscle, each was set to maximize the production of the different non-

essential amino acids or their glycolytic and TCA cycle-derived precursors glycerate-3-phospate (3pg) and alpha-ketogluterate (α-KG) as shown in Figure 10a.

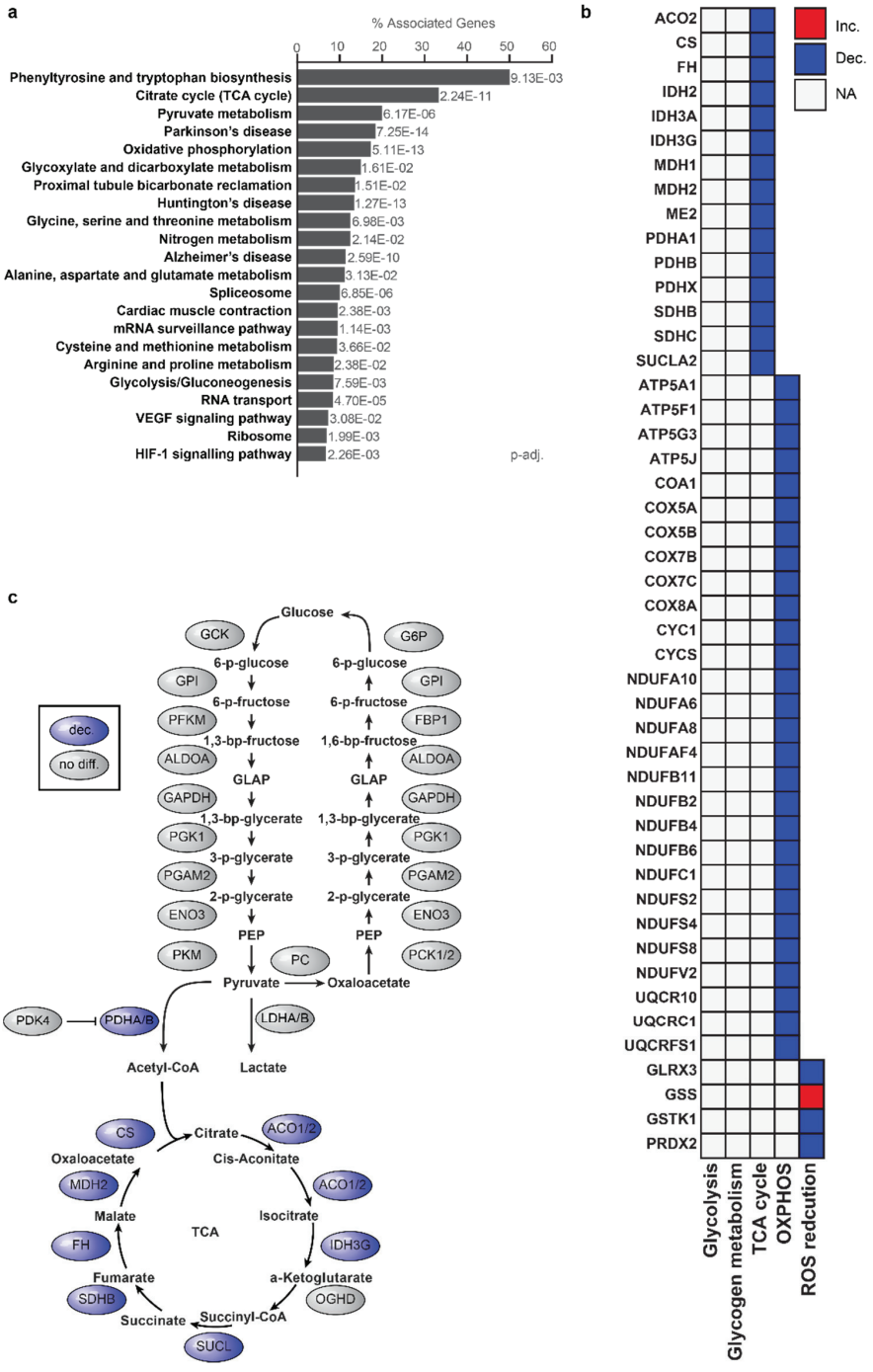

Figure 9: Changes in mRNA levels in aging skeletal muscle indicate alterations in metabolic regulation.
(a) KEGG pathways with mRNAs regulated in aging female muscle. In grey are the adjusted p-values per term. (b) The majority of metabolism-related transcripts are decreased in aging muscle. (c) Transcriptional changes in central glucose metabolism in aging muscle. Inc.: increased, Dec: decreased, NA: not applicable.

The relative change in the maximum producible levels of each metabolite during hibernation is summarized in Figure 10b. While α-KG steady state levels were predicted to be lower during hibernation, the levels of glutamate (Glu), alanine (Ala), glutamine (Gln) and proline (Pro) which derive from it were all increased. Arginine (Arg), aspartate (Asp) and asparagine (Asn) were unchanged, together with the 3pg-derived NEAAs glycine (Gly) and cysteine (Cys). The steady state levels of 3pg itself during hibernation were predicted to be increased, so was serine (Ser) for which it also serves as a precursor. Tyrosine (Tyr), which can be derived from phenylalanine (Phe) by hydroxylation, was also predicted to be increased during hibernation. Two age-dependent models were similarly generated using transcriptional data from young and older female vastus lateralis muscle biopsies to assess their impact on NEAA synthesis, and compared them to changes in hibernation. Seven NEAAs were predicted to have lower steady state levels in aging female muscles. Six of the NEAAs predicted to decrease in aging muscle were predicted to increase during hibernation (Figure 10c).

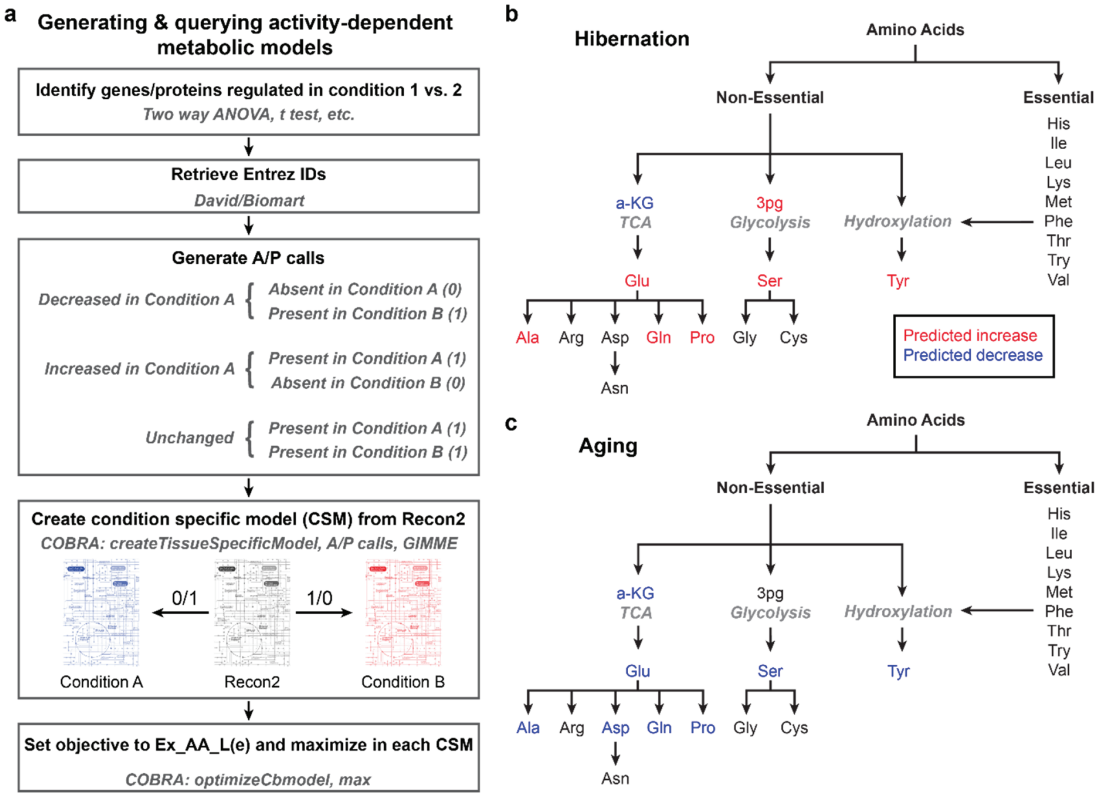

Figure 10: Metabolic modelling predicts differential regulation of non-essential amino acid (NEAA) levels in hibernation versus human ageing.
(a) Generation of activity-dependent metabolic models. (b) Predicted changes in steady state levels of NEAAs and their main precursors in GA during hibernation. (c) Prediction of age-dependent changes in NEAA metabolism in human vastus lateralis muscle.

4.1.5 Increasing NEAA availability increases myotube size in cell culture.

The results of the metabolic models suggest that intramuscular NEAA levels increase in hibernation which is a condition of muscle mass retention, but decreases with age when muscle mass is lost. This raised the question of whether NEAAs regulate muscle mass.

One way NEAAs could enhance muscle mass, is by contributing 50% of the precursors needed for protein synthesis. In hibernation NEAAs were predicted to increase, which could selectively increase NEAA-rich proteins due to the availability of a larger substrate pool. To test this hypothesis, the distribution of NEAA content in the proteins increased versus those decreased during hibernation were compared. Although NEAA-rich proteins (> 65% NEAAs) were only represented in the proteins increased in hibernation, their number was too low to be statistically significant, making the overall distribution across both groups similar (Figure 11a).

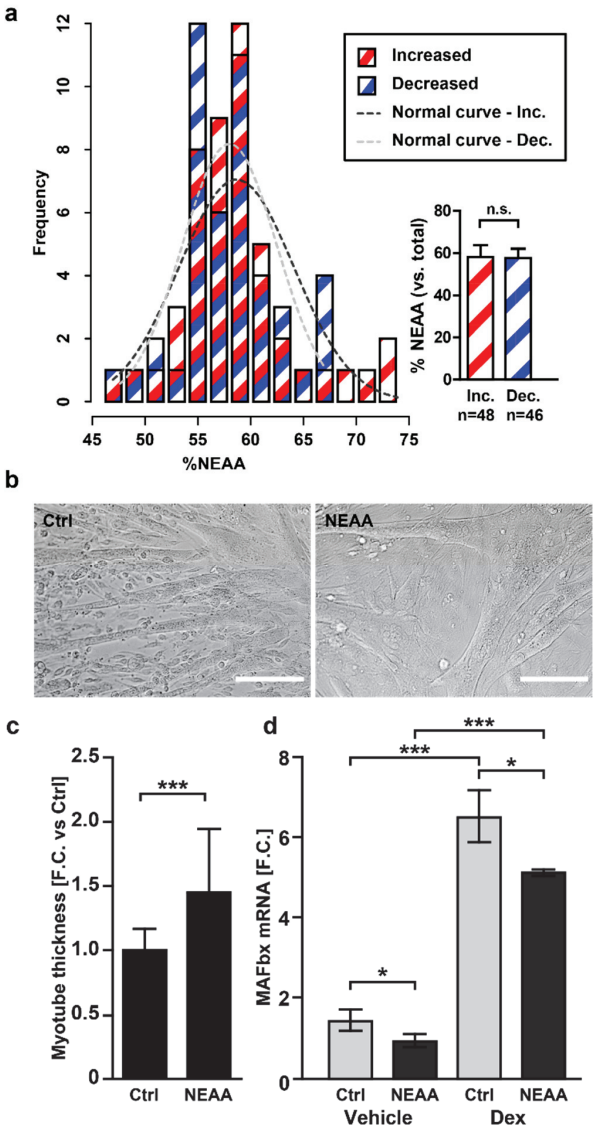

Figure 11: Distribution of non-essential amino acids (NEAAs) in proteins regulated during hibernation and their effect on myotube thickness.
(a) NEAA content in the proteins increased (red) or decreased (blue) during hibernation is not significantly changed (mean ± s.d., two-tailed t-test; estimated normal distributions of the two populations as black and grey dotted lines). (b, c) NEAA supplementation significantly increases myotube diameter (mean ± s.d., t-test). Size bar; 50 µM. (d) Effect of NEAA supplementation on MAFbx levels in differentiated C2C12 cells with and without Dexamethasone (n=3, mean ± s.e.m., two-way ANOVA, Bonferroni post-hoc test). Ctrl, control; Dex, dexamethasone.

It is thus unlikely that NEAA availability affects protein synthesis only by increasing the pool of precursors. To test if NEAAs could increase myotube size by affecting cellular process other than NEAA-dependent peptide elongation, C2C12 cells differentiated into myotubes were supplemented with a commercial solution of NEAA and compared to untreated cells. Upon comparison, myotube thickness was significantly greater when cells were supplemented with NEAAs (Figure 11b, c). This was associated with a decrease in levels of the muscle-specific E3 ubiquitin ligase MAFbx (Figure 11d), which is elevated in atrophic muscle under most reported cases (Lecker et al., 2004). These data support the hypothesis that increasing NEAA availability could increase muscle size, possibly by affecting the signalling events that control MAFbx production.

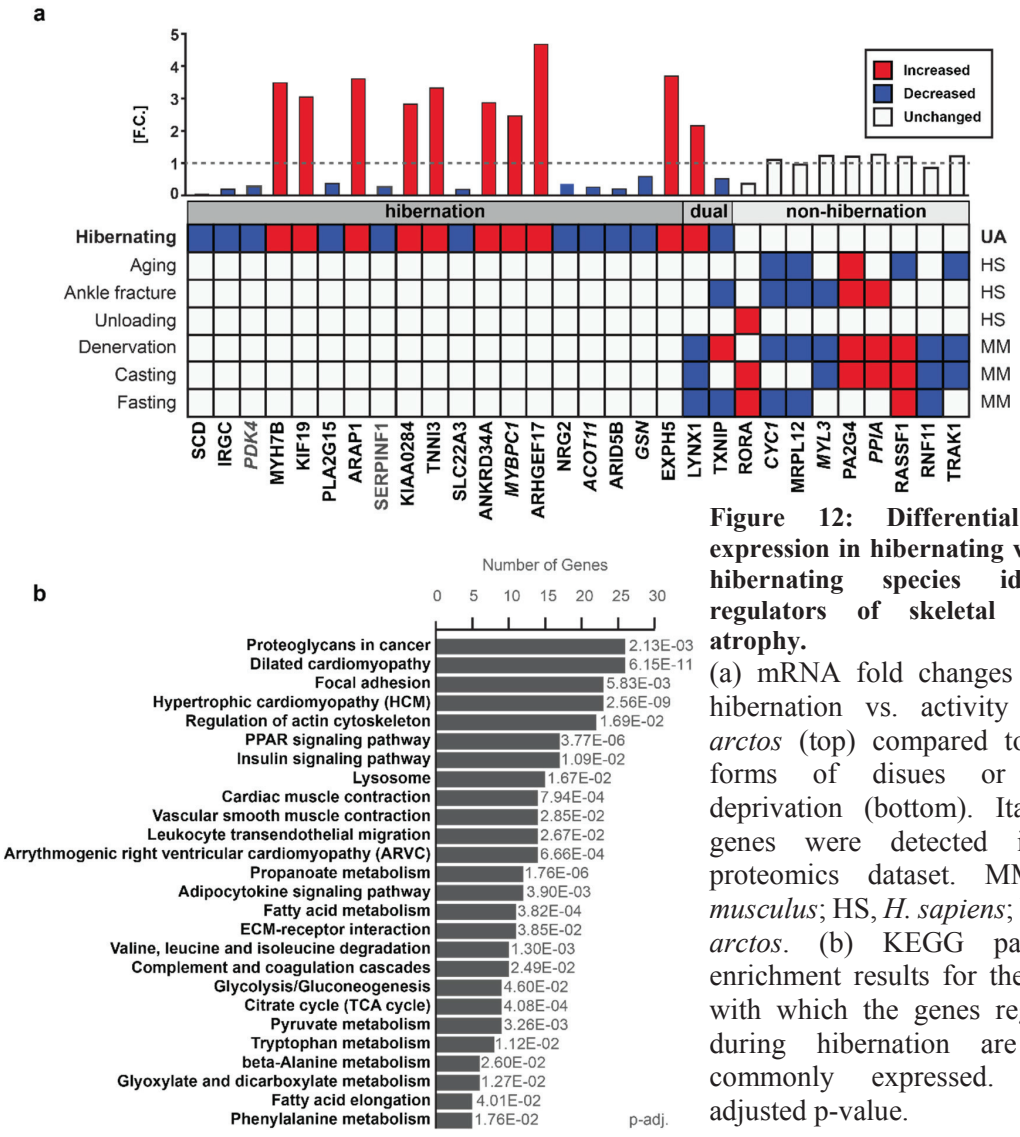

Figure 12: Differential gene expression in hibernating vs. non-hibernating species identifies regulators of skeletal muscle atrophy.
(a) mRNA fold changes during hibernation vs. activity in *U. arctos* (top) compared to other forms of disues or food-deprivation (bottom). Italicized genes were detected in the proteomics dataset. MM, *M. musculus*; HS, *H. sapiens*; UA, *U. arctos*. (b) KEGG pathways enrichment results for the genes with which the genes regulated during hibernation are most commonly expressed. p.adj.: adjusted p-value.

4.1.6 Identifying atrophy-associated genes by comparing changes in skeletal muscle mRNA expression under different atrophy-inducing conditions.

To identify genes that contribute to the hibernating bear's ability to resist muscle atrophy under caloric restriction and immobilization, we compared changes in mRNA expression during hibernation and six other atrophy-inducing conditions. The six conditions affect humans and mice, and are associated with a decrease in food intake and/or muscle mobility. The comparison was based on the directionality of change under the different conditions and resulted in the identification of three main groups of genes (Figure 12a). The first group includes the genes regulated during hibernation but in none of the other datasets. These genes were taken to be regulated selectively during hibernation, and thus suspected to contribute to the muscle's ability to resist atrophy. The second, smaller group of genes was regulated during hibernation and in at least half of the other conditions (similar or opposite direction). The third group contained genes that were not regulated during hibernation, but changed in at least half of the other datasets. Several of the genes in the three groups have been previously associated with muscle size or function. The third group contains genes that are not regulated during hibernation, but in at least half of the other datasets. Several of the genes in the three groups have been previously associated with muscle size or function (Table 18).

4.1.7 Validating the effect of Pdk4 and Serpinf1 on atrophy signalling in C2C12 cells.

To experimentally validate the effect of the genes in group one on atrophy, two were selected to be stably knocked down in C2C12 cells using gene-specific shRNAs. The two genes were Pdk4, a metabolic enzyme important in shuttling pyruvate into the TCA cycle (Zhang et al., 2014); and Serpinf1, a Nfκb activator in non-muscle cells (Yabe et al., 2005). After differentiation into myotubes and treatment with the atrophy-inducing, synthetic glucocorticoid dexamethasone (Clarke et al., 2007) or empty vehicle, levels of the atrophy marker MAFbx were compared by qRT-PCR. Pdk4 knockdown cells expressed higher levels of MAFbx compared to the controls when treated with only vehicle, an effect which was enhanced in the presence of dexamethasone (Figure 13a-d). The opposite was observed in the case of Serpinf1, where knockdown cells expressed lower levels of MAFbx compared to controls. The dexamethasone-induced increase was also stunted in the absence of Serpinf1, though not completely rescued (Figure 13e-h). Together these results support the relevance of the genes found differentially expressed in hibernation to the muscle's ability to reduce muscle loss not only in hibernation, but also in non-hibernating species.

Table 18. Genes differentially regulated in hibernation relate to striated muscle growth.

Gene	OMIM	Summary	Disease
RASSF1	605082	Increased expression in patients with heart failure. Larger hearts in Rassf1 knockout mice after TAC-surgery to induce pressure overload (Oceandy et al., 2009).	Heart failure, cardiac hypertrophy
MYL3	16079	Essential myosin light chain. Mutations have been associated with cardiac hypertrophy and skeletal muscle disease (Poetter et al., 1996; Olson et al., 2002).	Cardiac hypertrophy, skeletal muscle disease
CYC1	123980	Component of the electron transfer chain (ETC). A mutation in CYC1 reduces protein stability in muscle of a patient with growth retardation (Gaignard et al., 2013).	Skeletal myopathy, growth retardation
MYBPC1	160794	Myosin binding protein. Mutations are associated with Distal arthrogryposis type I, characterized by reduced muscle mass (Gurnett et al., 2010).	Distal arthrogryposis type I, muscle atrophy
TNNI3	191044	Associated with hypertrophic cardiomyopathy (Kimura et al., 1997).	Hypertrophic cardiomyopathy
RNF11	612598	Involved in NFKB signalling (Shembade et al., 2009; Maddirevula et al., 2012, 11).	n.a.
PPIA	123840	Encodes Cyclophilin A, which is secreted in response to increased ROS production. Knockout mice have smaller hearts in response to high ROS levels (Satoh et al., 2011).	n.a.
PA2G4	602145	Knockouts are smaller with reduced circulating IGF-1 (Zhang et al., 2008).	n.a.
RORA	600825	Involved in circadian regulation and induces Bmal1 expression (Akashi and Takumi, 2005; Sato et al., 2004), which affects muscle function and size, increases PDK4 while reducing Pdha activity (Dyar et al., 2014).	n.a.
ARID5B	608538	Decreased genomic methylation has been associated with reduced birth weight (Engel et al., 2014).	n.a.
NRG2	603818	Growth retardation in knockout mice (Britto et al., 2004).	n.a.
SERPINF1	172860	Enhances NFKB signalling (Yabe et al., 2005).	n.a.

n.a.: not available

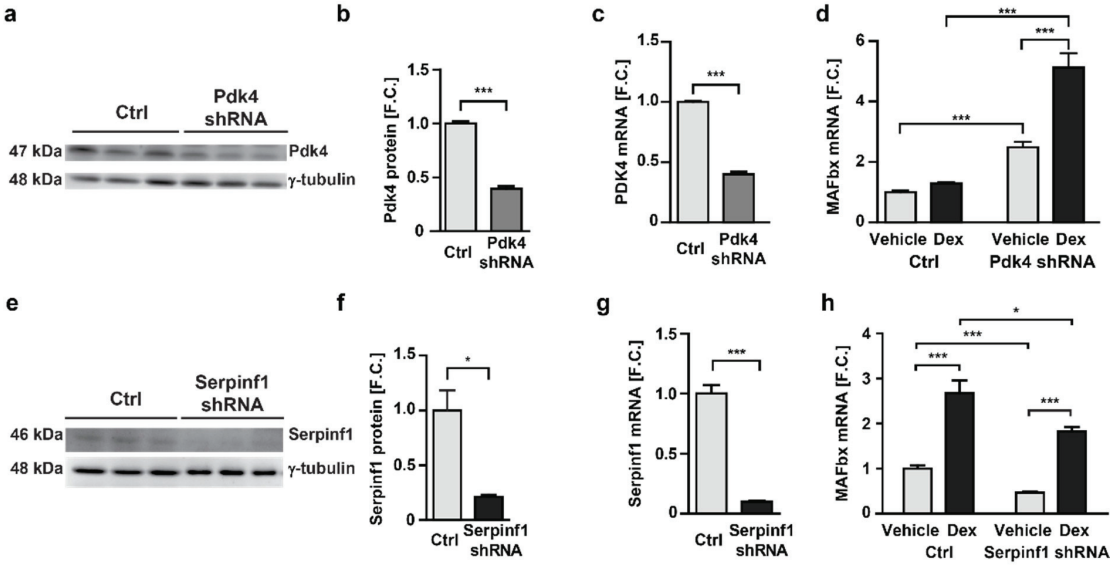

Figure 13: Validation of the effect of Pdk4 and Serpinf1 on muscle atrophy signalling in murine cells.

(a, b) Downregulation of Pdk4 in C2C12 cells after shRNA-mediated knockdown was validated by immunoblot analysis with >50% reduction of Pdk4 protein levels (n=3, mean ± s.d., t-test). (c) Pdk4 mRNA levels are reduced by >50% as determined by qRT-PCR (n=3, mean ± s.e.m., t-test). (d) Knockdown of Pdk4 increases RNA levels the atrophy marker MAFbx and amplifies the effect of dexamethasone (Dex) on MAFbx. Pdk4 downregulation increases the dexamethasone effect >5-fold (n=3, mean ± s.e.m., two-way ANOVA, Bonferroni post-hoc test). (e-g) After shRNA treatment, protein and RNA levels of Serpinf1 are reduced to <20% (n=3, mean ± s.d./s.e.m. (protein/mRNA), t-test). (h) MAFbx mRNA levels are decreased after the knockdown of Serpinf1. The increase of MAFbx mRNA expression after dexamethasone treatment is partially reverted. (n=3, mean ± s.e.m., two-way ANOVA, Bonferroni post-hoc test).

4.2 Titin's kinase domain (TK) affects metabolic and growth signalling in striated muscle.

TK regulates intracellular processes via its ability to form complexes with proteins such as Nbr1, p62 and Murf2 (Lange et al., 2005), but the consequence of such events on myocyte function have not been shown to date. To investigate its role as a signalling mediator, I generated a cell culture model stably expressing an inducible T7-tagged TK in C2C12 myoblasts (Figure 14a). The construct was designed to be suppressed with doxycycline (Dox; Tet-OFF system; Figure 14b). However, the addition of Dox to these cells appeared to independently affect some of the signalling pathways we were interested in studying. Accordingly TK expression was not silenced in the subsequently reported experiments, and all results were compared between the T7-TKCD expressing cells (TK+ cells) and the parental controls (TK– cells) that only express the Tet-responsive element. This cell line was

characterized together with a TK knockout (TKKO) animal model that was generated in our laboratory. The animals were previously shown to exhibit macro-and microscopic changes including cardiac hypertrophy and a resistance to denervation-induced atrophy in skeletal muscle. The characterization of the cell and animal models helped build a complementary picture of how TK affects metabolic and trophic signalling events in the myotube as illustrated in the following sections.

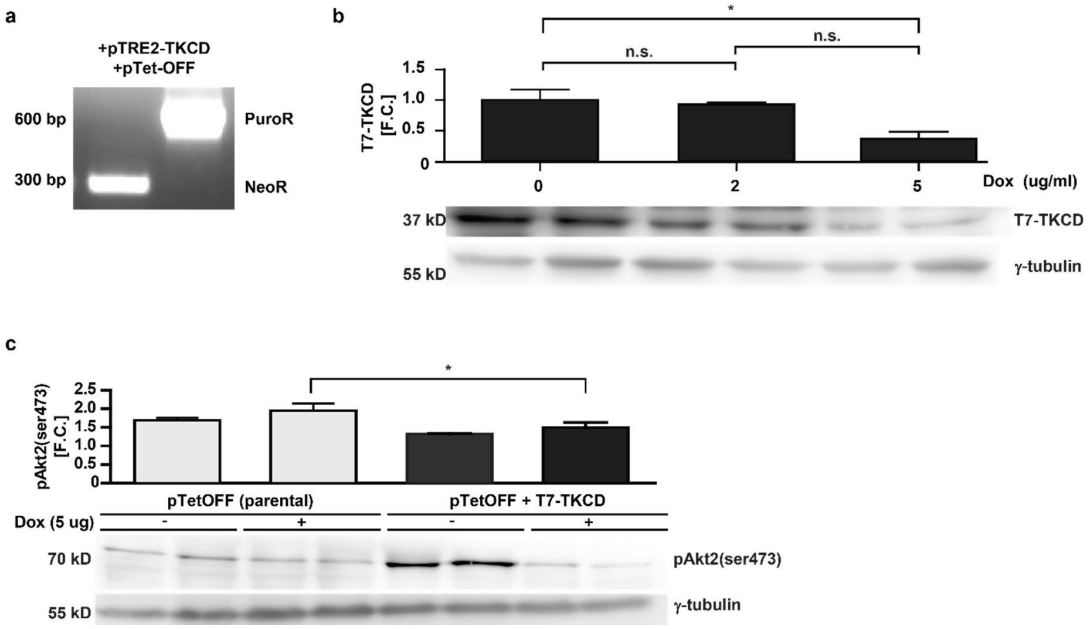

Figure 14: T7-tagged TKCD expression is responsive to Doxycycline (Dox) in the selected clone.

(a) The double stable clone is both positive for the Neomycin and Puromycin resistance genes (NeoR and PuroR). (b) T7-tagged TKCD expression can be significantly suppressed in the presence of 5 ug/ml Dox (n=2, mean ± s.d, One-way ANOVA, Bonferroni post-hoc test). (c) Dox addition increases the levels of insulin-induced pAkt (ser473) in both parental and T7-TKCD expressing cells, and the presence of TKCD decreases overall levels of pAkt (ser473) in C2C12 cells (n=2, mean ± s.d, Two-way ANOVA, Bonferroni post-hoc test).

4.2.1 Expression of soluble titin kinase changes myocyte metabolism.

The genes differentially expressed in the TK+ cells were used in a KEGG pathway enrichment analysis to obtain an overview of the processes that were affected in the presence of TK. Metabolic genes were the group most largely represented followed by genes of the insulin signalling pathway (Figure 15a). Specifically, mRNA levels of components of the pentose phosphate (PPP) and glycolytic pathways were elevated in the TK+ cells, while components of the electron transport chain (ETC) and the CO_2-buffering enzyme Car13 were supressed (Figure 15b). The changes are summarised in relation to central glucose metabolism in Figure 15c.

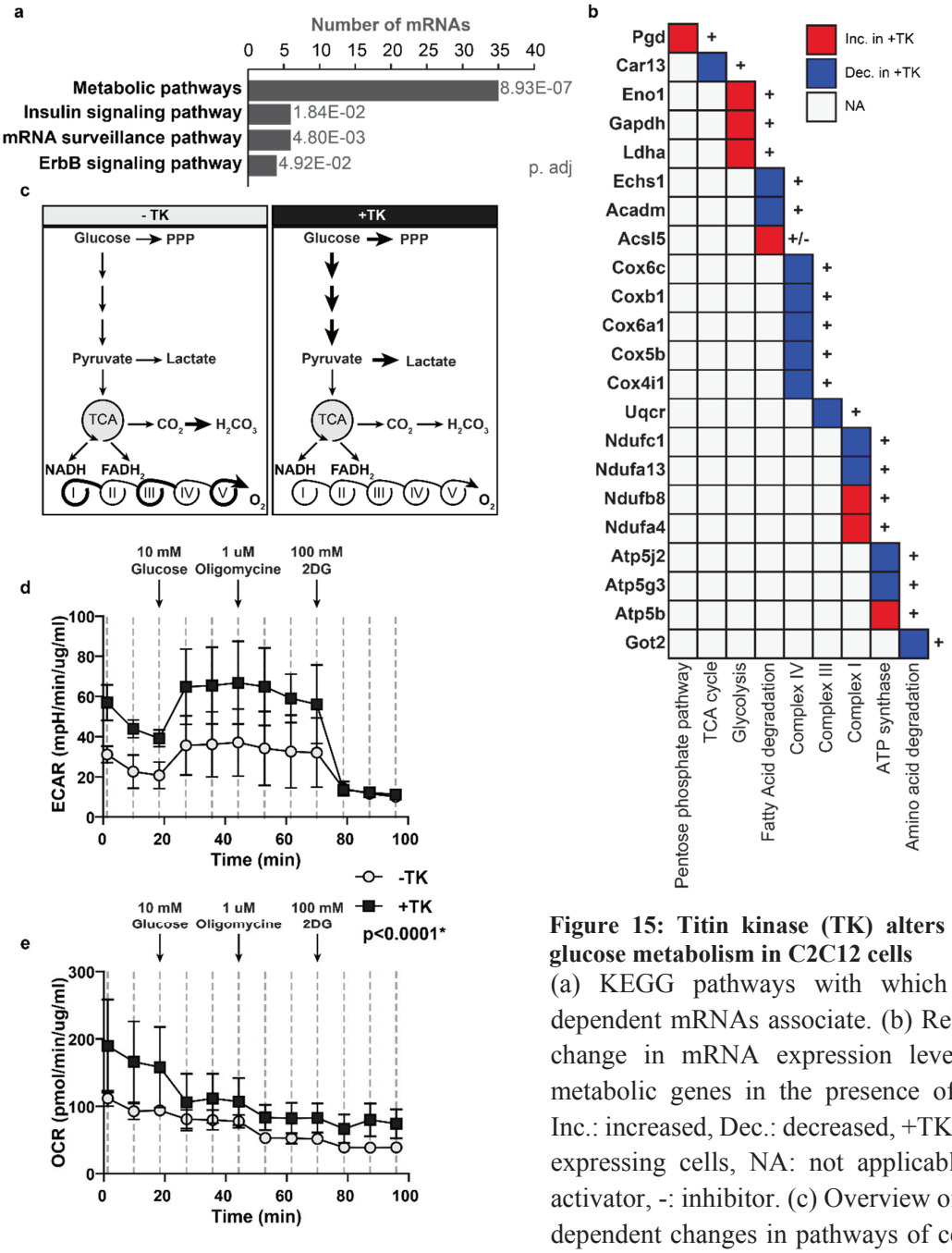

Figure 15: Titin kinase (TK) alters glucose metabolism in C2C12 cells

(a) KEGG pathways with which TK-dependent mRNAs associate. (b) Relative change in mRNA expression levels of metabolic genes in the presence of TK. Inc.: increased, Dec.: decreased, +TK: TK-expressing cells, NA: not applicable, +: activator, -: inhibitor. (c) Overview of TK-dependent changes in pathways of central glucose metabolism as indicated by (b). (d, e) TK-expressing cells have higher levels of basal extracellular acidification rate (ECAR) as well as a higher oxygen consumption rate (OCR) (n=4, mean ± s.d., Two-way ANOVA, Bonferroni post-hoc test).

To determine whether these transcriptional changes have consequences at the functional level, changes in glycolysis and oxidative phosphorylation were measured and compared using a SeaHorse® XF^{e}24 analyzer. We used a glycolytic stress kit, which allows the measurement of the changes in two parameters over time. The first parameter is the extracellular acidification rate (ECAR) used as a surrogate for glycolytic activity (based on the amount of lactate produced during glycolysis). The second parameter is the oxygen consumption rate (OCR), which reflects the activity of the ETC. TK+ cells kept in glucose-free medium have both higher ECAR and OCR, reflecting higher glycolytic and oxidative phosphorylation capacity (Figure 15d, e). Upon addition of 10 μM glucose, both cell lines shift from oxidative phosphorylation to mostly anaerobic respiration as evident by the increase in ECAR and decrease in OCR, but TK+ cells maintain a slightly higher OCR, and a much higher ECAR compared to TK- cells. While the addition of the ATP synthase inhibitor Oligomycin (1 μM) doesn't affect ECAR in either cell type, there is a slight decrease in OCR in both cell lines reflecting a decrease in oxidative phosphorylation, but TK-expressing cells continue to maintain higher ECAR and OCR levels. The addition of 2-deoxyglucose (2-DG) at 100 x the concentration of glucose, suppresses ECAR in both cell types, as it is a competitive inhibitor of hexokinase, the enzyme that catalyses the first step in glycolysis. This confirms that the increase in ECAR is glucose-dependent. OCR remained unaffected in either cell type, as the levels maintained post glucose-addition are glucose-independent (Nicholls et al., 2010). These results suggest an increase in the rate of glycolysis and oxidative phosphorylation in TK-expressing cells. The mRNA expression changes of Eno1, Gapdh and Ldha are consistent with an increase in glycolysis but the decrease in the majority of the regulated ETC components is the opposite of the observed increase in OCR in the TK+ cells.

4.2.2 Titin kinase-expressing C2C12 cells are less responsive to Insulin.

As changes in the gene expression and pathway enrichment analyses suggested that insulin signalling could be perturbed in TK+ cells, they were treated with insulin after at least eight hours of serum-starvation and compared to TK- cells treated similarly. Levels of pAkt2 (ser473) were measured as an output of insulin stimulation. While control cells responded normally to insulin, as indicated by the significant increase in pAkt (ser473) levels after treatment, there was no significant increase in TK-expressing cells (Figure 16a, b). Total Akt levels were unchanged in either cell-line (Figure. 16c, d).

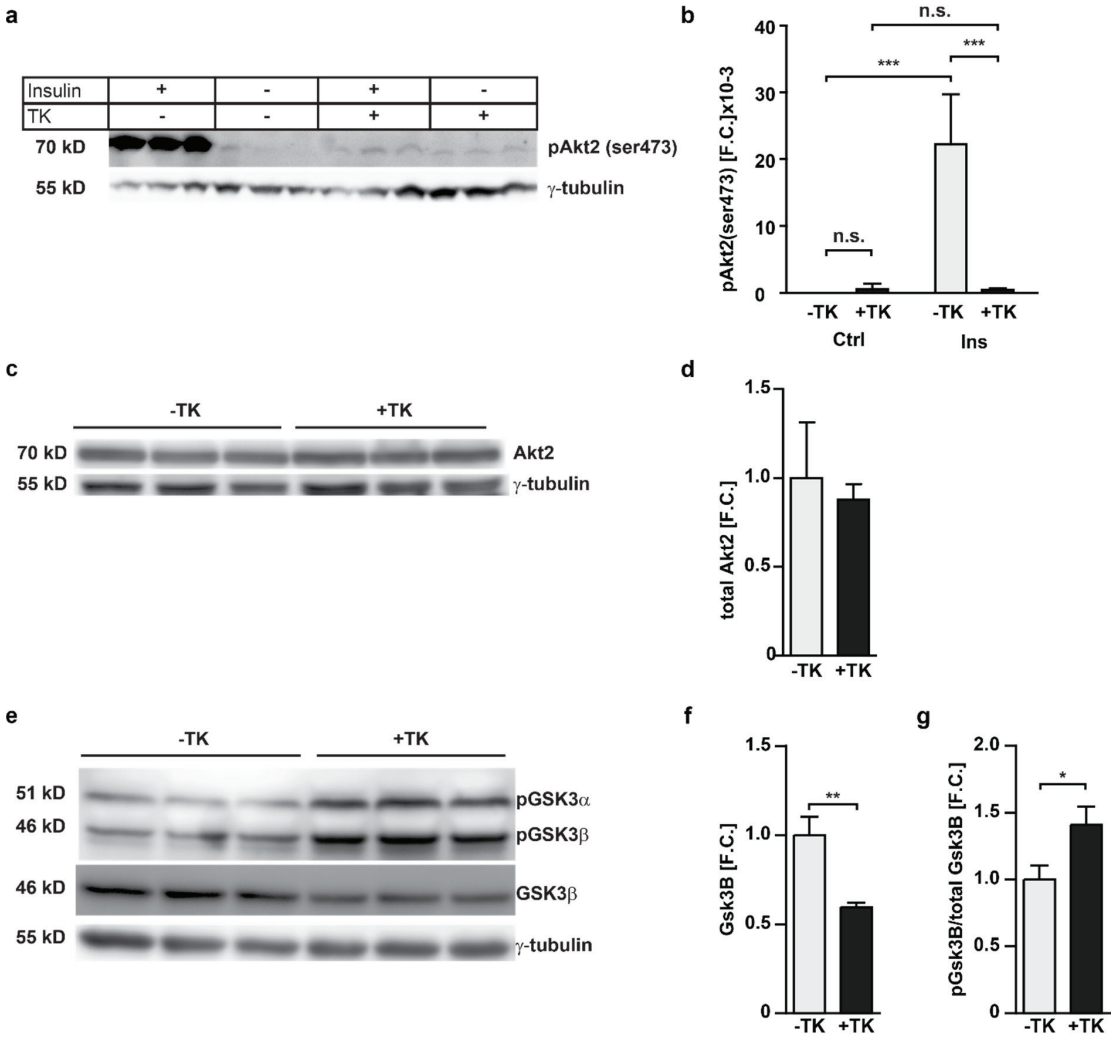

Figure 16: TK suppresses insulin-induced Akt activation in C2C12 cells.
(a, b) The presence of TK inhibits Akt2 phosphorylation at ser473 in response to insulin (n=3, mean ± s.d, Two-way ANOVA, Bonferroni post-hoc test). (c, d) Total levels of Akt2 are not different in TK-expressing cells (n=3, mean ± s.d., t-test). (e-g) TK enhances Gsk3-alpha/beta phosphorylation at ser9, although total Gsk3-β levels are lower (n=3, mean ± s.d., t-test).

Contrary to pAkt levels, phosphorylation of the Akt target Gsk3β was increased in TK+ cells, despite a decrease in total protein levels (Figure 16. e-g). Regulators of Akt phosphorylation were also checked including the indirect Akt phosphorylation inhibitor, PTEN, which was increased in TK+ cells (Figure 17 a-c). Levels of the Irs-1-binding protein and activator p62 (Geetha et al., 2012) were decreased in these cells (Figure 17d, e), so were the levels of the Akt activator Igf-1 (Figure 17f, g). The changes in all three Akt upstream regulators is consistent with the decrease in Akt phosphorylation levels observed in these cells.

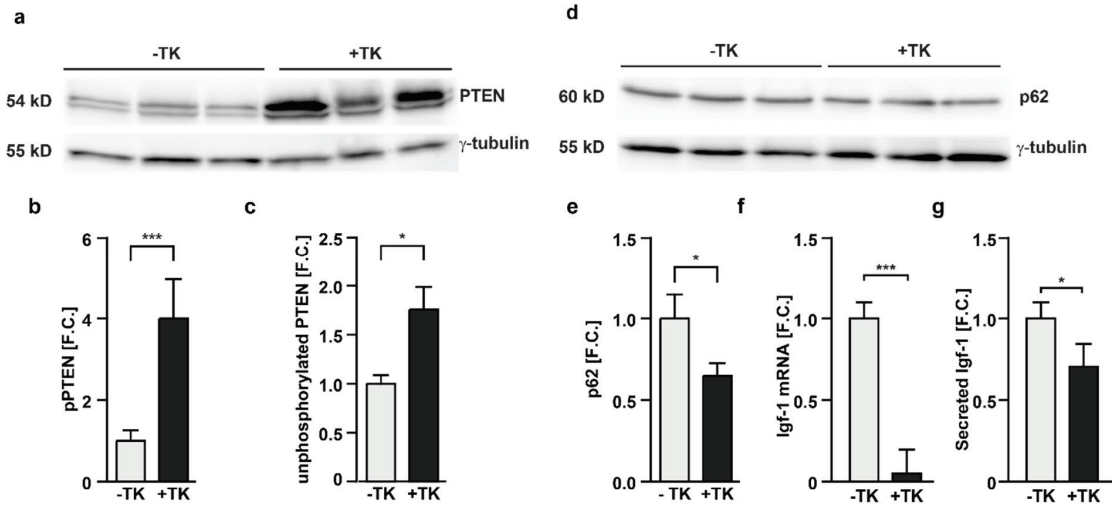

Figure 17: Dysregulation in insulin signalling effectors upstream of Akt in C2C12 cells expressing Titin kinase (TK).
(a-c) Total PTEN levels are higher in the presence of TK (n=3, mean ± s.d., t-test). (d, e) p62 levels are lower in TK-expressing cells (n=3, mean ± s.d., t-test). (f, g) TK expression reduces Igf-1 expression on both the mRNA and protein level (n=3, mean ± s.d., t-test).

4.2.3 Nfkb1 is differentially regulated in Titin-kinase expressing C2C12 cells.

The expression of TK suppressed Igf-1 mRNA and protein which argues for a TK-mediated change in transcription. To determine how TK might affect the transcription of Igf-1, I checked the transcription factor binding sites upstream of the Igf-1 gene as predicted by SA Bioscience's text mining application together with the UCSD Genome browser. One of the top transcription sites predicted was Nfκb (Figure 18a). I then compared the changes in mRNA levels in TK+ cells to those in the skeletal muscle of a published Nfkb1 knockout mouse which is resistant to disuse atrophy (GSE23497) (Wu et al., 2011). Both datasets share a total of 19 regulated genes, a significant majority of which are co-regulated (p-value = 0.022, permutation test; Figure 18b). Among the co-regulated genes are Sgk1, Eifbp4 and Igf-2 which are involved in the Pi3k-Akt pathway (Taniguchi et al., 2006; Andres-Mateos et al., 2013; Manning and Cantley, 2007). This comparison suggests that the presence of TK decrease Nfkb1-mediated transcription.

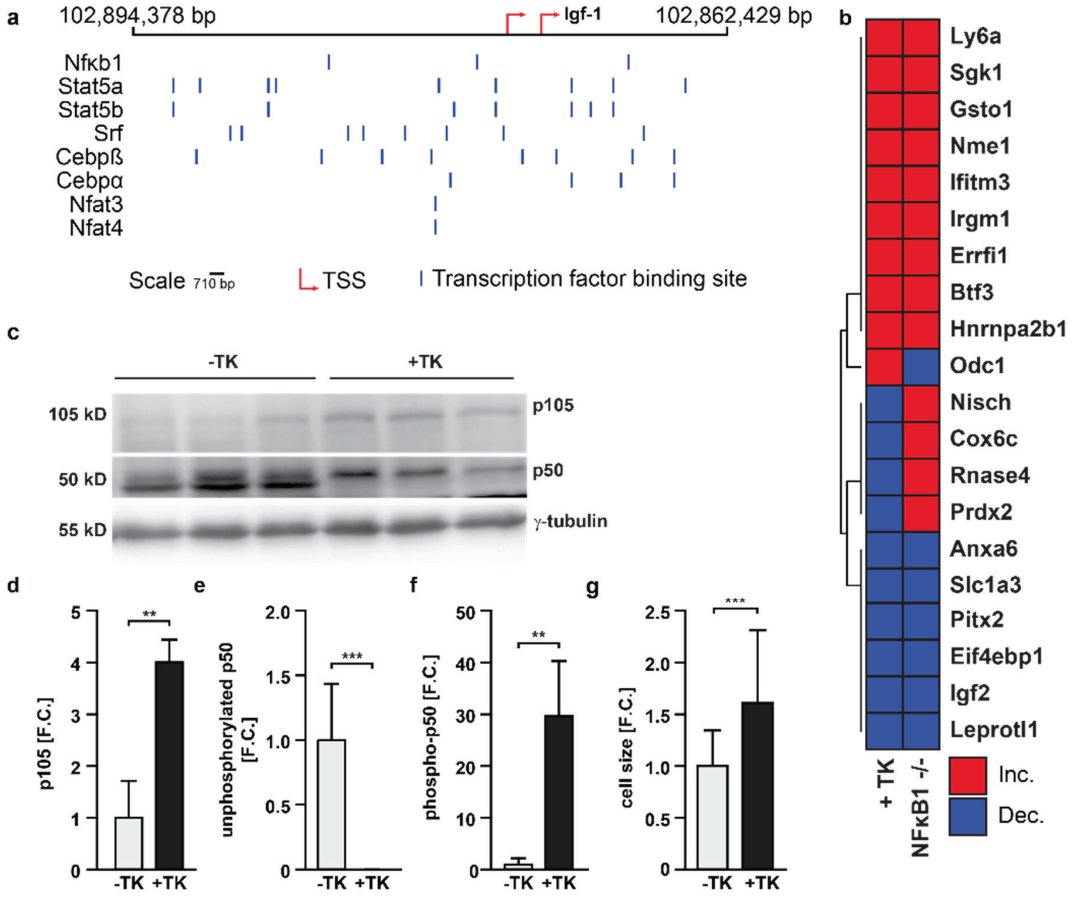

Figure 18: TK affects Nfkb1 protein levels and Nfkb1-dependent expression patterns in C2C12 cells.
(a) Predicted transcription factor binding sites upstream of Igf-1 include Nfκb sites (adopted from Qiagen's EpiTect ChIP qPCR Primer search output). (b) Nfkb1 knockout muscle and TK-expressing cells share a significant number of coregulated mRNAs (p-value<10xE-6, permutation test). (c-f) Preprocessed Nfkb1 (p105) levels are higher in the presence of TK as are the levels of phosphorylated p50 (the processed form of Nfkb1), while unphosphorylated levels of p50 are less (n=3, mean ± s.d., t-test). (g) TK increases the size of C2C12 cells (n=3, mean ± s.d., t-test).

Accordingly I checked if Nfkb1 protein levels were changed in TK+ cells. Indeed, TK expression increased pre-processed Nfkb1 (p105) and decreased processed Nfkb1 (p50). Furthermore, p50 was mostly modified in TK+ cells as suggested by the increase in intensity of a higher Mwt band (Figure 18c-f)). Consistent with a decrease in Nfkb1-mediated atrophy signalling, the average cell area of TK+ cells was significantly greater than controls (Figure 18g).

4.2.4 Titin kinase knockout mice (TKKO) are resistant to denervation-induced atrophy.

Although the skeletal muscle fibres of unchallenged TKKO mice are similar in size to wildtypes (WT), the observed regulation of Nfkb1 in cell culture suggests the possibility of a disuse-dependent phenotype as was reported for Nfkb1 KO mice (Hunter and Kandarian, 2004). Indeed denervated TKKO muscle was more resistant to atrophy than WT counterparts (Figure 19a). To gain insight into the underlying molecular mechanism, we compared changes in the mRNA expression profiles of WT and TKKO skeletal muscle 2 and 14 days post-denervation after normalization to the innervated contralateral leg (n=3 per group). Genes significantly regulated in a genotype-dependent manner (Two-way ANOVA) were assigned to functional groups by a KEGG pathway enrichment analysis (Figure 19b).

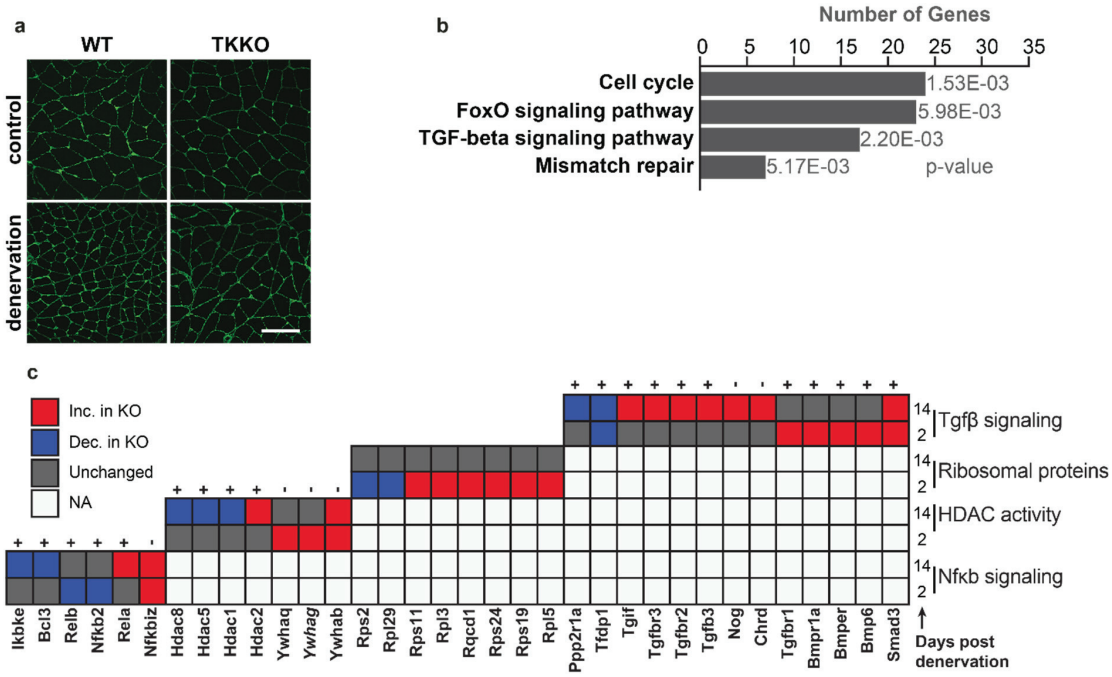

Figure 19: Titin kinase knockout (TKKO) muscle is resistant to denervation-induced atrophy.
(a) Denervated TKKO muscle is larger than wildtype (WT) as indicated by a laminin staining of the respective myofibers before and after sciatic nerve lesion (curtesy of Dr. M. Radke, unpublished). (b) KEGG pathways associated with the genes regulated during denervation depending on genotype during denervation as per a two-way ANOVA (p-value<0.05). (c) Relative change in mRNA levels of the genes involved in important atrophy pathways between TKKOs and WTs. Genes also regulated on the protein level are indicated in italics. +: activator, -: inhibitor.

FoxO and TGF-beta signalling pathways were highly enriched and include a large subset of histone deacetylase (Hdac)-related genes which are not represented as an independent term in the KEGG database. Both pathways have previously been linked to the regulation of muscle

size (Sandri et al., 2004; Sartori et al., 2013). A number of Nfkb-related and ribosomal proteins were regulated although not significantly enriched. Changes in genes related to Nfkb-, Hdac- and Tgf-beta signalling, as well as ribosomal proteins are summarized in Figure 19c. Activators of Nfkb-signalling are expressed at lower levels in the KOs after denervation compared to controls while the inhibitors are decreased which is consistent with the atrophy-resistant phenotype. Most Hdacs are expressed at lower levels in the KOs post-denervation, while the Hdac-binding family of Ywha (14-3-3) proteins are increased. These proteins help sequester Hdacs in the cytoplasm, preventing them from localizing to nucleus, where they induce the expression of atrophy-inducing genes (Moresi et al., 2010). These changes are also consistent with a decrease in Hdac-mediated atrophy signalling in denervated KO skeletal muscle. A large number of ribosomal proteins and components of the TGF-pathway are expressed at higher levels in denervated TKKO muscle, suggesting an increase in protein translation and TGF-β growth signalling in the absence of TKCD in murine muscle.

4.2.5 Nfkb/RelA, Cebpb and Xbp1 explain a large part of the Titin-kinase dependent, denervation-induced transcriptional changes.

To determine which transcription factors mediate titin kinase-dependent changes in denervated skeletal muscle I performed separate transcription factor binding site enrichment analyses on the mRNA expression profiling data acquired two and 14 days after denervation. Nfκb2 was the only transcription factor that was regulated and had binding sites upstream a significant number of the genes regulated two days after denervation. 14 days after denervation, Nfκb-binding sites were still enriched in a significant number of the regulated genes but neither Nfkb2 nor Nfkb1 themselves were changed on the mRNA level. However, RelA (p65) - another member of the NfκB transcription factor family - Cebpb and Xbp1 were regulated and also had a significant number of deregulated targets 14-days post-denervation. Together, the three transcription factors share a total of 456 targets regulated differently between KOs and WTs 14 days after denervation (Figure 20a), explaining more than half of the transcriptional changes observed. 54 of these genes are targets common to all three transcription factors, and most were transcriptionally increased (n=35). Among the increased common targets were Tgf-β and FoxO signalling components Smad3, Tgfbr3 and Araf; as well as titin itself (Figure 20b).

The observation that Nfκb-related transcription factor binding sites were enriched in genes regulated at both time points post denervation (Nfκb in both and RelA at 14 days) prompted a deeper analysis of NfκB-dependent changes.

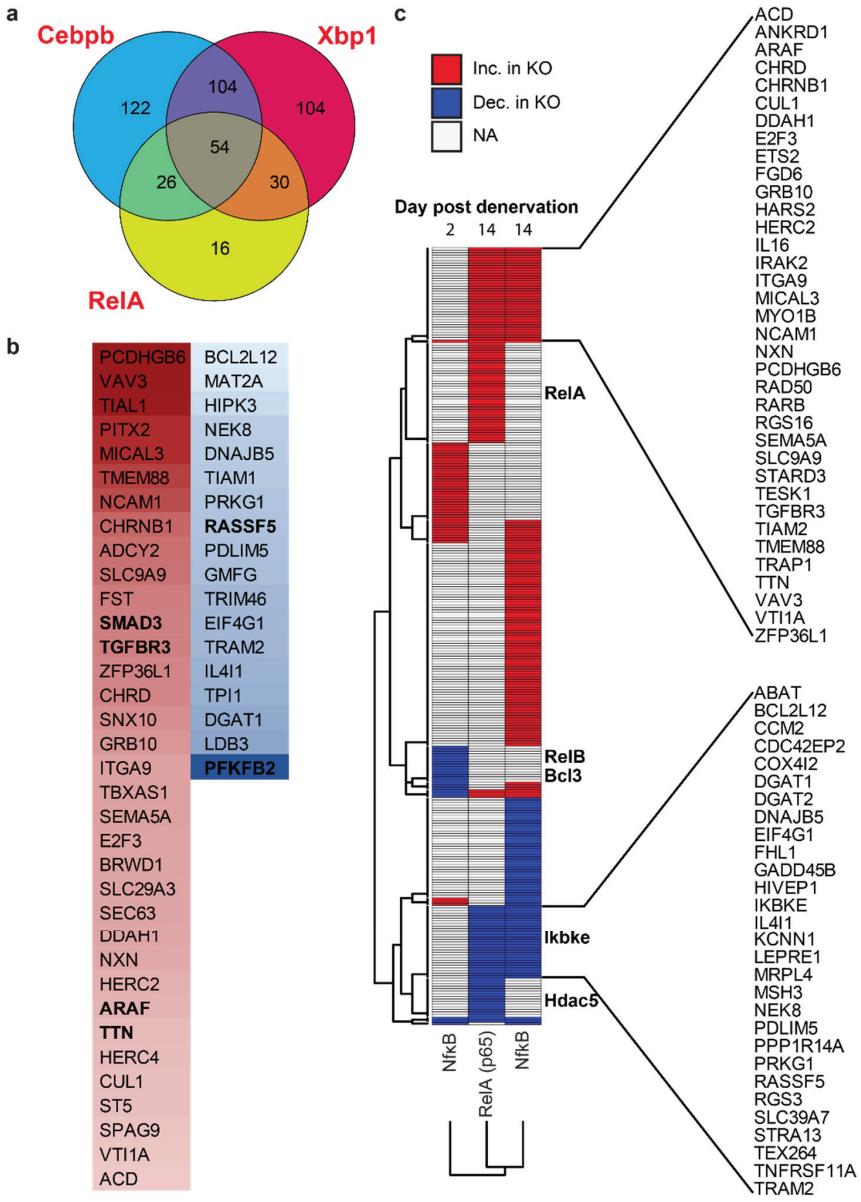

Figure 20: Titin kinase alters Nfkb transcriptional activity in denervated muscle.

(a) Venn diagram of the targets of the three transcription factors (TF) differentially regulated between WT and KO muscle 14 days after denervation. (b) The relative regulation of the 54 genes with TF binding sites for the three TFs in (a). (c) The regulation of the targets of Nfκb TFs two and 14 days post denervation reflects little overlap between the targets at the two time points, that RelA and Nfκb share several targets at 14 days and that the Nfκb components are themselves regulated in an Nfκb-dependent manner. Inc.: increased, Dec.: decreased, NA: not applicable, KO: knockout.

Only a small subset of the predicted Nfκb targets are regulated two and 14 days after denervation (n=22, corresponding to 33.3% of the targets at day two and 16.2% of those at day 14; Figure 20c). 13 of these genes were co-regulated but none are RelA targets, while 9 were counter-regulated including three RelA targets. There were no targets shared between RelA at 14 days and Nfkb at day 2 that were not also Nfkb targets at 14 days. A large number of RelA and Nfkb targets were shared at 14 days, all of which were coregulated. Among the Nfκb targets suppressed in TKKOs vs WTs two days post-denervation were RelB and Bcl3, which also regulate Nfκb transcription (Gilmore, 2006). RelA expression was increased in the TKKOs compared to controls 14 days post-denervation, while expression of the Nfκb inhibitor Iκbke (a target of both RelA and Nfkb) was reduced. These findings suggest that the Nfκb transcription factors regulate their own production (Tian et al., 2005; Lombardi et al., 1995; Ten et al., 1992; Bren et al., 2001), in a way that decreases Bcl3 and p52/RelB-mediated transcription, but supports transcription mediated by RelA/p50. Genes targeted by both RelA and Nfkb 14 days post denervation have been associated with the regulation of striated muscle size such as Ankrd1 (Zhong et al., 2015) and Titin (Peng et al., 2007, 2006), which were increased in the knockouts as well as Fhl1 (Cowling et al., 2008), which was suppressed. In C2C12 cells, the Nfkb2 precursor p100 was elevated in TK+ cells, while p52 levels were not significantly changed (Figure 21a-c). Fhl2, a functional and structural homolog of Fhl1 (Ding et al., 2009) was increased in TK+ cells (Figure. 21d, e), while Hdac5 post-translational modification was altered as evident by the appearance of a band at a slightly lower Mwt (Figure 22a-c).

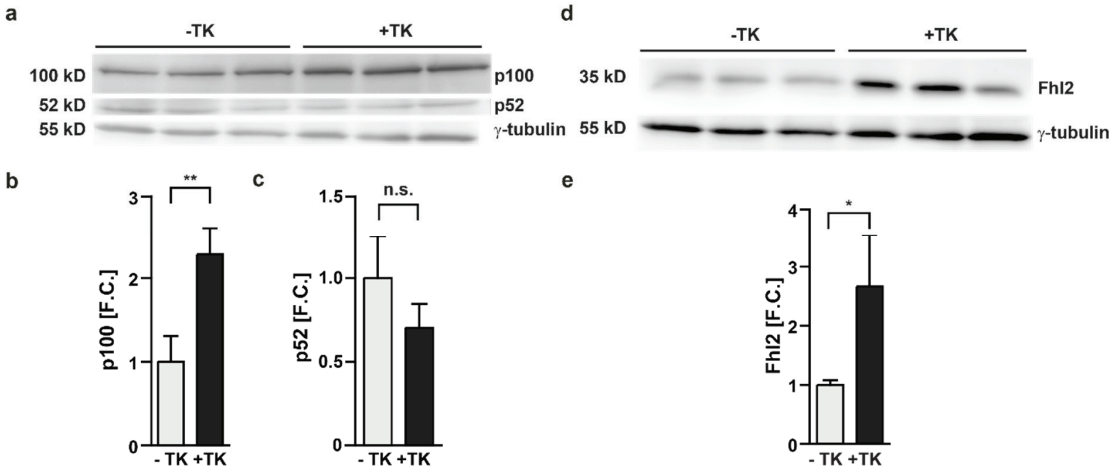

Figure 21: Titin kinase (TK) changes Nfkb2 and Fhl2 levels in C2C12 cells.
(a-c) TK increases the levels of unprocessed Nfkb2 (p100), while p52 are not significantly different (n=3, mean ± s.d., t-test). (d, e) Fhl2 levels are higher in TK-expressing C2C12 cells (n=3, mean ± s.d., t-test).

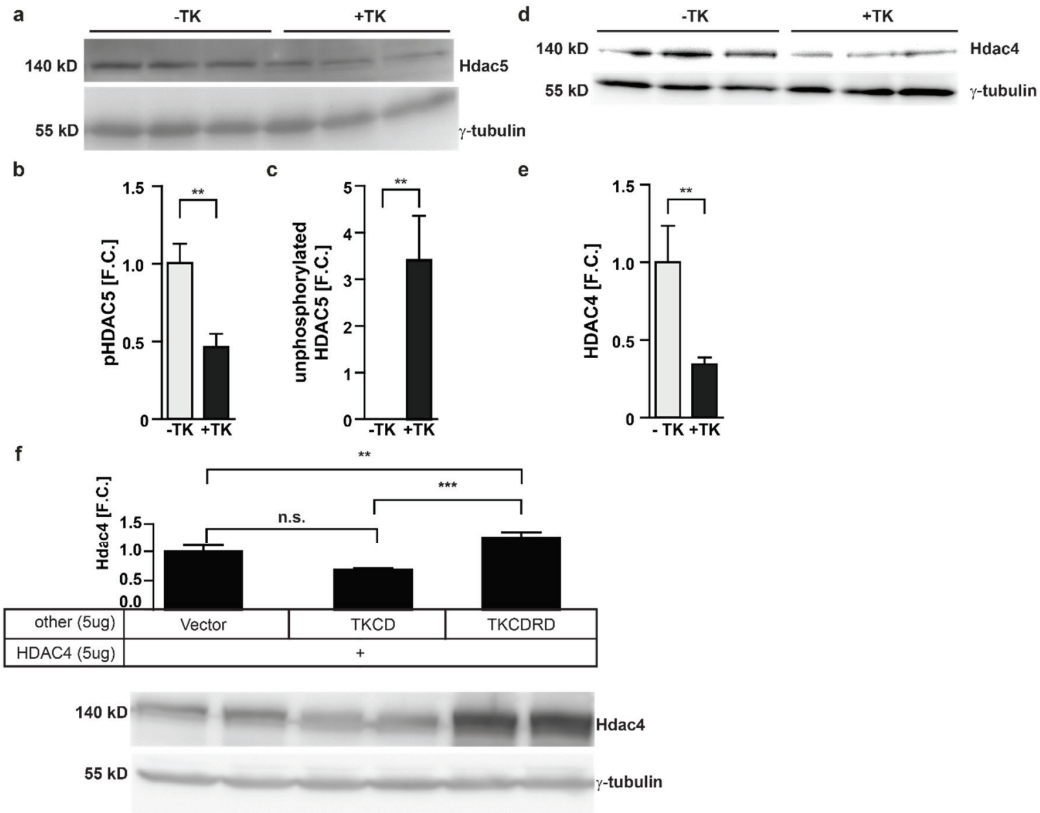

Figure 22: Titin kinase (TK) alters class II HDAC expression levels in C2C12 cells.

(a-c) TK decreases the levels of phosphorylated Hdac5 (upper band) in C2C12 cells while increasing the levels of the unphosphorylated form (lower band) (n=3, mean ± s.d., t-test). (d, e) Total Hdac4 levels are lower in TK-expressing C2C12 cells (n=3, mean ± s.d., t-test). (f) HEK293 cells transiently transfected with only the catalytic from of TK (TKCD) have relatively lower levels of Hdac4 than those transfected with empty vector or the autoinhibited form (TKCDRD) while the latter have higher levels of Hdac4 than both TKCD and control-transfected cells (n=3, mean ± s.d., One-way ANOVA, Bonferroni post-hoc test).

Hdac4 levels were also lower in TK+ cells (Figure 22d, e) and the same was observed in Hek293 cells cotransfected with Hdac4 and the catalytic domain of TK (Figure 22f).

4.2.6 Titin kinase knockout hearts are hypertrophic and have higher levels of glucose-derived metabolites.

The effect of titin's kinase domain was obvious in knockout hearts as TKKO hearts were significantly larger and heavier than their WT counterparts (Figure 23a, b). To investigate the molecular changes associated with this increase in cardiac size, I analysed Affymetrix expression differences between TKKOs and WTs. 100 genes were significantly regulated ($p<0.05$) between the genotypes, of which only ribosomal proteins were significantly enriched

as per a KEGG pathway enrichment analysis ($p<0.05$). All the regulated transcripts encoding ribosomal proteins were increased in the TKKO hearts (Rpl36, Rps12, Rps15a, Rps21, Rps24). The hypertrophy markers Myh6, Adrb1, and Nppa (Dorn et al., 2003) were also upregulated in TKKO hearts, consistent with the increase in cardiac muscle size. The gene expression analysis was complemented by a phospho-protein study of WT vs. KO left ventricular protein lysate using label-free mass spectrometry. Phosphorylation of the TK-interaction partner p62, Raptor, Akt2 (ser473) and Irs-1(Ser1101) were increased (Figure 23.c), suggesting elevated Insulin/Igf-1 signalling in TKKO hearts. In line with these changes was an increase in phospho-Ndrg2 (Figure 23.d), a gene that was overexpressed on the mRNA and protein level in hibernating grizzly bear skeletal muscle (Figure 6a) and is involved in insulin-induced cardio-protection against ischemia reperfusion injury (Sun et al., 2013).

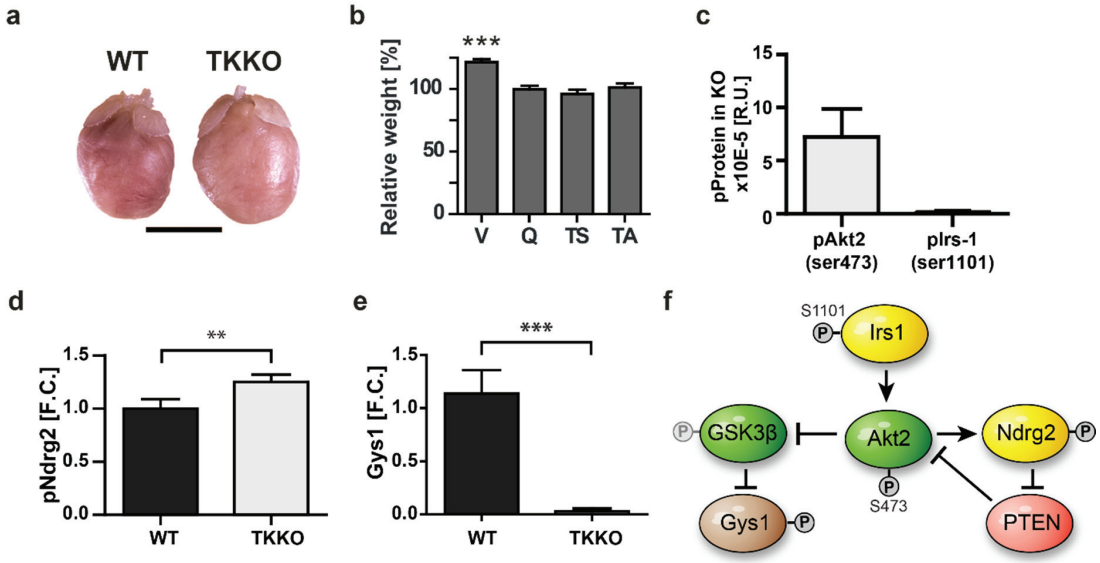

Figure 23: Titin kinase knockout (TKKO) hearts are hypertrophic and have a hyperactive Akt pathway.
(a) TKKO hearts are larger than wildtypes (WT). (b) Unlike the different skeletal muscle types depicted (Q: Quadriceps; TS: Triceps Surae, TA: Tibialis Anterior), ventricular (V) weight of TKKOs is significantly higher than WTs (Curtesy Dr. M. Radke, unpublished). (c) Levels of pAkt2 (ser473) and pIrs-1 (ser1101) are detectable in TKKO hearts but undetected in WTs. (d) pNdrg2 levels are higher in TKKO hearts while (e) pGys1 levels are lower. (f) pAkt phosphorylates Ndrg2 and indirectly dephosphorylates Gys1.

The phosphorylation of Glycogen synthase (Gys1) was reduced in TKKO hearts (Figure 21e), which is also Akt-dependent (Manning and Cantley, 2007) (Figure 23.f). A metabolomics study of the same hearts used for the phospho-proteomics analysis, revealed alterations in the levels of several amino-acids, the majority of which were non-essential (70%). All of the affected NEAAs were increased in the TKKO hearts (Figure 24a-g), while the EAAs were decreased, except for methionine (Figure 24h-j). Lactate levels were increased in the TKKO hearts (Figure 24k), as is later shown in skeletal muscle (Figure 25j).

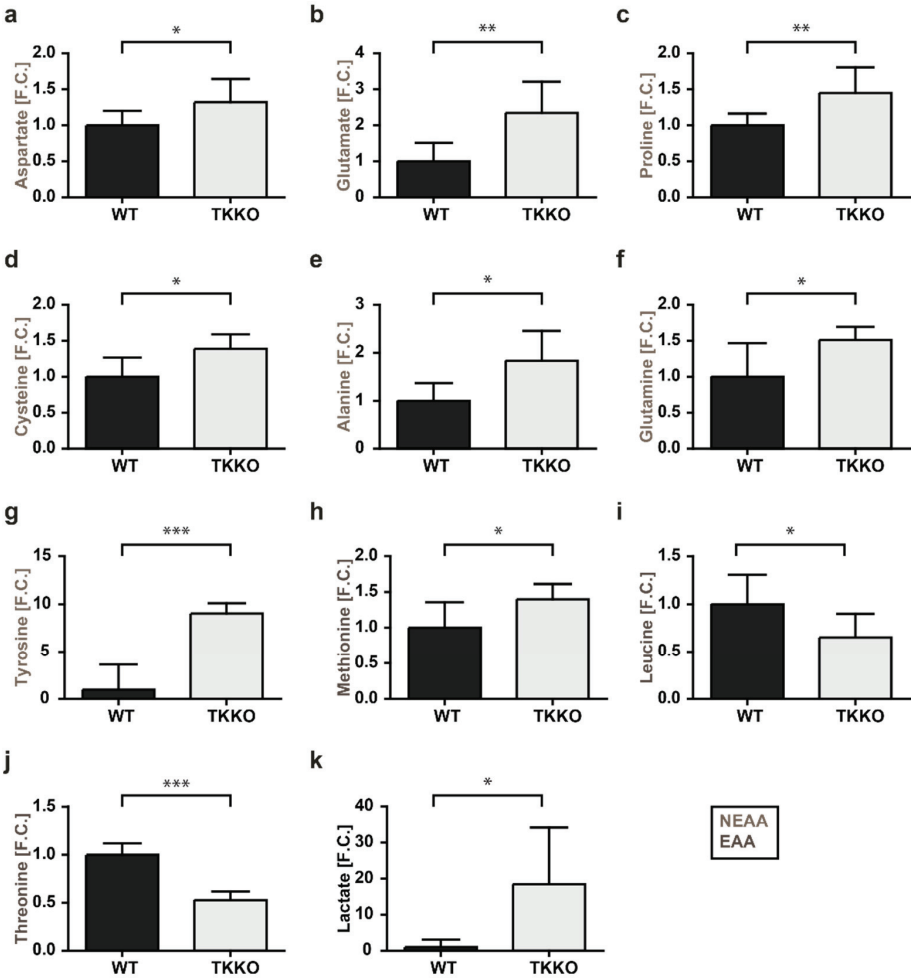

Figure 24: Amino acid and lactic acid levels are altered in Titin kinase knockout (TKKO) hearts.

(a-g) Several non-essential amino acids (NEAA) are increased in TKKO hearts. (h-j), while two of the essential amino acids (EAA) are decreased. (k) Lactate levels are higher in TKKO hearts.

4.2.7 Glucose metabolism is deregulated in TKKO skeletal muscle.

In C2C12 cells, titin kinase regulated not only cell size but also metabolism. To analyse if metabolism was also altered in TKKO skeletal muscle, mRNA expression profiles of three WT and three KO animals were compared (Figure 25a).

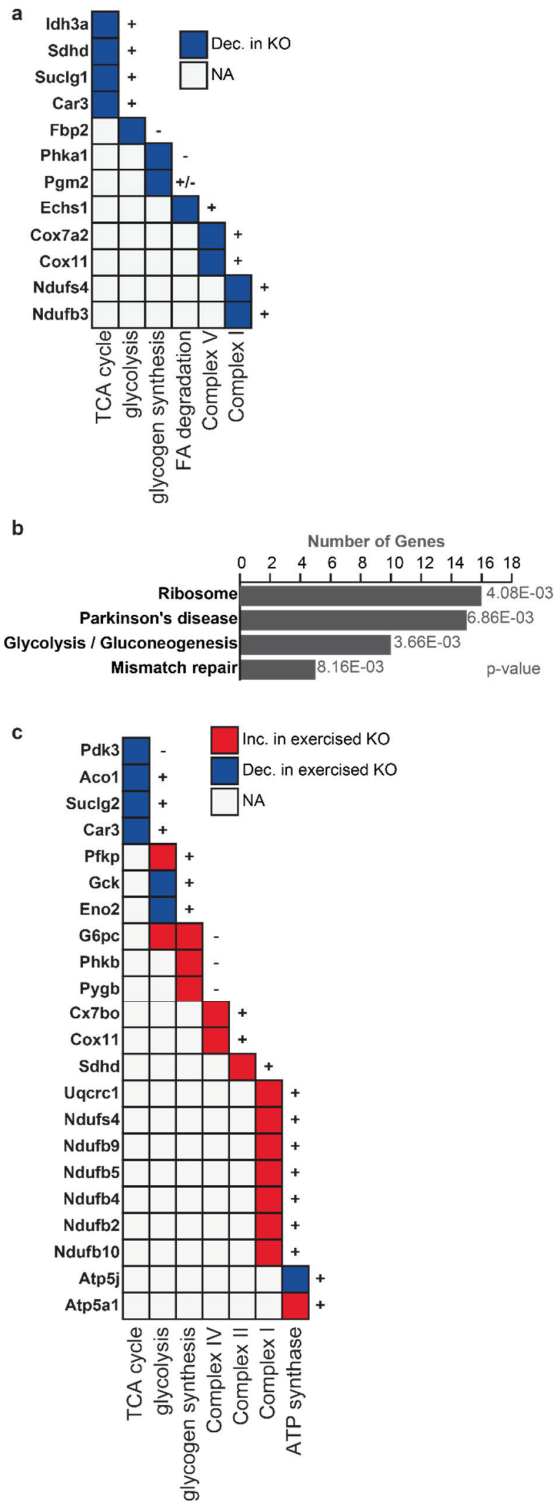

Figure 25: Transcriptional deregulation of central glucose metabolic enzymes in titin kinase knockout (TKKO) skeletal muscle. (a) Several genes involved in central glucose metabolism are deregulated on the mRNA level in TKKO gastrocnemius (GA) muscle. (b) The genes regulated between trained WTs and KOs enrich to KEGG terms related to protein synthesis and metabolic deregulation among others. (c) The relative regulation of metabolic genes on the mRNA level in KOs after a month of training suggest an adaptive increase (inc.) in oxidative phosphorylation while TCA cycle enzymes remain lower (dec.). NA: not applicable.

Indeed, several enzymes related to glucose and energy metabolism were decreased in unchallenged KO muscles. However the number of enzymes is not high enough to be significantly represented in a Gene ontology analysis. After a month of regular treadmill training, changes in metabolic gene expression become more evident (Figure 25b) and are for the most part reversed compared to the changes in unchallenged animals (Figure 25 c). For example components of the ETC and glycogen breakdown are higher in TKKOs, while expression levels of the TCA cycle enzymes remain lower in TKKOs even after training. Proteins regulated in TKKOs as determined by SILAC include the components of Complex I of the ETC Ndufa1 and Ndufv2 and several TCA proteins, all of which were decreased (Figure 26a-e). Phkg1, the catalytic domain of the glycogen phosphorylase kinase complex and Ugp2, which catalyses the first step in glycogen synthesis were also decreased (Figure 26f-g). The enzymatic changes were complemented with an increase in glucose, lactate and malate (Figure 26h-j) as well as glycogen. The changes in metabolites and enzymes of glycolysis/gluconeogenesis, TCA cycle and glycogen metabolism are summarized in Figure 26k. These changes suggest that ATP production in TKKO muscle is lower, and glycogen immobilization more difficult, making these animals less capable of generating the energy necessary to support strenuous physical activity.

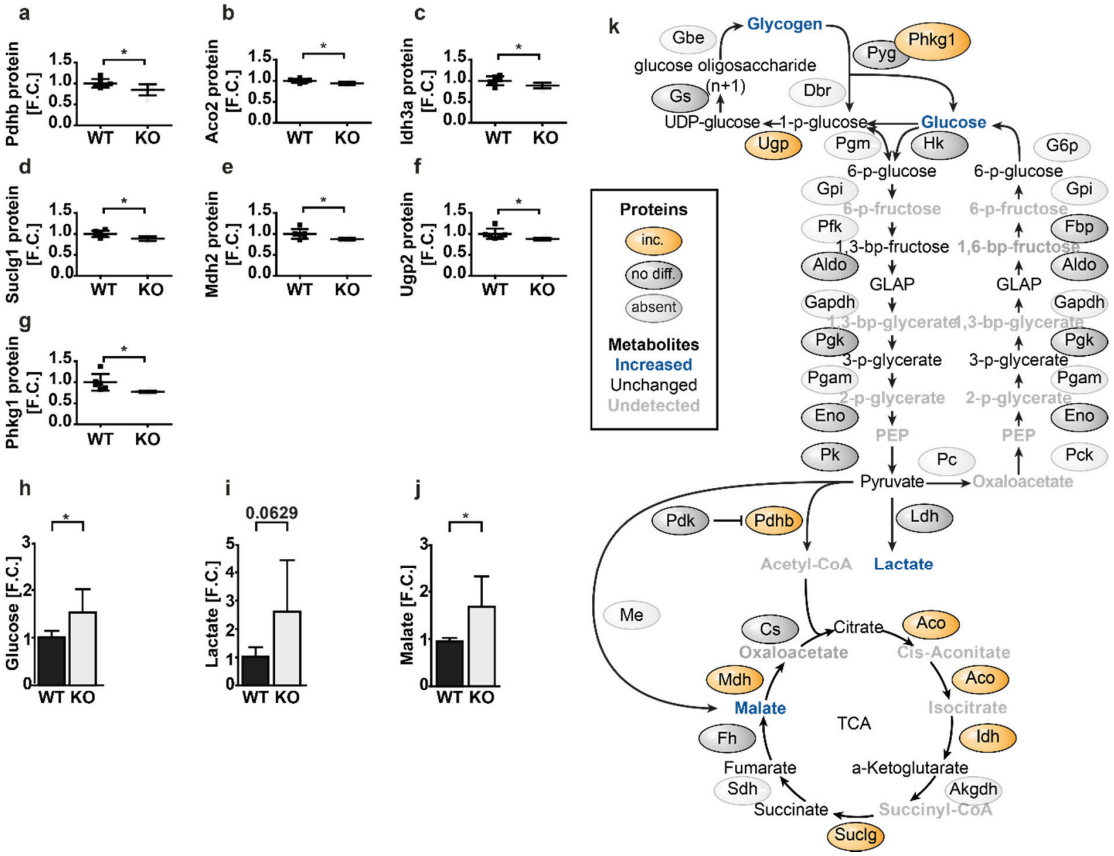

Figure 26 TCA cycle activity is decreased in titin kinase knockout (TKKO) skeletal muscle.

(a-g) Enzymes of central glucose metabolism are decreased in the KO GA, while (h-j) glucose, lactate and malate are increased. (k) Overlaying the protein and metabolite changes in TKKO muscle to central glucose metabolism indicates that most changes are in glycogen synthesis and breakdown, and the (Tricarboxylic acid) TCA cycle activity under basal activity levels. No diff.: unchanged, NA: not available.

5 Discussion

Striated muscle size and function is regulated in response to changes in use. Muscles used frequently or that work against a greater load adjust by increasing their size to adapt to the increase in demand. The opposite is true if a muscle is used less frequently, or in adjustment to a decreased load. Depending on the context, a change in muscle size can be favourable or detrimental. For example, cardiac and skeletal muscle hypertrophy often occur in athletes (Scharf et al., 2010), improving their cardiac output, supporting better skeletal muscle oxygenation and strengthening the skeletal muscle used during exercise which improves the athletes' performance over time. On the other hand, astronauts in space experiences cardiac and skeletal muscle atrophy, which subjects them to complications when back on Earth (LeBlanc et al., 1995). Skeletal muscle atrophy is common in many other situations as well, such as long-periods of hospitalization, bone fracture, aging, muscle denervation and situations of calorie restriction (Glass, 2003). Increasing our understanding of muscle size regulation could thus help us enhance favourable and prevent detrimental changes in muscle. For this reason, a lot of research has been done to understand how muscle size is regulated under different conditions implicating a range of pathways including the Pi3k-Akt-mTor (Rommel et al., 2001), Nfκb (Hunter and Kandarian, 2004), Tgf-β-Bmp (Sartori et al., 2013) and HDAC/HAT (Moresi et al., 2010) signalling pathways. Nevertheless, pharmaceutical companies are still on the search for better therapeutic targets/approaches to help prevent pathological muscle atrophy and/or hypertrophy more efficiently, and with minimal side effects as many of these pathways have been associated with other functions such as cell survival, carcinogenesis, and inflammation.

While innervation supplies stimuli about muscle use, mechanical stimulation has been shown to improve muscle function in patients with decreased neuroskeletal communication and astronauts in microgravity (Bunse et al., 2003; Layne et al., 1998). Also, hibernating bears, which are resistant to muscle atrophy despite a decrease in muscle load and food intake in winter, are able to maintain muscle mass even after denervation (Lin et al., 2012). This suggests innervation-independent pathways that regulate muscle size, which prompted us to study the molecular changes occurring in the skeletal muscle of hibernating bears, as well as in the muscle of mice that lack a domain, which has long been considered a mechanical sensor that communicates to intracellular signalling pathways.

5.1 Metabolic changes in hibernating and aging muscle suggest changes in NEAA availability that affect myotube size.

We chose hibernating bears as a model of atrophy-resistance because - unlike small mammalian hibernators - bears maintain their body temperature at about 30 ^{o}C throughout hibernation while the small hibernators go into torpor (Carey et al., 2003). Torpor involves decreasing body temperatures to as low as -2 ^{o}C in some cases (Carey et al., 2003). At such low temperatures metabolism is largely suppressed and so is believed to play an important role in decreasing muscle loss in these animals. In bears, the relatively mild decrease in temperature compared to torpor was shown to be independent of the decrease in temperature (Tøien et al., 2011). According to my results, this decrease in metabolism in the muscle is attributable to a decrease in protein levels of a large number of metabolic enzymes. The change in these enzymes leads to a decrease in ATP production in muscle during hibernation according to the metabolic models constructed using this data. Despite the suppression of several metabolic enzymes, some of those affecting glycolysis and TCA cycle activity were increased, which suggests that they are maintained for metabolic processes besides energy production. Indeed, the models predict an increase in some glycolytic and TCA-cycle-derived NEAAs. Although no previous studies have reported a change in NEAA levels in bear skeletal muscle during hibernation, changes in plasma levels are known to differ (Stenvinkel et al., 2013a). On the other hand, according to the metabolic models generated using data from skeletal muscle of aging females, older female subjects with less muscle mass have lower levels of the same NEAAs that were increased in the metabolic model of skeletal muscle in hibernation. An example of a physiological condition in which NEAA concentrations were measured and associated with changes in skeletal muscle size include a study of ewes. In this study NEAA levels were lower in twin foetuses which usually have lower muscle mass than a single foetus close to birth (Sales et al., 2014). Together with the findings reported here, this supports the hypothesis that NEAA availability in skeletal muscle is associated with an increase in muscle mass. According to the data, in C2C12 cells, an increase in NEAA levels in muscle might not just co-occur with other changes that increase muscle size, but also contributes to growth, as supplementing NEAAs to the cells increased myotube size and suppressed the atrophy marker MAFbx. This effect is not necessarily due to an increase in NEAA-rich proteins as these proteins are not significantly increased during hibernation according to the data. It is likely that NEAAs have a role in atrophy signalling, as has already been shown for arginine (Jewell et al., 2015) and glutamine (MacLennan et al., 1987) which affect mTOR activity. mTOR mediates protein synthesis via

inhibiting 4ebp1 and activating ribosomal protein S6 (Figure 27). It also activates Akt by phosphorylation at Ser-473, which in turn suppressed FoxO1-mediated MAFbx expression, which could explain the decrease in MAFbx upon NEAA supplementation.

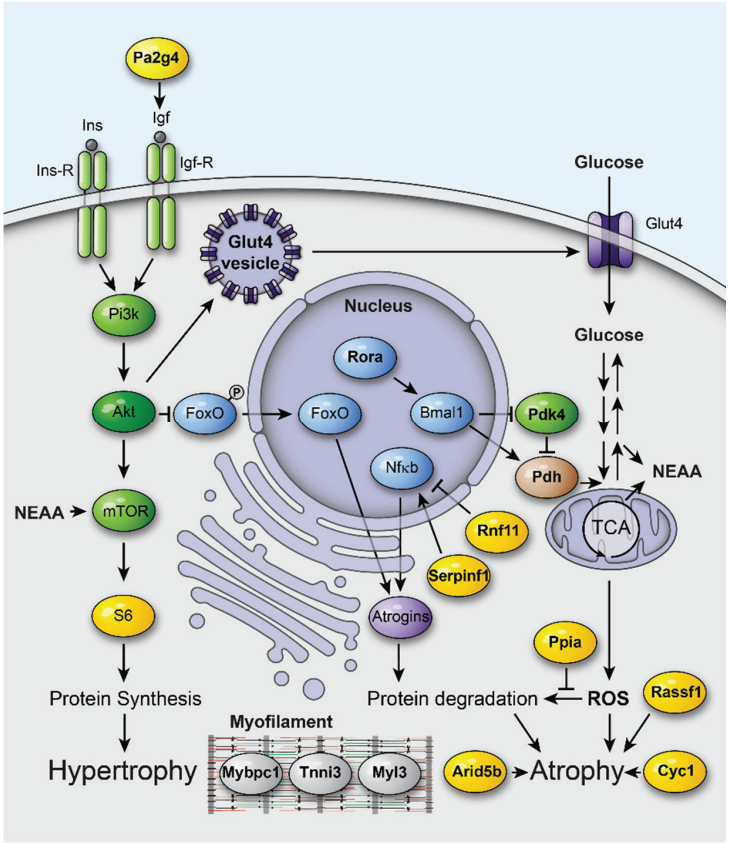

Figure 27: Summary of trophic signalling in skeletal muscle of hibernating grizzly bears.
Genes differentially regulated in hibernation vs. skeletal muscle atrophy (bold) relate to trophic signalling and metabolism. NEAA: non-essential amino acids; ROS: reactive oxygen species; TCA: Tricarboxylic acid cycle.

5.2 Hibernation-specific transcriptional changes implicate Pdk4, Serpinf1 and insulin signalling in the regulation of muscle mass.

The transcriptional changes occurring during hibernation helped identify genes that are important in controlling muscle size. By comparing the changes in mRNA levels in hibernation to those in several atrophy-inducing conditions we identified a group of genes that are regulated in the majority of the groups, some of which have already been implicated in the regulation of muscle size and function (Table 18). We also identified a group that was selectively regulated in hibernation, which I followed up on more closely. Genes regulated selectively in hibernation

could help explain the bear's specific ability to maintain its mass during hibernation compared to humans and mice in comparable situations. Although the majority of these genes have not been linked to altered muscle function or size, they are co-expressed with genes that are important in regulating basic organ function according to a guilt-by-association approach. Two of the genes that have not been reported to affect muscle size include a metabolic enzyme Pdk4 (Zhang et al., 2014) which was also regulated on the protein level and a Nfkb activator, Serpinf1 (Yabe et al., 2005). Based on its function as an inhibitor of TCA cycle activity, Pdk4 reduces ROS production as it indirectly limits oxidative phosphorylation, an important source for ROS production in the cell (Zhang et al., 2014). A reduction in ROS production decreases protein damage and degradation, which would help preserve muscle mass. A reduction of Pdk4 levels in C2C12 cells, resulted in increased transcription of the atrophy marker MAFbx, consistent with an increase in protein degradation. This supports the hypothesis that during hibernation Pdk4 protein levels are primarily increased and that changes in mRNA levels are secondary. On the other hand, the reduction of Serpinf1 decreased MAFbx levels in C2C12 cells. This could be explained by its role as an Nfkb activator (Yabe et al., 2005). Since Nfkb signalling mediates disuse atrophy (Hunter and Kandarian, 2004), the loss of Serpinf1 can be expected to cause atrophy via decreased Nfκb activity, which increases MAFbx expression. In this scenario, suppressing Serpfin1 transcription could be the primary level of regulation during hibernation, and not necessarily secondary to changes in protein level or activity. These findings support the relevance of the genes regulated only in hibernation to the regulation of atrophy signalling in non-hibernators, but indicate that the directionality of change alone does not indicate whether these genes promote or inhibit atrophy. Since the regulation of these genes was driven by natural selection to improve the survival chances of bears during and soon after hibernation they potentially serve as good drug targets in therapies developed to reduce muscle loss with minimal side effects. The utility of biomimicry for the conservation of muscle mass has been demonstrated for Sgk1, which is regulated in squirrel muscle during hibernation and increases muscle size in mice (Andres-Mateos et al., 2013).

In hibernating bears there were changes in a significant number of insulin signalling components, and all these changes reflect alterations that could enhance the pathway's activity if maintained at the protein level. An increase in insulin sensitivity in muscle would be favourable during hibernation considering the pathway's positive effect on muscle growth (Rommel et al., 2001), and argues for a tissue-specific regulation of insulin sensitivity in hibernation, during which circulating insulin levels are unchanged (Figure 28). Contrary to the

observations in muscle, adipose tissue is insulin-resistant during hibernation (Nelson et al., 2014), facilitating lipid breakdown and increasing the availability of glycerol which is not only the major energy source during hibernation, but also contributes to the synthesis of non-essential amino acids (Ahlquist et al., 1984). This keeps blood glucose levels constant, while decreasing the demand on muscle protein as an amino acid and energy source during the period of reduced caloric intake. Together, an increase in skeletal muscle sensitivity and adipose tissue resistance to insulin could work together to help maintain muscle mass during hibernation (Figure 28).

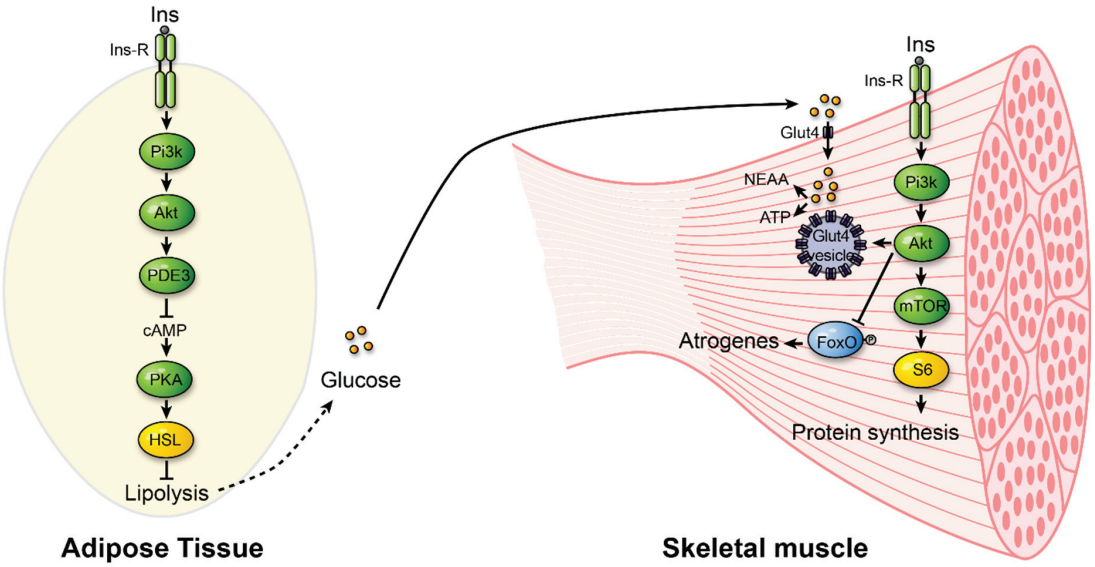

Figure 28: Differential insulin sensitivity between adipose tissue and skeletal muscle in hibernating bears.
Insulin inhibits lipolysis in adipose tissue, while stimulating glucose uptake, protein synthesis and muscle growth in skeletal muscle.

5.3 Titin kinase regulates energy metabolism and muscle growth by modulating NfκB and Akt signalling.

The giant muscle protein titin contains a serine/threonine kinase domain that resembles the structure of the myosin light chain kinases (MLCK), suggesting a role in signalling (Mayans et al., 1998). Titin's kinase domain rearranges when titin is stretched, exposing the catalytic core but not at resting forces, suggesting that it could serve as a mechanotransducer (Puchner et al., 2008). The identification of mechanotransducers in skeletal muscle could help explain how - independent of neural input - muscle can adopt to changes in use (Linke, 2008). Although titin kinase targets and binding partners have been identified (Mayans et al., 1998; Lange et al., 2005), little is known about the effect of titin kinase on muscle growth and metabolism or if the

kinase function is necessary for these effects. Here we show that the absence of titin kinase has a favourable effect on muscle size based on observations made in denervated skeletal muscle and hearts of mice lacking the catalytic domain of titin's kinase region (TKKO). Transcriptional changes occurring in the skeletal muscle of the denervated TKKOs compared to WTs suggest that alterations in Nfκb, Hdac Class I and II and Tgf-β signalling occur in the absence of titin's catalytic domain. Two days post-denervation a significant number of the deregulated transcripts in the TKKOs are potential NfκB targets and Nfkb2 itself is decreased on the mRNA level. The decrease in Nfkb2 levels in the TKKO muscle could, in part, explain why TKKOs are resistant to denervation-induced atrophy. Nfκb transcription factors have been shown to regulate one another, and this is also reflected in the transcriptional changes in denervated TKKO muscle. The decrease in Nfkb2 early after denervation is accompanied by a decrease in its Nfκb-related targets RelB and Bcl3. RelB binds DNA only when dimerized with other Nfκb transcription factors, the most common of which is the processed Nfkb2 (p52), while Bcl3 is known to enhance p50-mediated transcription. Together Bcl3 and p50 are important in mediating disuse atrophy in muscle (Hunter and Kandarian, 2004). Thus, changes in Nfkb2 early after denervation help-mediate changes in other atrophy-related genes in TKKO skeletal muscle. 14 days after denervation, Nfκb2 levels are not significantly different between WTs and KOs, but Nfκb transcriptional targets are nevertheless enriched. On the other hand, targets of another NfκB transcription factor, RelA, are enriched at this time point and its mRNA levels are also increased. Unlike p50 and Bcl3, RelA does not regulate disuse (Hunter et al., 2002). And according to the data it is likely that RelA-p50 transcription is enhanced 14 days after denervation in the TKKOs, promoting the transcription of growth-associated genes (eg: Ankrd1, E2F3, Titin) while suppressing the transcription of atrogenes such as Fhl1 (Cowling et al., 2008) and the Nfκb inhibitor Ikbke (Figure 29). These genes are among the list of a significant number of common RelA and Nfkb targets deregulated in TKKO muscle 14 days after denervation. RelA also enhances its own transcription and suppress that of Hdac5, amplifying the RelA-dependent transcriptional changes, while suppressing Hdac5-mediated atrophy (Moresi et al., 2010). This suggests that changes in Hdac5 signalling might be secondary to changes in Nfkb transcription in TKKO skeletal muscle. However, Hdac5 was not the only component of Hdac signalling that was regulated in TKKO muscle. Several 14-3-3 proteins were increased early and later after denervation in TKKOs, including 14-3-3-γ, which was also decreased on the protein level in unchallenged TKKO muscle. These proteins are important in shuttling and sequestering class II Hdacs in the cytosol (Martin et al., 2007), preventing them from enhancing atrogene transcription.

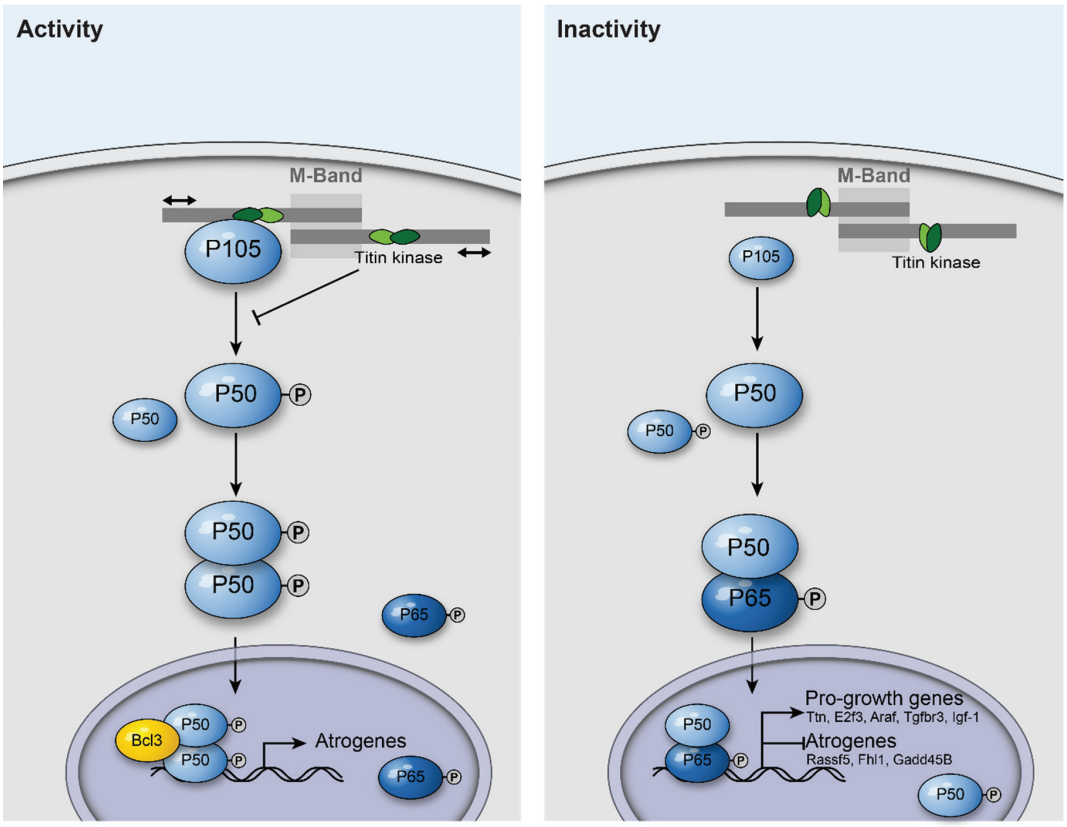

Figure 29: The effect of Titin kinase (TK) on NfκB1-mediate growth signalling. Upon stretch Titin kinase's catalytic domain binds p105 preventing its processing into p50. Also whatever p50 is present in the cell is predominantly phosphorylated, increasing the avidity of p50 for DNA and enhancing the binding of p50-p50 homodimers. Together with higher levels of Bcl3, p50-p50 activates the transcription of atrogenes. This decreases the chances of p65-p50 heterodimer formation, which is usually the predominant dimer in the cells and inhibits atrogene expression, while enhancing the expression of growth promoters.

Thus, an increase in their levels in TKKO muscle could help explain its resistance to denervation-induced atrophy. Furthermore, Hdac2, a class I HDAC was increased in TKKO muscle after denervation. Unlike Hdac5, Hdac2 is mostly nuclear as it does not contain a nuclear export signal (NES) and is thus not affected by 14-3-3 proteins (de Ruijter et al., 2003). It is known to increase cardiac size in mice (Trivedi et al., 2007). An increase in the majority of regulated ribosomal protein-coding mRNAs in TKKO muscle suggests an increase in protein synthesis during denervation, while the majority of the changes in the components of the Tgf-β pathway reflect changes that enhance signalling down this pathway. Enhanced Tgf-β signalling increases organ size and helps explain why TKKOs are more resistant to denervation-induced atrophy (McPherron et al., 1997) Expression changes in Tgf-β signalling components such as Tgfbr3 and Smad3 14 days post-denervation are possibly mediated by Cebpb, Xbp1

and/or RelA as they have binding sites for all three TFs. Unlike RelA, little is known about the role of Xbp1 in regulating muscle size, but Cebpb interacts with RelA in modulating gene transcription (Xia et al., 1997), and regulates cardiac growth in response to exercise (Boström et al., 2010). In C2C12 cells, the expression of the catalytic domain of titin kinase increases the levels of unprocessed Nfkb1 and 2 (p105 and p100 respectively), and decreases the levels of processed Nfkb1 (p50) but only mildly affects p52 levels. The increase in p105 and p100 levels could be due an increase in transcription, but were unchanged according to the mRNA expression profiling data. Another possibility is altered processing in the presence of TK, which explains the accompanying decrease in the processed form of p105 (p50) and the trend seen in case of p52. A decrease in p50 could explain the resemblance between the mRNA expression profiles of Nfkb1 knockouts and TK+ cells as well as the increase in cell size compared to controls. Despite the decrease in p50 in the TK+ cells, the majority of it exists in a modified form as suggested by a higher migration band in immunoblots for the protein. One of the most common modifications of p50 is phosphorylation, which increases the binding affinity of p50 for DNA (Misteli et al., 1998). In this case, DNA-binding p50 homodimers could be more abundant in these cells, mediating the expression of a subset of genes different to those regulated by p50-RelA heterodimers. Similar changes might not be detectable in the complete Nfkb1 KO mice, and could explain the discrepancy seen between the Nfkb1 KOs and TK+ cells with respect to the minor subset of counter-regulated genes. Currently little is known about the role of TK in regulating Nfkb1 and only with further experiments on skeletal muscle tissue could we get a more accurate picture of the associated changes. However, one possibility is that in WT muscle, the presence of titin's kinase domain alters Nfkb1 protein levels in a way that promotes the formation of phospho-p50 homodimers, even if p105 processing is suppressed, which, together with increasing levels of Bcl3, would enhance disuse/denervation-induced atrophy in comparison to TKKOs. Although many of the transcriptional changes seen in the TKKO skeletal muscle were not detected in the C2C12 cells, some were changed on the protein level such as Hdac5, of which the unphosphorylated from was increased in TK+ cells. This suggests that TK increases the levels of unphosphorylated Hdac5, which is the form that is present and active in the nucleus (Martin et al., 2007). A similar change in skeletal muscle could help explain why muscles lacking TK are more resistant to atrophy. Another class II HDAC, Hdac4, was decreased in the presence of TK and no changes in migration were detectable suggesting that total protein levels might be lower in the presence of TK. An increase in Hdac4 levels alone in TKKO muscle could not explain why it is more atrophic as Class II knockouts have less atrophy and it is possible that Hdac4 levels are decreased in the presence

of TK in C2C12 cells to compensate for the increase in active Hdac5. Levels of Fhl2 are lower in TK- cells, while its homolog - Fhl1 - is lower on the transcriptional level in TKKOs. This suggests that the regulation of this family of proteins is titin kinase dependent in both systems. Fhl proteins 1-3 suppress growth (Ding et al., 2009). A relative decrease in Fhl protein levels in denervated TKKO muscle could explain why they are more resistant to atrophy compared to WTs.

Unlike striated muscle, very few changes in signalling components are regulated between TKKO and WT hearts according to the mRNA profiling data. The largest group of regulated mRNAs are those that encode ribosomal proteins, which as in the denervated skeletal muscle, are mostly increased. Individual markers of cardiac hypertrophy such as Nppa, Myh6 and Adrb1 were also elevated in the TKKO hearts. On the total protein level, few changes were detected, while changes in Akt signalling was prominent according to changes in phospho-protein profiles. The changes mainly reflect an increase in Akt-signalling (Figure 30). For example, pAkt and pIrs-1 levels were not detectable in the WTs, but measurable in TKKO hearts, suggesting that these phosphoproteins are increased in the absence of TK. Phosphorylation of Akt at ser473 is associated with an increase in activity, while the serine phosphorylation of Irs-1 is mostly inhibitory and Irs-1-dependent as part of a negative feedback loop (Taniguchi et al., 2006). These changes were also accompanied with an increase in the Akt-responsive protein Ndrg-2, while levels of Gys1 were decreased, an event which requires that Akt suppress Gsk3β by phosphorylating it at Ser9 (Manning and Cantley, 2007). Gsk3β however was not detected in this dataset. As increased Akt activity has been shown to increase organ size, these changes suggest that titin kinase suppressed Akt signalling muscle in cardiac muscle, which is why WT hearts are smaller than TKKOs. In C2C12 cells, TK+ cells expressed lower levels of pAkt upon insulin stimulation, arguing that TK suppresses insulin-induced signalling in these cells. This was accompanied by a decrease in the levels of the Akt-signalling activator Igf-1 (Rommel et al., 2001), and the Irs-1 activator p62 (Geetha et al., 2012), while the Akt inhibitor PTEN was decreased (Manning and Cantley, 2007). Worth noting is that p62 was shown to exist together in a complex with the muscle specific ubiquitin ligase MuRF2 and TK at the sarcomeric M-band (Lange et al., 2005). This could explain why it is decreased in the presence of TK, which enables p62 binding to MuRF2 and its subsequent degradation Unlike the hearts, where pGsk3β is likely higher in the absence of TK, C2C12 cells lacking TK express lower levels of pGsk3β, suggesting the involvement of another Akt-like kinase in its regulation. One such kinase could be Sgk1 which is transcriptionally increased in the TK+, and

similarly increased in Nfkb1 knockout muscle. This suggests that Sgk1 up-regulation in TK+ cells is secondary to the decrease in p50 levels.

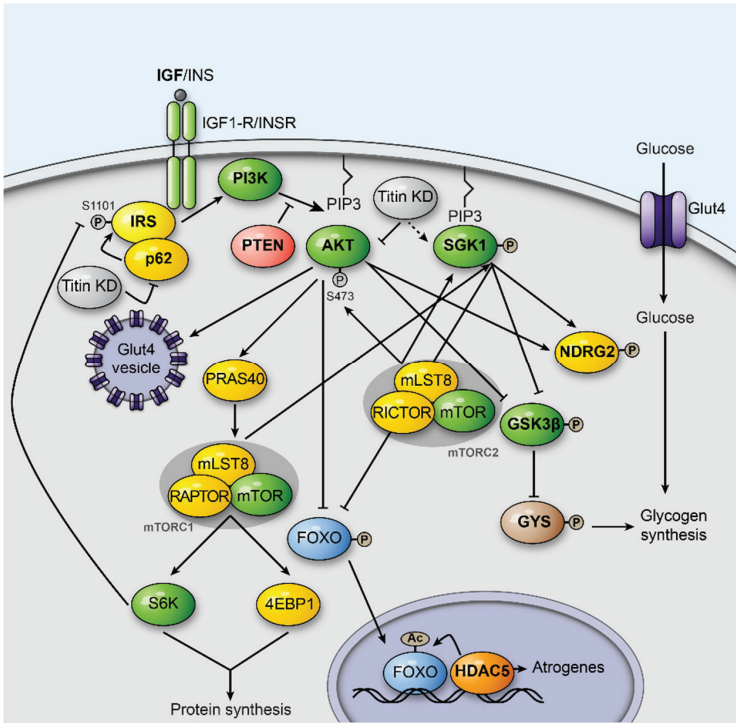

Figure 30: The effect of Titin kinase (TK) on Akt signalling.
TK suppresses Akt phosphorylation at Ser473, which leads to a decrease in pNdrg2 levels as well as Gsk3β in KO hearts. This is accompanied by a decrease in the inhibitory serine phosphorylation of Irs1 as downstream effects are already in check. A decrease in Akt activity would also lead to a decrease in FoxO inhibition by phosphorylation, and consequently an increase in atrogene transcription. Also Akt activation of the mTORC1 complex would decreased in the presence of TK, which translates to a decrease in protein synthesis. A less active Akt would also means less Glut4 vesicle translocation to the membrane, decreasing glucose uptake in these cells. In C2C12 cells, Sgk1 is higher in the presence of TK overriding the effect of decreased Akt activity on Gsk3β and other events downstream. A decrease in pAkt could be due to a decrease in p62 or Igf-1 levels, an increase in PTEN or all three together. Names in bold correspond to signalling components that were regulated in the hearts or C2C12 cells in a TK-dependent manner.

Like Akt, Sgk1 is known to increase muscle size by regulating similar downstream targets (Andres-Mateos et al., 2013). In fact, hibernating squirrels resist atrophy due to an increase in Sgk1 signalling, despite a decrease in pAkt levels (Andres-Mateos et al., 2013). No indication of a similar change is evident in the heart according to the different types of data generated from the murine hearts, which could explain the discrepancy in signal propagation beyond Akt. TKKO hearts also have higher levels of several NEAAs, and a decrease in two of three

deregulated EAAs. This suggests that NEAA also play a role in increasing cardiac size in TKKOs. The decrease in EAAs could be due to their increasing incorporation into proteins in the hypertrophic hearts, while methionine, the EAA that was increased in these hearts is taken up at high levels as it is essential in priming the synthesis of all new peptides. A possible explanation for the increase in NEAA levels in TKKO hearts is the hyperactive Akt pathway, which regulates the uptake of more glucose by increasing Glut4 translocation to the membrane (Taniguchi et al., 2006). Because the heart relies on lipid oxidation for energy generation, excess glucose might be shuttled towards the production of other metabolites, such as NEAAs or lactate, which was also notably increased in the TKKO hearts. Thus the results suggest that TK suppresses striated muscle growth in both hearts and skeletal muscle, but achieves that by regulating different pathways in the two muscle types (Figure 31). There is no difference in the size of TKKO and WT skeletal muscle, but the results suggest that they are less capable of producing of ATP. Indications to that include the decrease in several glycolytic, TCA cycle and respiratory chain enzymes on the mRNA and protein level in TKKO muscle. This is accompanied by an increase in glucose, lactate, malate and glycogen. Together these changes suggest that TKKO skeletal muscle cannot efficiently shuttle the pyruvate generated from glycolysis into the TCA cycle which decreases the amount of electron carriers generated and shuttled towards ATP generation via oxidative phosphorylation (Figure 32a). As a result, pyruvate is shuttled towards lactate or malate production, explaining why they are elevated in TKKO muscle. Because the amount of ATP produced in TKKO skeletal muscle is less, the muscle likely enhances glucose uptake to compensate, explaining the increase in glucose levels in the muscle. Glucose is consequently not only shuttled towards glycolysis, but also towards glycogen synthesis. Many of the changes in the mRNA levels of the glucose metabolic genes is reversed when the animals are exercised on a treadmill regularly for a month suggesting that exercise can rectify some of the changes in glucose metabolism, including oxidative respiration, and glycogen turnover. However, TCA cycle enzymes remain less in the exercised TKKOs arguing that TK is important for TCA cycle enzyme transcription, a function that is not compensated by the induction of other signalling pathways in response to increased exercise (muscle use). One possible mechanism by which TCA enzyme levels are regulated is via p52-RelB. P52-RelB heterodimers are important for mitochondrial biogenesis via regulating Pgc1b levels (Bakkar et al., 2012). Knocking down either of these genes impairs oxidative phosphorylation in skeletal muscle, and since TKKO muscles have lower levels of these two genes, they might be incapable of transcribing Pgc1b and possibly other genes that are important for mitochondrial biogenesis, including TCA cycle enzymes.

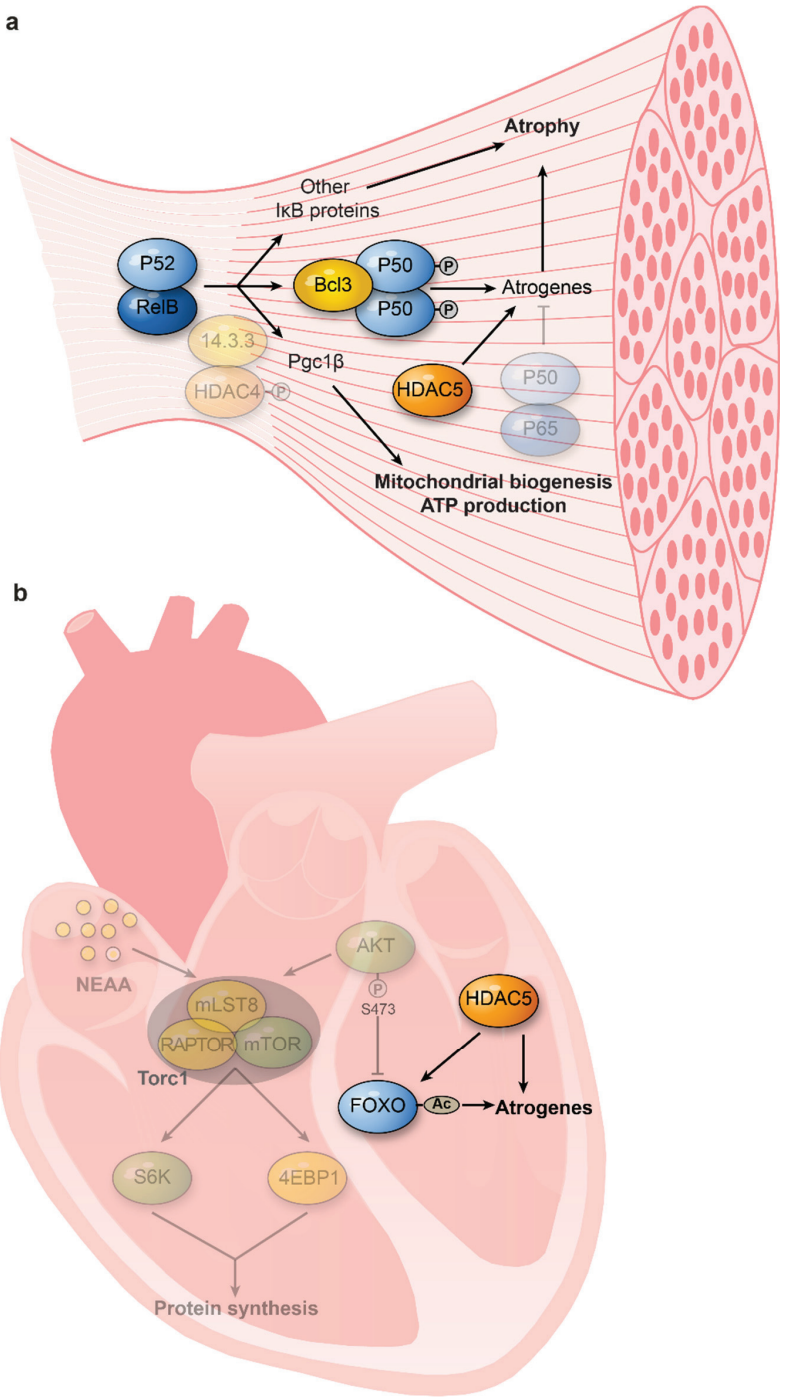

Figure 31: Titin kinase (TK) affects different regulatory pathways in skeletal and cardiac muscle.
(a) In skeletal muscle Nfκb signalling is the predominant Titin kinase effector pathway, affecting atrogene expression and mitochondrial biogenesis. (b) In the heart Akt signalling is predominantly affected by TK. In both, Hdac5 signalling is likely affected.

In C2C12 cells expressing TK, glycolytic and respiratory chain activity were both increase as indicated by these cells' higher ECAR and OCR levels,. This suggests that, in this system, TK expression is also associated with an increase in energy production even though the changes in the mRNA levels of many of the respiratory chain components are decreased, which could be secondary to an increase in protein levels or activity in these cells (Figure 32b).

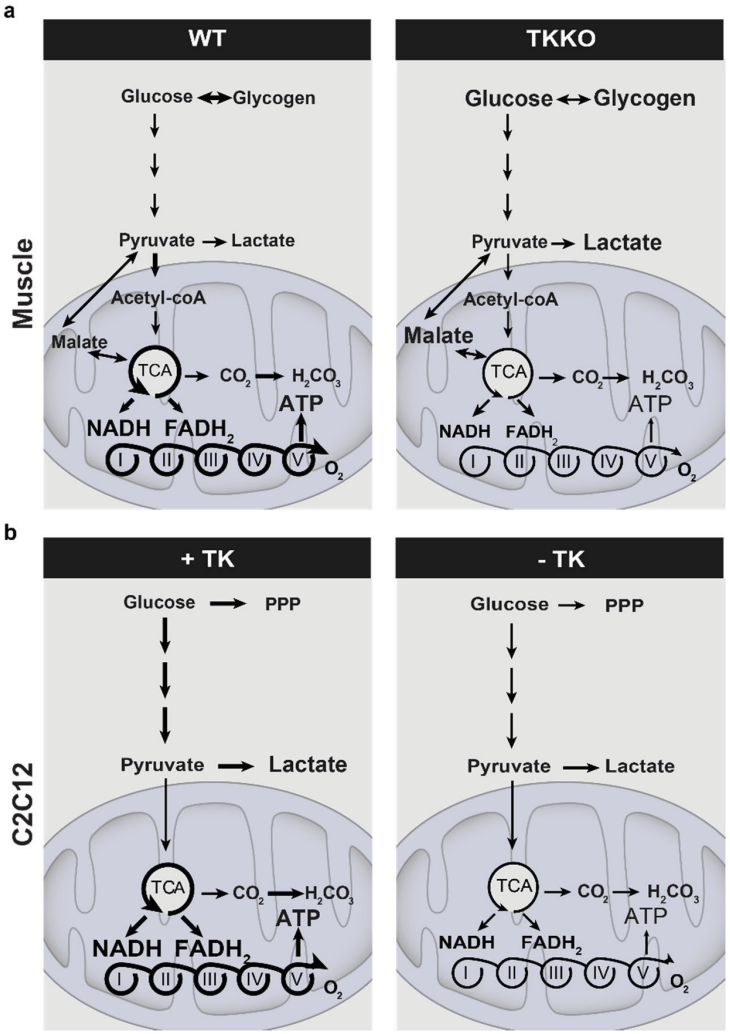

Figure 32: Titin kinase (TK) increases ATP production in both C2C12 cells and murine muscle.
(a) TK knockouts (TKKOs) have lower oxidative phosphorylation capacity than wildtypes (WT), so they compensate by uptaking more glucose which is mostly converted to glycogen and lactic acid. This decreases the amount of ATP produced in TKKO muscle. (b) TK expressing C2C12 cells have both more aerobic and anaerobic activity, which results in the production of more CO2, lactic acid and eventually more ATP than controls.

Besides the change in NEAAs, an increase in lactate is the only obviously difference in glucose-derived metabolites in TKKO hearts. This is similar to the changes in skeletal muscle lactate levels. However a functional analysis done on these hearts has shown that they are similar to WT hearts (Dr. M. Radke, personal communication), suggesting that these hearts are capable of efficiently producing the energy they need to meet demands in unchallenged animals. This is also supported by the absence of major changes in metabolic enzyme mRNA and protein levels in these hearts. Also, if Nfkb signalling is not largely affected by TK in the hearts, and the skeletal muscle phenotype is indeed p52-RelB-dependent, the absence of TK would not be expected to have a great effect on the heart. Thus the data suggest that titin kinase is important in the regulation of ATP production in both C2C12 cells and skeletal muscle, but not so much in the heart. Further experiments would need to be conducted on the TKKOs to verify if the changes in metabolism are of functional consequence on the animals' ability to perform strenuous activity compared to WTs.

5.4 Primary and secondary effectors of titin kinase-mediated signalling.

The initial idea behind generating a cell line expressing TK in an inducible manner was to facilitate the generation of time resolved data, providing insight into early (primary) and late (secondary) TK-dependent molecular changes. Unfortunately, preliminary experiments indicated a mild effect of Doxycycline - the drug used to suppress TK expression in these cells - on some of the signalling pathways we were interested in studying. This complicated the use of the system for the generation of the time resolved data, making drug-induced versus TK-induced changes harder to discriminate. The changes reported here were all at steady, as the cells were used as normal stable cells in the absence of Doxycycline. Thus, a statement about primary and secondary effects are mostly speculative and made in context of existing knowledge about the Titin kinase binding partners and crosstalk between the different signalling pathways.

The titin kinase as a structure is similar to the serine/threonine CaMK kinase family and has long been thought to be catalytically active when not inhibited by its autoregulatory domain that folds back on and blocks its catalytic core in the absence of stretch (Puchner et al., 2008). In vitro, the only substrate confirmed to be phosphorylated in a kinase-dependent manner is Tcap, a protein that caps titin's N-terminus and stabilizes its integration at the Z-disc (Mayans et al., 1998). However, a recent report by the author of the original Tcap paper argues that what was reported as a titin kinase-dependent change in Tcap phosphorylation was actually an

artefact mediated by a contaminating kinase present in the insect cells in which TK was expressed, and that titin kinase itself is not catalytically active due to the presence of two non-canonical amino acids; methionine-34 and aspartate-147 in sequences in which are mostly absent in active kinases (Bogomolovas et al., 2014; Lange et al., 2005). Nevertheless, titin kinase affects proteins binding at the M-band (Bogomolovas et al., 2014). Among the proteins that differentially bind at the M-band based on the presence of TK are MuRF1 and MuRF2, both muscle-specific ubiquitin ligases that affect protein turnover, and could explain part of the changes we see in the signalling pathways described in this thesis.

The effect of Titin kinase on Akt signalling can be mainly explained via its ability to bind p62 in a Nbr1-dependent manner (Lange et al., 2005). This interaction was shown to recruit Murf2 to p62, an event which could lead to an increase in p62 ubiquitination and degradation. P62 enhances Irs-1-mediated signalling, and thus enhances Akt signalling (Geetha et al., 2012). In the absence of TK, cells have higher levels of p62, and are capable of phosphorylating Akt upon insulin stimulation, a response which is dampened in the presence of TK. This is in line with the observations made in both animals and C2C12 cells, suggesting that this could be one of the primary events occurring in a TK-dependent manner.

The effect of titin kinase on NfκB signalling holds in both C2C12 cells and animal skeletal muscle. Nfkb transcription factors regulated themselves and one another, making the identification of a primary culprit difficult without further interaction data. However, it is likely that TK affects the processing of Nfkb1 from p105 to p50, which alters the amount of total p50 as well as its DNA binding capacity (Figure 31) and subsequently alters the transcription of various other NfκB signalling components, including Nfkb2, which is important for Pgc1β and RelB transcription. In this scenario one would imagine that TK enhances the p50 homodimer-Bcl3 mediated disuse-atrophy response, as well as p52-RelB mediated mitochondrial biogenesis (Figure 32). This could explain why Nfκb1 is not deregulated on the mRNA level in these animals since all NfκB-related transcriptional changes seen in the TKKOs are secondary to a shift in p105 processing and p50 versus phospho-p50 stoichiometry. However, if this is because of p105 binding TK, sequestering it from degradation or if this is secondary to the binding and MuRF-mediated degradation of an IκK needs to be validated by co-immunoprecipitation experiments. In C2C12 cells, we see a decrease in the levels of Hdac4 in the presence of TK, which suggests that its degradation might also be regulated in a TK-MuRF dependent manner. Total Hdac5 levels might not be changed, with only a shift from phosphorylated to unphosphorylated in the presence of TK, supporting that this is not a kinase-

dependent effect, but secondary to a change in the expression levels of a Hdac5 kinase in the presence of TK. Both CamkI and CamkIId are increased on the mRNA level in the TKKO skeletal muscle, suggesting that a decrease in their expression level in the presence of TK could explain the decrease in Hdac5 phosphorylation. Interestingly, Camk1 has a NfκB binding site in its promoter, suggesting that its transcriptional regulation might also be Nfκb-mediated.

5.5 Conclusion and perspective

This work compares how disuse atrophy is communicated in different mammalian systems. One of them is the hibernating grizzly bear, which is naturally resistant to disuse atrophy. By identifying the evolutionary changes that confer bears with the ability to maintain muscle mass, we hoped to identify pathways that could be harnessed for improved therapy of patients who suffer from muscle atrophy. Indeed, we found metabolic changes that not only suppress unnecessary energy expenditure in muscle during hibernation, but also enhance the production of non-essential amino acids, which might help prevent muscle atrophy in these animals. Furthermore, non-essential amino acids increase the size of cultured murine cells, suggesting that this treatment could support an increase in muscle mass in non-hibernating species. This is relevant for affordable healthcare as non-essential amino acids are, on average, cheaper than essential amino acids. Unlike essential amino acids, non-essential amino acids can be synthesized by the organism and treatments that support their production in muscle could improve local availability.

In addition we identified a set of genes that are differentially expressed only during hibernation, and not in six other atrophy-inducing conditions in murine and human muscle, suggesting that these contribute to the ability of grizzly bear muscle to resist atrophy. Several of these genes have previously been linked to the regulation of muscle size and/or function and I show that two of these genes not previously associated with muscle growth affect atrophy signalling in murine myotubes. This further supports the relevance of this approach to extending our knowledge of growth regulators not only in bears but also other mammals. Indeed, we utilize pathways selected over thousands of years to prevent atrophy in one species to achieve the same in humans, while minimizing the negative effect on other critical aspects of muscle function. The targeting of more than one gene in combination might further improve outcome for patients.

In a complementary approach to identifying growth regulators in a large animal model protected from disuse atrophy, we used a knockout mouse lacking the mechanically activated titin kinase domain to understand how muscle activity regulates growth.

I show that the absence of this mechanosensor in murine skeletal muscle could lead to a decrease in ATP production, compromising the ability of these animals to perform strenuous physical activity. The disruption of NfκB signalling could underlie this change in metabolic

activity in the absence of TK. TK-dependant changes in NfκB signalling were also important in regulating muscle size in response to disuse.

The effect on muscle growth extends to the unchallenged heart, which is bigger in the absence of the kinase, without additional functional consequences. The main changes in signalling in this case relate to Akt signalling, suggesting differences in the function of the kinase domain as a signalling intermediate in skeletal versus cardiac muscle (Figure 32). Together, these findings confirm the role of titin kinase in communicating information about muscle use and link titin kinase to metabolic and trophic signalling pathways.

In summary, titin's kinase domain is an important regulator of striated muscle signalling, which expands on our knowledge of how mechanical input is converted into a biochemical signal. The work links titin kinase to the NfκB and Akt pathway, and shows that grizzly bear muscle is resistant to disuse atrophy, in part, because of its ability to modulate signalling down these same pathways. Importantly not only these pathways can be targeted in a clinical setting to help prevent muscle atrophy, but also others differentially regulated in hibernating and non-hibernating mammals.

6 Bibliography

Ahlquist, D., R. Nelson, Steiger, Jones, and Ellefson. 1984. Glycerol metabolism in the hibernating black bear. *Journal of Comparative Physiology B*. 75–79.

Akashi, M., and T. Takumi. 2005. The orphan nuclear receptor RORalpha regulates circadian transcription of the mammalian core-clock Bmal1. *Nat. Struct. Mol. Biol.* 12:441–448.

Alway, S.E., J.D. MacDougall, D.G. Sale, J.R. Sutton, and A.J. McComas. 1988. Functional and structural adaptations in skeletal muscle of trained athletes. *J. Appl. Physiol.* 64:1114–1120.

Anderson, M.E., J.H. Brown, and D.M. Bers. 2011. CaMKII in myocardial hypertrophy and heart failure. *J. Mol. Cell. Cardiol.* 51:468–473.

Andres-Mateos, E., H. Brinkmeier, T.N. Burks, R. Mejias, D.C. Files, M. Steinberger, A. Soleimani, R. Marx, J.L. Simmers, B. Lin, et al. 2013. Activation of serum/glucocorticoid-induced kinase 1 (SGK1) is important to maintain skeletal muscle homeostasis and prevent atrophy. *EMBO Mol Med*. 5:80–91.

Bakkar, N., K. Ladner, B.D. Canan, S. Liyanarachchi, N.C. Bal, M. Pant, M. Periasamy, Q. Li, P.M.L. Janssen, and D.C. Guttridge. 2012. IKKα and alternative NF-κB regulate PGC-1β to promote oxidative muscle metabolism. *J. Cell Biol.* 196:497–511.

Baskin, K.K., B.R. Winders, and E.N. Olson. 2015. Muscle as a "Mediator" of Systemic Metabolism. *Cell Metab.* 21:237–248.

Berenji, K., M.H. Drazner, B.A. Rothermel, and J.A. Hill. 2005. Does load-induced ventricular hypertrophy progress to systolic heart failure? *Am. J. Physiol. Heart Circ. Physiol.* 289:H8–H16.

Berridge, M.J., M.D. Bootman, and H.L. Roderick. 2003. Calcium signalling: dynamics, homeostasis and remodelling. *Nat Rev Mol Cell Biol*. 4:517–529.

Bialek, P., C. Morris, J. Parkington, M. St Andre, J. Owens, P. Yaworsky, H. Seeherman, and S.A. Jelinsky. 2011. Distinct protein degradation profiles are induced by different disuse models of skeletal muscle atrophy. *Physiol. Genomics*. 43:1075–1086.

Bindea, G., B. Mlecnik, H. Hackl, P. Charoentong, M. Tosolini, A. Kirilovsky, W.-H. Fridman, F. Pagès, Z. Trajanoski, and J. Galon. 2009. ClueGO: a Cytoscape plug-in to decipher functionally grouped gene ontology and pathway annotation networks. *Bioinformatics*. 25:1091–1093.

Bodine, S.C. 2013. Hibernation: the search for treatments to prevent disuse-induced skeletal muscle atrophy. *Exp. Neurol.* 248:129–135.

Bogomolovas, J., A. Gasch, F. Simkovic, D.J. Rigden, S. Labeit, and O. Mayans. 2014. Titin kinase is an inactive pseudokinase scaffold that supports MuRF1 recruitment to the sarcomeric M-line. *Open Biol*. 4.

Boström, P., N. Mann, J. Wu, P.A. Quintero, E.R. Plovie, D. Panáková, R.K. Gupta, C. Xiao, C.A. MacRae, A. Rosenzweig, et al. 2010. C/EBPβ controls exercise-induced cardiac growth and protects against pathological cardiac remodeling. *Cell*. 143:1072–1083.

Boudina, S., and E.D. Abel. 2007. Diabetic cardiomyopathy revisited. *Circulation*. 115:3213–3223.

Bren, G.D., N.J. Solan, H. Miyoshi, K.N. Pennington, L.J. Pobst, and C.V. Paya. 2001. Transcription of the RelB gene is regulated by NF-kappaB. *Oncogene*. 20:7722–7733.

Britto, J.M., S. Lukehurst, R. Weller, C. Fraser, Y. Qiu, P. Hertzog, and S.J. Busfield. 2004. Generation and characterization of neuregulin-2-deficient mice. *Mol. Cell. Biol.* 24:8221–8226.

Bunse, M., N. Bit-Avragim, A. Riefflin, A. Perrot, O. Schmidt, F.R. Kreuz, R. Dietz, W.I. Jung, and K.J. Osterziel. 2003. Cardiac energetics correlates to myocardial hypertrophy in Friedreich's ataxia. *Ann Neurol*. 53:121–123.

Carey, H.V., M.T. Andrews, and S.L. Martin. 2003. Mammalian hibernation: cellular and molecular responses to depressed metabolism and low temperature. *Physiol. Rev.* 83:1153–1181.

Centner, T., J. Yano, E. Kimura, A.S. McElhinny, K. Pelin, C.C. Witt, M.L. Bang, K. Trombitas, H. Granzier, C.C. Gregorio, et al. 2001. Identification of Muscle Specific Ring Finger Proteins as Potential Regulators of the Titin Kinase Domain. *J Mol Biol*. 306:717–726.

Chen, Y.W., P. Zhao, R. Borup, and E.P. Hoffman. 2000. Expression profiling in the muscular dystrophies: identification of novel aspects of molecular pathophysiology. *J Cell Biol*. 151:1321–1336.

Clapham, D.E. 2007. Calcium signaling. *Cell*. 131:1047–1058.

Clarke, B.A., D. Drujan, M.S. Willis, L.O. Murphy, R.A. Corpina, E. Burova, S.V. Rakhilin, T.N. Stitt, C. Patterson, E. Latres, et al. 2007. The E3 Ligase MuRF1 degrades myosin heavy chain protein in dexamethasone-treated skeletal muscle. *Cell Metab.* 6:376–385.

Clark, K.A., A.S. McElhinny, M.C. Beckerle, and C.C. Gregorio. 2002. Striated muscle cytoarchitecture: an intricate web of form and function. *Annu. Rev. Cell Dev. Biol.* 18:637–706.

Cowling, B.S., M.J. McGrath, M.-A. Nguyen, D.L. Cottle, A.J. Kee, S. Brown, J. Schessl, Y. Zou, J. Joya, C.G. Bönnemann, et al. 2008. Identification of FHL1 as a regulator of skeletal muscle mass: implications for human myopathy. *J Cell Biol*. 183:1033–48.

Van Dam, S., T. Craig, and J.P. de Magalhães. 2015. GeneFriends: a human RNA-seq-based gene and transcript co-expression database. *Nucleic Acids Res.* 43:D1124–1132.

DeFronzo, R.A., and D. Tripathy. 2009. Skeletal muscle insulin resistance is the primary defect in type 2 diabetes. *Diabetes Care*. 32 Suppl 2:S157–163.

Dietz, V., G. Colombo, and L. Jensen. 1994. Locomotor activity in spinal man. *Lancet*. 344:1260–1263.

Ding, L., Z. Wang, J. Yan, X. Yang, A. Liu, W. Qiu, J. Zhu, J. Han, H. Zhang, J. Lin, et al. 2009. Human four-and-a-half LIM family members suppress tumor cell growth through a TGF-beta-like signaling pathway. *J. Clin. Invest.* 119:349–361.

Dorn, G.W., J. Robbins, and P.H. Sugden. 2003. Phenotyping hypertrophy: eschew obfuscation. *Circ. Res*. 92:1171–1175.

Dyar, K.A., S. Ciciliot, L.E. Wright, R.S. Biensø, G.M. Tagliazucchi, V.R. Patel, M. Forcato, M.I.P. Paz, A. Gudiksen, F. Solagna, et al. 2014. Muscle insulin sensitivity and glucose metabolism are controlled by the intrinsic muscle clock. *Mol Metab*. 3:29–41.

Emig, D., N. Salomonis, J. Baumbach, T. Lengauer, B.R. Conklin, and M. Albrecht. 2010. AltAnalyze and DomainGraph: analyzing and visualizing exon expression data. *Nucleic Acids Res*. 38:W755–762.

Engel, S.M., B.R. Joubert, M.C. Wu, A.F. Olshan, S.E. Håberg, P.M. Ueland, W. Nystad, R.M. Nilsen, S.E. Vollset, S.D. Peddada, et al. 2014. Neonatal genome-wide methylation patterns in relation to birth weight in the Norwegian Mother and Child Cohort. *Am. J. Epidemiol.* 179:834–842.

Faulkner, J.A., C.S. Davis, C.L. Mendias, and S.V. Brooks. 2008. The aging of elite male athletes: age-related changes in performance and skeletal muscle structure and function. *Clin J Sport Med*. 18:501–507.

Fedorov, V.B., A.V. Goropashnaya, N.C. Stewart, Ø. Tøien, C. Chang, H. Wang, J. Yan, L.C. Showe, M.K. Showe, and B.M. Barnes. 2014. Comparative functional genomics of adaptation to muscular disuse in hibernating mammals. *Mol. Ecol.* 23:5524–5537.

Fill, M., and J.A. Copello. 2002. Ryanodine Receptor Calcium Release Channels. *Physiological Reviews*. 82:893–922.

Finkel, T., and N.J. Holbrook. 2000. Oxidants, oxidative stress and the biology of ageing. *Nature*. 408:239–247.

Gaignard, P., M. Menezes, M. Schiff, A. Bayot, M. Rak, H. Ogier de Baulny, C.-H. Su, M. Gilleron, A. Lombes, H. Abida, et al. 2013. Mutations in CYC1, encoding cytochrome c1 subunit of respiratory chain complex III, cause insulin-responsive hyperglycemia. *Am. J. Hum. Genet.* 93:384–389.

Geetha, T., C. Zheng, N. Vishwaprakash, T.L. Broderick, and J.R. Babu. 2012. Sequestosome 1/p62, a Scaffolding Protein, Is a Newly Identified Partner of IRS-1 Protein. *J. Biol. Chem.* 287:29672–29678.

Gilmore, T.D. 2006. Introduction to NF-kappaB: players, pathways, perspectives. *Oncogene*. 25:6680–6684.

Glass, D.J. 2003. Signalling pathways that mediate skeletal muscle hypertrophy and atrophy. *Nat Cell Biol*. 5:87–90.

Gurnett, C.A., D.M. Desruisseau, K. McCall, R. Choi, Z.I. Meyer, M. Talerico, S.E. Miller, J.-S. Ju, A. Pestronk, A.M. Connolly, et al. 2010. Myosin binding protein C1: a novel gene for autosomal dominant distal arthrogryposis type 1. *Hum. Mol. Genet.* 19:1165–1173.

Hakvoort, T.B.M., P.D. Moerland, R. Frijters, A. Sokolović, W.T. Labruyère, J.L.M. Vermeulen, E. Ver Loren van Themaat, T.M. Breit, F.R.A. Wittink, A.H.C. van Kampen, et al. 2011. Interorgan coordination of the murine adaptive response to fasting. *J. Biol. Chem.* 286:16332–16343.

Hoshijima, M. 2006. Mechanical stress-strain sensors embedded in cardiac cytoskeleton: Z disk, titin, and associated structures. *Am J Physiol Heart Circ Physiol*. 290:H1313–H1325.

Huang, D.W., B.T. Sherman, and R.A. Lempicki. 2008. Systematic and integrative analysis of large gene lists using DAVID bioinformatics resources. *Nat. Protocols*. 4:44–57.

Hunter, R.B., and S.C. Kandarian. 2004. Disruption of either the Nfkb1 or the Bcl3 gene inhibits skeletal muscle atrophy. *J. Clin. Invest.* 114:1504–1511.

Hunter, R.B., E. Stevenson, A. Koncarevic, H. Mitchell-Felton, D.A. Essig, and S.C. Kandarian. 2002. Activation of an alternative NF-kappaB pathway in skeletal muscle during disuse atrophy. *FASEB J.* 16:529–538.

Jewell, J.L., Y.C. Kim, R.C. Russell, F.-X. Yu, H.W. Park, S.W. Plouffe, V.S. Tagliabracci, and K.-L. Guan. 2015. Metabolism. Differential regulation of mTORC1 by leucine and glutamine. *Science*. 347:194–198.

Karpac, J., and H. Jasper. 2011. Metabolic homeostasis: HDACs take center stage. *Cell*. 145:497–499.

Kempa, S., J. Hummel, T. Schwemmer, M. Pietzke, N. Strehmel, S. Wienkoop, J. Kopka, and W. Weckwerth. 2009. An automated GCxGC-TOF-MS protocol for batch-wise extraction and alignment of mass isotopomer matrixes from differential 13C-labelling experiments: a case study for photoautotrophic-mixotrophic grown Chlamydomonas reinhardtii cells. *J. Basic Microbiol.* 49:82–91.

Kempa, S., W. Rozhon, J. Samaj, A. Erban, F. Baluska, T. Becker, J. Haselmayer, E. Schleiff, J. Kopka, H. Hirt, et al. 2007. A plastid-localized glycogen synthase kinase 3 modulates stress tolerance and carbohydrate metabolism. *Plant J.* 49:1076–1090.

Kimura, A., H. Harada, J.E. Park, H. Nishi, M. Satoh, M. Takahashi, S. Hiroi, T. Sasaoka, N. Ohbuchi, T. Nakamura, et al. 1997. Mutations in the cardiac troponin I gene associated with hypertrophic cardiomyopathy. *Nat. Genet.* 16:379–382.

Lange, S., F. Xiang, A. Yakovenko, A. Vihola, P. Hackman, E. Rostkova, J. Kristensen, B. Brandmeier, G. Franzen, B. Hedberg, et al. 2005. The Kinase Domain of Titin Controls Muscle Gene Expression and Protein Turnover. *Science*. 308:1599–1603.

Layne, C.S., A.P. Mulavara, C.J. Pruett, P.V. McDonald, I.B. Kozlovskaya, and J.J. Bloomberg. 1998. The use of in-flight foot pressure as a countermeasure to neuromuscular degradation. *Acta Astronaut*. 42:231–246.

LeBlanc, A., R. Rowe, V. Schneider, H. Evans, and T. Hedrick. 1995. Regional muscle loss after short duration spaceflight. *Aviat Space Environ Med*. 66:1151–1154.

Lecker, S.H., R.T. Jagoe, A. Gilbert, M. Gomes, V. Baracos, J. Bailey, S.R. Price, W.E. Mitch, and A.L. Goldberg. 2004. Multiple types of skeletal muscle atrophy involve a common program of changes in gene expression. *FASEB J*. 18:39–51.

Lin, D.C., J.D. Hershey, J.S. Mattoon, and C.T. Robbins. 2012. Skeletal muscles of hibernating brown bears are unusually resistant to effects of denervation. *J. Exp. Biol.* 215:2081–2087.

Linke, W.A. 2008. Sense and stretchability: the role of titin and titin-associated proteins in myocardial stress-sensing and mechanical dysfunction. *Cardiovasc. Res*. 77:637–648.

Li, R., H. Zhu, J. Ruan, W. Qian, X. Fang, Z. Shi, Y. Li, S. Li, G. Shan, K. Kristiansen, et al. 2010. De novo assembly of human genomes with massively parallel short read sequencing. *Genome Res.* 20:265–272.

Lombardi, L., P. Ciana, C. Cappellini, D. Trecca, L. Guerrini, A. Migliazza, A.T. Maiolo, and A. Neri. 1995. Structural and functional characterization of the promoter regions of the NFKB2 gene. *Nucleic Acids Res.* 23:2328–2336.

MacLennan, P.A., R.A. Brown, and M.J. Rennie. 1987. A positive relationship between protein synthetic rate and intracellular glutamine concentration in perfused rat skeletal muscle. *FEBS Lett.* 215:187–191.

Maddirevula, S., M. Anuppalle, T.-L. Huh, S.H. Kim, and M. Rhee. 2012. Rnf11-like is a novel component of NF-κB signaling, governing the posterior patterning in the zebrafish embryos. *Biochem. Biophys. Res. Commun.* 422:602–606.

Manning, B.D., and L.C. Cantley. 2007. AKT/PKB signaling: navigating downstream. *Cell*. 129:1261–1274.

Martin, M., R. Kettmann, and F. Dequiedt. 2007. Class IIa histone deacetylases: regulating the regulators. *Oncogene*. 26:5450–5467.

Mayans, O., P.F. van der Ven, M. Wilm, A. Mues, P. Young, D.O. Fürst, M. Wilmanns, and M. Gautel. 1998. Structural basis for activation of the titin kinase domain during myofibrillogenesis. *Nature*. 395:863–9.

McKinsey, T.A., C.L. Zhang, and E.N. Olson. 2000. Activation of the myocyte enhancer factor-2 transcription factor by calcium/calmodulin-dependent protein kinase-stimulated binding of 14-3-3 to histone deacetylase 5. *Proc Natl Acad Sci U S A*. 97:14400–14405.

McPherron, A.C., A.M. Lawler, and S.J. Lee. 1997. Regulation of skeletal muscle mass in mice by a new TGF-beta superfamily member. *Nature*. 387:83–90.

Means, A.R. 2000. Regulatory cascades involving calmodulin-dependent protein kinases. *Mol. Endocrinol.* 14:4–13.

Mihaylova, M.M., D.S. Vasquez, K. Ravnskjaer, P.-D. Denechaud, R.T. Yu, J.G. Alvarez, M. Downes, R.M. Evans, M. Montminy, and R.J. Shaw. 2011. Class IIa histone

deacetylases are hormone-activated regulators of FOXO and mammalian glucose homeostasis. *Cell*. 145:607–621.

Misteli, T., J.F. Cáceres, J.Q. Clement, A.R. Krainer, M.F. Wilkinson, and D.L. Spector. 1998. Serine phosphorylation of SR proteins is required for their recruitment to sites of transcription in vivo. *J. Cell Biol.* 143:297–307.

Moresi, V., A.H. Williams, E. Meadows, J.M. Flynn, M.J. Potthoff, J. McAnally, J.M. Shelton, J. Backs, W.H. Klein, J.A. Richardson, et al. 2010. Myogenin and class II HDACs control neurogenic muscle atrophy by inducing E3 ubiquitin ligases. *Cell*. 143:35–45.

Nelson, O.L., H.T. Jansen, E. Galbreath, K. Morgenstern, J.L. Gehring, K.S. Rigano, J. Lee, J. Gong, A.J. Shaywitz, C.A. Vella, et al. 2014. Grizzly bears exhibit augmented insulin sensitivity while obese prior to a reversible insulin resistance during hibernation. *Cell Metab.* 20:376–382.

Nicholls, D.G., V.M. Darley-Usmar, M. Wu, P.B. Jensen, G.W. Rogers, and D.A. Ferrick. 2010. Bioenergetic Profile Experiment using C2C12 Myoblast Cells. *J Vis Exp*.

Oceandy, D., A. Pickard, S. Prehar, M. Zi, T.M.A. Mohamed, P.J. Stanley, F. Baudoin-Stanley, R. Nadif, S. Tommasi, G.P. Pfeifer, et al. 2009. Tumor suppressor Ras-association domain family 1 isoform A is a novel regulator of cardiac hypertrophy. *Circulation*. 120:607–616.

Oeckinghaus, A., M.S. Hayden, and S. Ghosh. 2011. Crosstalk in NF-κB signaling pathways. *Nat. Immunol.* 12:695–708.

Ojuka, E.O., V. Goyaram, and J.A.H. Smith. 2012. The role of CaMKII in regulating GLUT4 expression in skeletal muscle. *Am. J. Physiol. Endocrinol. Metab.* 303:E322–331.

Olson, T.M., M.L. Karst, F.G. Whitby, and D.J. Driscoll. 2002. Myosin light chain mutation causes autosomal recessive cardiomyopathy with mid-cavitary hypertrophy and restrictive physiology. *Circulation*. 105:2337–2340.

Patti, M.E., A.J. Butte, S. Crunkhorn, K. Cusi, R. Berria, S. Kashyap, Y. Miyazaki, I. Kohane, M. Costello, R. Saccone, et al. 2003. Coordinated reduction of genes of oxidative metabolism in humans with insulin resistance and diabetes: Potential role of PGC1 and NRF1. *Proc. Natl. Acad. Sci. U.S.A.* 100:8466–8471.

Peng, J., K. Raddatz, S. Labeit, H. Granzier, and M. Gotthardt. 2006. Muscle atrophy in Titin M-line deficient mice. *J Muscle Res Cell Motil*. 1–8.

Peng, J., K. Raddatz, J.D. Molkentin, Y. Wu, S. Labeit, H. Granzier, and M. Gotthardt. 2007. Cardiac hypertrophy and reduced contractility in hearts deficient in the titin kinase region. *Circulation*. 115:743–751.

Poetter, K., H. Jiang, S. Hassanzadeh, S.R. Master, A. Chang, M.C. Dalakas, I. Rayment, J.R. Sellers, L. Fananapazir, and N.D. Epstein. 1996. Mutations in either the essential or regulatory light chains of myosin are associated with a rare myopathy in human heart and skeletal muscle. *Nat. Genet.* 13:63–69.

Pratipanawatr, W., T. Pratipanawatr, K. Cusi, R. Berria, J.M. Adams, C.P. Jenkinson, K. Maezono, R.A. DeFronzo, and L.J. Mandarino. 2001. Skeletal muscle insulin resistance in normoglycemic subjects with a strong family history of type 2 diabetes is associated with decreased insulin-stimulated insulin receptor substrate-1 tyrosine phosphorylation. *Diabetes*. 50:2572–2578.

Puchner, E.M., A. Alexandrovich, A.L. Kho, U. Hensen, L.V. Schäfer, B. Brandmeier, F. Gräter, H. Grubmüller, H.E. Gaub, and M. Gautel. 2008. Mechanoenzymatics of titin kinase. *Proc. Natl. Acad. Sci. U.S.A*. 105:13385–13390.

Reich, K.A., Y.-W. Chen, P.D. Thompson, E.P. Hoffman, and P.M. Clarkson. 2010. Forty-eight hours of unloading and 24 h of reloading lead to changes in global gene expression patterns related to ubiquitination and oxidative stress in humans. *J. Appl. Physiol.* 109:1404–1415.

Ren, H., D. Accili, and C. Duan. 2010. Hypoxia converts the myogenic action of insulin-like growth factors into mitogenic action by differentially regulating multiple signaling pathways. *Proc. Natl. Acad. Sci. U.S.A*. 107:5857–5862.

Rommel, C., S.C. Bodine, B.A. Clarke, R. Rossman, L. Nunez, T.N. Stitt, G.D. Yancopoulos, and D.J. Glass. 2001. Mediation of IGF-1-induced skeletal myotube hypertrophy by PI(3)K/Akt/mTOR and PI(3)K/Akt/GSK3 pathways. *Nat Cell Biol*. 3:1009–1013.

Rondinone, C.M., L.M. Wang, P. Lonnroth, C. Wesslau, J.H. Pierce, and U. Smith. 1997. Insulin receptor substrate (IRS) 1 is reduced and IRS-2 is the main docking protein for phosphatidylinositol 3-kinase in adipocytes from subjects with non-insulin-dependent diabetes mellitus. *Proc. Natl. Acad. Sci. U.S.A*. 94:4171–4175.

Rose, A.J., and M. Hargreaves. 2003. Exercise increases Ca2+-calmodulin-dependent protein kinase II activity in human skeletal muscle. *J. Physiol. (Lond.)*. 553:303–309.

De Ruijter, A.J.M., A.H. van Gennip, H.N. Caron, S. Kemp, and A.B.P. van Kuilenburg. 2003. Histone deacetylases (HDACs): characterization of the classical HDAC family. *Biochem. J.* 370:737–749.

Sales, F.A., D. Pacheco, H.T. Blair, P.R. Kenyon, G. Nicholas, M. Senna Salerno, and S.A. McCoard. 2014. Identification of amino acids associated with skeletal muscle growth in late gestation and at weaning in lambs of well-nourished sheep. *J. Anim. Sci.* 92:5041–5052.

Sandri, M., C. Sandri, A. Gilbert, C. Skurk, E. Calabria, A. Picard, K. Walsh, S. Schiaffino, S.H. Lecker, and A.L. Goldberg. 2004. Foxo Transcription Factors Induce the Atrophy-Related Ubiquitin Ligase Atrogin-1 and Cause Skeletal Muscle Atrophy. *Cell*. 117:399–412.

Sarbassov, D.D., D.A. Guertin, S.M. Ali, and D.M. Sabatini. 2005. Phosphorylation and regulation of Akt/PKB by the rictor-mTOR complex. *Science*. 307:1098–1101.

Sartori, R., E. Schirwis, B. Blaauw, S. Bortolanza, J. Zhao, E. Enzo, A. Stantzou, E. Mouisel, L. Toniolo, A. Ferry, et al. 2013. BMP signaling controls muscle mass. *Nat. Genet.* 45:1309–1318.

Satoh, K., P. Nigro, A. Zeidan, N.N. Soe, F. Jaffré, M. Oikawa, M.R. O'Dell, Z. Cui, P. Menon, Y. Lu, et al. 2011. Cyclophilin A promotes cardiac hypertrophy in apolipoprotein E-deficient mice. *Arterioscler. Thromb. Vasc. Biol.* 31:1116–1123.

Sato, T.K., S. Panda, L.J. Miraglia, T.M. Reyes, R.D. Rudic, P. McNamara, K.A. Naik, G.A. FitzGerald, S.A. Kay, and J.B. Hogenesch. 2004. A functional genomics strategy reveals Rora as a component of the mammalian circadian clock. *Neuron*. 43:527–537.

Scharf, M., M.H. Brem, M. Wilhelm, U.J. Schoepf, M. Uder, and M.M. Lell. 2010. Atrial and ventricular functional and structural adaptations of the heart in elite triathletes assessed with cardiac MR imaging. *Radiology*. 257:71–79.

Schiaffino, S., and C. Reggiani. 2011. Fiber types in mammalian skeletal muscles. *Physiol. Rev.* 91:1447–1531.

Shagin, D.A., D.V. Rebrikov, V.B. Kozhemyako, I.M. Altshuler, A.S. Shcheglov, P.A. Zhulidov, E.A. Bogdanova, D.B. Staroverov, V.A. Rasskazov, and S. Lukyanov. 2002. A novel method for SNP detection using a new duplex-specific nuclease from crab hepatopancreas. *Genome Res.* 12:1935–1942.

Shannon, P., A. Markiel, O. Ozier, N.S. Baliga, J.T. Wang, D. Ramage, N. Amin, B. Schwikowski, and T. Ideker. 2003. Cytoscape: A Software Environment for Integrated Models of Biomolecular Interaction Networks. *Genome Res.* 13:2498–2504.

Shembade, N., K. Parvatiyar, N.S. Harhaj, and E.W. Harhaj. 2009. The ubiquitin-editing enzyme A20 requires RNF11 to downregulate NF-kappaB signalling. *EMBO J.* 28:513–522.

Shen, M.J., and D.P. Zipes. 2014. Role of the autonomic nervous system in modulating cardiac arrhythmias. *Circ. Res.* 114:1004–1021.

Stenvinkel, P., O. Fröbert, B. Anderstam, F. Palm, M. Eriksson, A.-C. Bragfors-Helin, A.R. Qureshi, T. Larsson, A. Friebe, A. Zedrosser, et al. 2013a. Metabolic changes in summer active and anuric hibernating free-ranging brown bears (Ursus arctos). *PLoS ONE*. 8:e72934.

Stenvinkel, P., A.H. Jani, and R.J. Johnson. 2013b. Hibernating bears (Ursidae): metabolic magicians of definite interest for the nephrologist. *Kidney Int.* 83:207–212.

Stitt, T.N., D. Drujan, B.A. Clarke, F. Panaro, Y. Timofeyva, W.O. Kline, M. Gonzalez, G.D. Yancopoulos, and D.J. Glass. 2004. The IGF-1/PI3K/Akt Pathway Prevents Expression of Muscle Atrophy-Induced Ubiquitin Ligases by Inhibiting FOXO Transcription Factors. *Mol. Cell*. 14:395–403.

Sun, Z., G. Tong, N. Ma, J. Li, X. Li, S. Li, J. Zhou, L. Xiong, F. Cao, L. Yao, et al. 2013. NDRG2: a newly identified mediator of insulin cardioprotection against myocardial ischemia-reperfusion injury. *Basic Res. Cardiol.* 108:341.

Taniguchi, C.M., B. Emanuelli, and C.R. Kahn. 2006. Critical nodes in signalling pathways: insights into insulin action. *Nat. Rev. Mol. Cell Biol.* 7:85–96.

Tarazona, S., F. García-Alcalde, J. Dopazo, A. Ferrer, and A. Conesa. 2011. Differential expression in RNA-seq: a matter of depth. *Genome Res.* 21:2213–2223.

Ten, R.M., C.V. Paya, N. Israël, O. Le Bail, M.G. Mattei, J.L. Virelizier, P. Kourilsky, and A. Israël. 1992. The characterization of the promoter of the gene encoding the p50 subunit of NF-kappa B indicates that it participates in its own regulation. *EMBO J.* 11:195–203.

Thuret, S., L.D.F. Moon, and F.H. Gage. 2006. Therapeutic interventions after spinal cord injury. *Nat. Rev. Neurosci.* 7:628–643.

Tian, B., D.E. Nowak, M. Jamaluddin, S. Wang, and A.R. Brasier. 2005. Identification of direct genomic targets downstream of the nuclear factor-kappaB transcription factor mediating tumor necrosis factor signaling. *J. Biol. Chem.* 280:17435–17448.

Tøien, O., J. Blake, D.M. Edgar, D.A. Grahn, H.C. Heller, and B.M. Barnes. 2011. Hibernation in Black Bears: Independence of Metabolic Suppression from Body Temperature. *Science*. 331:906–909.

Trivedi, C.M., Y. Luo, Z. Yin, M. Zhang, W. Zhu, T. Wang, T. Floss, M. Goettlicher, P.R. Noppinger, W. Wurst, et al. 2007. Hdac2 regulates the cardiac hypertrophic response by modulating Gsk3 beta activity. *Nat. Med.* 13:324–331.

Welle, S., A.I. Brooks, J.M. Delehanty, N. Needler, and C.A. Thornton. 2003. Gene expression profile of aging in human muscle. *Physiol. Genomics*. 14:149–159.

Witczak, C.A., N. Jessen, D.M. Warro, T. Toyoda, N. Fujii, M.E. Anderson, M.F. Hirshman, and L.J. Goodyear. 2010. CaMKII regulates contraction- but not insulin-induced glucose uptake in mouse skeletal muscle. *Am. J. Physiol. Endocrinol. Metab.* 298:E1150–1160.

Wojtaszewski, J.F., Y. Higaki, M.F. Hirshman, M.D. Michael, S.D. Dufresne, C.R. Kahn, and L.J. Goodyear. 1999. Exercise modulates postreceptor insulin signaling and glucose transport in muscle-specific insulin receptor knockout mice. *J. Clin. Invest.* 104:1257–1264.

Wu, C.-L., S.C. Kandarian, and R.W. Jackman. 2011. Identification of genes that elicit disuse muscle atrophy via the transcription factors p50 and Bcl-3. *PLoS ONE*. 6:e16171.

Xia, C., J.K. Cheshire, H. Patel, and P. Woo. 1997. Cross-talk between transcription factors NF-kappa B and C/EBP in the transcriptional regulation of genes. *Int. J. Biochem. Cell Biol.* 29:1525–1539.

Yabe, T., T. Sanagi, J.P. Schwartz, and H. Yamada. 2005. Pigment epithelium-derived factor induces pro-inflammatory genes in neonatal astrocytes through activation of NF-kappa B and CREB. *Glia*. 50:223–234.

Yılmaz, Z.B., B. Kofahl, P. Beaudette, K. Baum, I. Ipenberg, F. Weih, J. Wolf, G. Dittmar, and C. Scheidereit. 2014. Quantitative dissection and modeling of the NF-κB p100-p105 module reveals interdependent precursor proteolysis. *Cell Rep*. 9:1756–1769.

Zaglia, T., G. Milan, M. Franzoso, E. Bertaggia, N. Pianca, E. Piasentini, V.A. Voltarelli, D. Chiavegato, P.C. Brum, D.J. Glass, et al. 2013. Cardiac sympathetic neurons provide

trophic signal to the heart via β2-adrenoceptor-dependent regulation of proteolysis. *Cardiovasc. Res.* 97:240–250.

Zhang, S., M.W. Hulver, R.P. McMillan, M.A. Cline, and E.R. Gilbert. 2014. The pivotal role of pyruvate dehydrogenase kinases in metabolic flexibility. *Nutr Metab (Lond)*. 11:10.

Zhang, Y., Y. Lu, H. Zhou, M. Lee, Z. Liu, B.A. Hassel, and A.W. Hamburger. 2008. Alterations in cell growth and signaling in ErbB3 binding protein-1 (Ebp1) deficient mice. *BMC Cell Biol.* 9:69.

Zhong, L., M. Chiusa, A.G. Cadar, A. Lin, S. Samaras, J.M. Davidson, and C.C. Lim. 2015. Targeted inhibition of ANKRD1 disrupts sarcomeric ERK-GATA4 signal transduction and abrogates phenylephrine-induced cardiomyocyte hypertrophy. *Cardiovasc. Res.*

Zhulidov, P.A., E.A. Bogdanova, A.S. Shcheglov, L.L. Vagner, G.L. Khaspekov, V.B. Kozhemyako, M.V. Matz, E. Meleshkevitch, L.L. Moroz, S.A. Lukyanov, et al. 2004. Simple cDNA normalization using kamchatka crab duplex-specific nuclease. *Nucleic Acids Res.* 32:e37.

7 Abbreviations

2-DG	2-Deoxyglucose
3pg	Glycerate-3-phosphate
A	
Ab	Antibody
Ach	Acetylcholine
Adrb1	Adrenergic receptor beta-1
AKT	Protein kinase B (PKB)
Ala	Alanine
Alpha-KG	Alpha-ketogluterate
ANOVA	Analysis of variance
AP	Action potential
Arg	Arginine
AS160	Akt substrate of 160 kD
Asn	Asparagine
Asp	Aspartate
ATP	Adenine tri-phosphate
B	
Bcl3	B cell leukemia 3
BSA	Bovine serum albumin
C	
Ca2+	Calcium ion
CaM	Calmodulin
CaMK	Ca2+-calmodulin-dependent kinase
Car3/13	Carbonic anhydrase-3/13
CBP	CREB-binding protein
cDNA	Complementary DNA
Cebpb	CCAAT/enhancer binding protein-beta
CO2	Carbon dioxide
C-terminus	Carboxyl-terminus
Cys	Cysteine
ddH2O	Double distilled water
D	
DDT	Dithiothreitol
Deptor	DEP domain-containing mTOR-interacting protein
Dex	Dexamethasone
DMEM	Dolbecco's Modified Eagle's Medium
DMSO	Dimethyl sulfoxide
DNA	Deoxyribonucleic acid
DNS	Duplex-specific nuclease
dNTP	Deoxynucleoside triphosphate
Dox	Doxycycline
E	
EAA	Essential amino acids
ECAR	Extracellular acidification rate
EDTA	Ethylenediaminetetraacetic acid
Eno1	Enolase-1
ERK1/2	Extracellular signal regulated kinase-1/2

ESI	Electron spray ionization
ETC	Electron transport chain
F	
FA	Fatty acid
FAD	Flavin adenine dinucleotide
FBS	Fetal bovine serum
FC	Fold change
FCd	Fold change discretized
FDR	False discovery rate
Fhl1/2	Four-and-a-half LIM protein-1/2
FN3	Fibronectin type III domain
FOXO	Forkhead box transcription factor Class O
G	
GA	Gastrocnemius
Gapdh	Glyceraldehyde-3-phosphate dehydrogenase
GC	Gas chromatography
GEO	Gene expression omnibus
Gln	Glutamine
Glu	Glutamate
GLUT-4	Glucose transporter type 4
Gly	Glycine
Gpi	Glucose phosphate isomerase
GRB2	Growth factor receptor bound protein 2
GSK3a/b	Glycogen Synthase kinase type alpha/beta
Gys1	Glycogen synthase 1
H	
h	Hour
H/L	Heavy to light ratio
H2O	Water
HAT	Histone acetyl transferase
HCl	Hydrochloride
HDAC	Histone deacetylase
Hif1-alpha	Hypoxia induced factor-1-alpha
H.S.	Horse serm
HS/H. sapiens	Homo Sapiens
Hz	Hertz
I	
IAUCUA	Institutional Animal Care and Use Committee
IGF	Insulin growth factor
IKB	Inhibitor of NFKB
IKK	IKB-kinase
Iκbke	Ikb kinase e
Ig	Immunoglobulin
INS	Insulin
IP3	Inositol tri-phosphate
IP3R	IP3-receptor
IRS	Insulin receptor substrate

L

LC	Liquid chromatography
Ldha	Lactate dehyrogenase-a
LTQ-FT	Linear ion trap quadrupole with Fourier transformation ion cyclotron resonance mass spectrometry
LV	Left ventricle

M

MAFbx	Muscle atrophy F-box
MAPK	Mitogen activated protein kinase
MCW	Methanol-chloroform-water
min	Minute
MIRKO	Muscle-insulin receptor knockout mice
MLC	Myosin light chain
MLCK	MLC-kinase
MM	Mus Musculus
mRNA	Messenger RNA
MS	Mass spectrometry
mTOR	Mammalian target of rapamycin
mTORC1/2	Mammalian target of rapamycin complex 1/2
MuRF	Muscle ring-finger protein
Mwt	Molecular weight
Myh6	Myosin heavy chain-6

N

NaCl	Sodium Chloride
NAD(H)	Nicotinamide adenine dinucleotide
Nbr1	Neighbour of BRCA1 gene 1
Ndrg2	N-Myc Downstream-Regulated Gene 2 Protein
Ndufa1	NADH Dehydrogenase (Ubiquinone) 1 Alpha subcomplex, 1
Ndufv2	NADH Dehydrogenase (Ubiquinone) Flavoprotein 2
NEAA	Non-essential amino acid
NEB	New England Biosciences
NES	Nuclear export signal
NFKB	Nuclear factor kappa-light-chain-enhancer of activated B cells
N-terminus	Amino-terminus

O

OCR	Oxygen consumption rate
Ogdh	α-ketogluterate dehydrogenase
OXPHOS	Oxidative phosphorylation

P

P100/p52	Unprocessed/processed NFKB2
P105/p50	Unprocessed/processed NFKB1
P300	E1A-binding protein p300

P62	Nucleopoorin p62 (Sequestosome 1)
p-adj.	P-value adjusted for multiple testing
pAkt	Phosphorylated-protein kinase B
PCR	Polymerase chain reaction
PDH-A/B	Pyruvate dehydrogenase subunit A/B
Pdk-3/4	Pyruvate dehydrogenase kinase-3/4
Pgc1a/b	Peroxisome proliferator-activated receptor gamma coactivator 1-alpha/beta
PH	Pleckstrin homology
Phe	Phenylalanine
Phkg1	Phosphorylase kinase subunit gamma 1
PI3K	Phosphoinositide-3-kinase
PIP3	Phosphatidylinositol 3-phosphate
Pp1	Protein phosphatase 1
PPAR-alpha	Peroxisome proliferator-activated receptor-alpha
ppm	Parts per million
PPP	Pentose phosphate pathway
Ppp1r3c	Protein phosphatase 1 regulatory subunit 3C
Pro	Proline
PTEN	Phosphatase and tensin homologue
Pyg	Glycogen phosphorylase

Q

qRT-PCR	Quantitative real time-PCR

R

RACE	Rapid amplification of cDNA ends
RD	Regulatory domain
REL	Reticuloendotheliosis oncogene cellular homolog
RNA	Ribonucleic acid
ROS	Reactive oxygen species
Rpl36	Ribosomal protein like-36
rpm	Revolutions per minute
Rps12/15a/21/24	Ribosomal protein subunit-12/15a/21/24
rRNA	Ribosomal RNA
RyR	Ryanodine receptor

S

s	Second
s.d.	Standard deviation
s.e.m.	Standard error of the mean
Ser	Serine
Serpinf1	Serpin peptidase inhibitor, clade F
shRNA	Short hairpin RNA

Socs	Suppressor of cytokine signalling
SR	Sarcoplasmic reticulum
SRF	Serum response factor
T	
TBS	Tris-buffered saline
TBS-T	Tris buffered saline with Tween 20
TCA	Tricarboxylic acid
Tcap	Telethonine/Titin cap
TF	Transcription factor
TFBS	TF binding site
TGF-beta	Tissue growth factor-Beta
Thr	Threonine
TK(CD)	Titin kinase catalytic domain
TKCDRD	Autoinhibited Titin kinase domain
TWA	Two-way ANOVA
Tyr	Tyrosine
U	
UA/U.Arctos	Urus Arctos
Ugp2	UDP-Glucose pyrophosphorylase-2
UPLC	Ultra performance liquid chromatography
US	United States
V	
V	Volt
W	
WT	Wild-type
X	
Xbp1	X-box binding protein 1
Y	
Ywha	14-3-3 protein

8 List of figures

9 List of tables